The Thesis Committee for John Robert Kintz
Certifies that this is the approved version of the following thesis:

Experimental Evaluation of Partial Depth Precast Concrete Deck Panels Subjected to Shear Loading

APPROVED BY
SUPERVISING COMMITTEE:

Todd Helwig, Supervisor

Michael Engelhardt

Experimental Evaluation of Partial Depth Precast Concrete Deck Panels Subjected to Shear Loading

by

John Robert Kintz, B.S.E.

Thesis

Presented to the Faculty of the Graduate School of

The University of Texas at Austin

in Partial Fulfillment

of the Requirements

for the Degree of

Master of Science in Engineering

The University of Texas at Austin

May 2017

Dedication

To my family, as your limitless love, guidance, and support make all things possible. To my cousin Alex Kintz and my grandmother Jean Holtman, who inspire me to be my best each and every day.

Acknowledgements

I would like to thank the Texas Department of Transportation, for the funding they provided made this research possible and paid for my graduate education.

I would also like to thank Dr. Todd Helwig and Dr. Michael Engelhardt for the opportunity to conduct research at the Ferguson Laboratory. Your guidance has been invaluable, and my experience at the lab under your mentorship has helped me grow as both an engineer and a person. Thank you also to Dr. Patricia Clayton, whose advice and enthusiasm were very valued during my time at The University of Texas.

Thank you to the Ferguson Laboratory staff who provided assistance in many phases of this research project. In particular, thank you David Braley, Mike Brown, John Bacon, Dennis Phillip, Elizabeth Clayton, Michelle Damvar, and Blake Stasney.

A special thanks to Colter Roskos, whose efforts were critical to the success of this project, and whose friendship I have greatly appreciated through every challenge and success. Thank you also to Hossein Yousefpour, whose help, advice, and friendship were truly valued during my time at FSEL.

I would also like to thank the students at the Ferguson Laboratory, especially Mark Eason, who was always willing to lend a helping hand and whom I consider myself lucky to call a friend.

To my parents Mary and Robert and my sister Rachel, thank you for your constant love and support. Thank you also to Jessica Salazar, who helped me cherish the good times and push through the tough ones. I couldn’t have done it without each and every one of you.

Finally, I would like to thank my Grandpops, James Kintz, who inspired me to write with his wonderful poem:

"PRECAST CONCRETE PANELS ON CURVED BRIDGES"

Tunnels are like funnels, they pour everything into a hole;
Bridges are like a ride into the sky on the wing of a soul.

Precast concrete panels are the wind beneath their wings;
To hold them up so their tires, with a happy song sings.

The panels need to have smooth shapes;
Not bumpy, grumpy, like an apes.

Panels must be very strong;
Or to the ground before very long;

They can be decorative and pretty;
To come across like a fast ditty.

When people look at them they will say;
The Civil Engineer had a very nice day.

And will say very loud;
JOHN, YOU MAKE US VERY PROUD.

Abstract

Experimental Evaluation of Partial Depth Precast Concrete Deck Panels Subjected to Shear Loading

John Robert Kintz, M.S.E.

The University of Texas at Austin, 2017

Supervisor: Todd Helwig

Horizontally curved girder bridges are often utilized for highway interchanges and other projects with restricted right-of-way. The large torsional demands caused by the girder geometry often require these systems to have extensive bracing, typically in the form of cross frames or diaphragms, to increase the torsional stiffness of the girder system during the construction phase. The most critical stage for the bracing is during the deck placement, when the noncomposite girders must resist the full construction load.

Partial depth precast concrete panels (PCPs) are prestressed concrete panels used primarily as stay-in-place (SIP) formwork for straight girder systems. They are placed on full-length extruded bedding strips epoxied to the girder top flange, and the remaining depth of the deck is cast above. This is a time-efficient method of construction, and has become an attractive option due to ease of constructability and deck longevity. Although the panels have not been used on horizontally curved girder systems, there is a desire by bridge owners and contractors to use the forms in some curved girder applications. In addition to using the panels on curved girder applications, engaging the in-plane shear

stiffness of the panels may lead to significant bracing in both straight and horizontally curved girder applications.

A research investigation focused on measuring the behavior of PCPs acting as a shear diaphragm, as well as to develop an adequate connection between the PCPs and the girders was conducted at The University of Texas at Austin. Four PCP connection details were developed and tested at two different bedding strip heights. These connections were designed for a range of capacities, and in-plane shear load was applied until failure using a frame mechanism assembly.

The experimental results showed that the connected PCPs had significant shear stiffness and strength, with the panels reaching shear capacities between 91 and 154 kips before failure depending on the connection detail that was utilized. A 46 to 70 percent increase in shear stiffness was also observed when the bedding strip height was reduced from 4 inches to ½ inch. All panels greatly exceeded the design capacity using the ACI design predictions, with 7 of 8 panels eventually failing due to concrete side face breakout. The eighth PCP failed from weld rupture in which the weld connecting the WT and the girder flange began to unzip.

Table of Contents

List of Tables

List of Figures

CHAPTER 1: INTRODUCTION

1.1 OVERVIEW

Horizontally curved girders are frequently utilized in the bridge industry for a variety of applications such as highway interchanges in urban settings that require a tight radius of curvature. The girders can be subjected to significant torsional demands as a result of gravity loads applied to the curved geometry. Many curved bridges employ either steel I-girders or tub girders and a major design consideration is the torsional stiffness of the system during construction. Many of these girders require extensive bracing during the construction of the concrete deck. Although steel girders have been the most widely used in horizontally curved girders, concrete U-beams have also been used in some applications. The torsional stiffness of the concrete U-beams is also a major design consideration.

In the completed bridge, the cured concrete deck provides substantial restraint to the girder systems. In general, the most critical stage to control torsional deformations and provide overall stability occurs during placement of the concrete bridge deck during construction. During these stages, the non-composite steel or concrete girder must support the entire construction load. To ensure sufficient stability, traditional bracing such as cross frames, diaphragms or lateral trusses are employed throughout the length. However, these braces are expensive to fabricate and erect and for steel girders can result in fatigue sensitive details that require significant inspection over the service life of the bridge. An example of a horizontally curved steel system with intermediate bracing is shown below in Figure 1.1.

Figure 1.1: Horizontally Curved Steel Girders with Intermediate Cross-Frames (Haskins, 2015)

Most conventional bridge construction makes use of stay-in-place (SIP) forming systems to provide support to the concrete bridge deck during construction. As the name implies, these forms stay on the bridge permanently. Most steel bridge systems make use of permanent metal deck forms (PMDF), while most concrete bridges in the state of Texas use partial depth precast concrete deck panels (PCPs) that are usually approximately 4 inches thick and span between adjacent girders. The PCPs are fabricated at precasting yards and in most situations are prestressed. A schematic of a typical PCP is shown in Figure 1.2. While the PCPs are widely used in Texas, the forming systems have primarily been limited to straight-girder applications. As shown in Figure 1.2, the forms are often supported on bedding strips that are inset from the edges of the panels so that the cast-in-place concrete in the field can flow under the edges of the panel providing good support in the finished bridge. Although the Texas Department of Transportation (TxDOT) has

recommended details for utilizing PCPs on steel girders, most steel girders make use of PMDF that is supported at the ends by cold-formed angles that are welded to the top flange of the girders. As a result the PMDF has a positive connection to the girder flanges, while the PCPs do not have a positive connection to the girders. Due to the lack of a positive connection, PCPs are not currently permitted in horizontally curved girder applications; however TxDOT would be interested in using the panels if the use can be shown to be safe. In addition to simply using the PCPs in steel and concrete girder applications, with a suitable connection to the tops of the supporting girders, the panels may provide significant bracing. For suitable bracing, the demand on the panels during construction must be established. In general, the torsional deformations of the girders during construction will result in a shearing deformation of the panel. For this bracing application, the PCP will act as a shear diaphragm.

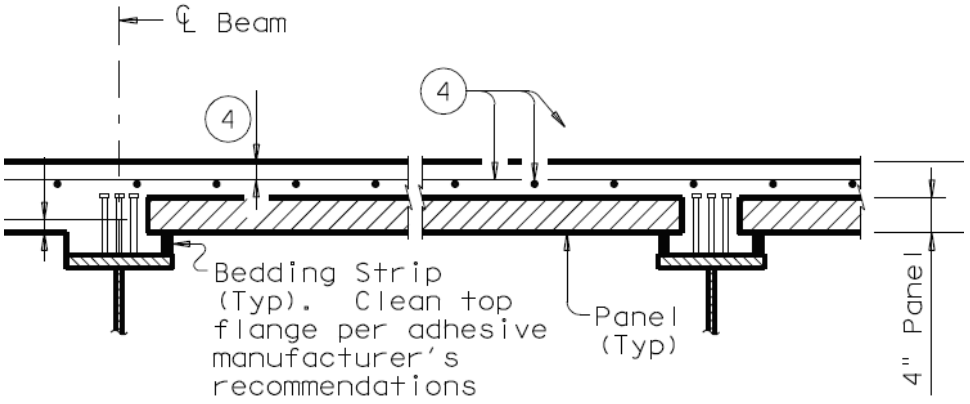

Figure 1.2: PCP Deck Panel Spanning Between Girder Lines (TxDOT, 2006)

1.2 RESEARCH OBJECTIVES

An investigation into the capabilities of PCPs as shear diaphragm bracing for horizontally curved girders during the construction phase is currently being conducted at The University of Texas at Austin with sponsorship from the TxDOT. The study includes both full-scale laboratory testing and computational modeling. The experimental testing consists of shear tests on the panels as well as full-scale buckling and torsion tests on steel I-girder and tub girders. The focus of this thesis is the panel shear tests that were carried out in the study.

Diaphragm bracing effectiveness relies not only on the stiffness of the diaphragm itself, but also on the stiffness of the connection attaching it to the girders. An example of this is the current practice method described in the previous section. Although the PCPs are believed to have high in-plane shear stiffness and strength, the impact of the bedding strip support on the stiffness is not well understood. In addition, a suitable connection between the PCPs and the girder flanges must be developed and evaluated. While this thesis is focused on the shear tests on the panels, a discussion of the full scale girder tests and computational modeling will be provided in a dissertation by Roskos. The following section provides an overview of the scope and layout of this thesis.

A total of eight shear panel tests have been carried out to date. The eight different panels were tested using a variety of connection details.

1.3 THESIS SCOPE

The concentration of this thesis is to portray the results of a research experiment investigating the capabilities of PCPs as shear diaphragm bracing members on straight and horizontally curved girder systems. This thesis focuses on the in-plane shear testing of PCPs using a proposed connection detail developed by the research team. The thesis

consists of five chapters. Following this introductory chapter, Chapter 2 discusses research background and previous work relevant to this investigation. An overview of the laboratory test setup is provided in Chapter 3. Findings from the in-plane shear tests experiments are presented in Chapter 4 and are discussed in detail within Chapter 5. Also included in Chapter 5 is an outline of future work that is outside the timeline of this thesis, and recommendations for consideration for future work.

CHAPTER 2: BACKGROUND AND LITERATURE REVIEW

2.1 OVERVIEW

This chapter provides a summary of background information and previous research pertinent to the scope of this thesis. Because the PCPs may be relied upon for beam bracing, a discussion of the lateral torsional buckling (LTB) failure mode of beam members and stability beam bracing is provided. Stiffness and strength requirements of member bracing, particularly as it pertains to diaphragms, are considered in addition to their effect on warping for steel systems. Given that this thesis focuses primarily on diaphragm-bracing of beam elements, research regarding the behavior of diaphragm braced beams is examined. One area that has been the subject of past stability research is the capability of permanent metal deck forms (PMDFs) as a bracing element, and a summary of this research is provided. Portions of this chapter were organized based on literature review work done by Jetann (2003), and some figures have been adapted for use in this thesis. For a comprehensive overview into the history of precast concrete panels and the in-plane shear behavior of concrete, please refer to the literature review work done by McCammon (2015), which was work carried out as part of the present study.

2.2 BUCKLING AND BRACING OF STEEL BEAMS

2.2.1 Lateral Torsional Buckling

The critical stage for lateral torsional buckling (LTB) in bridges often occurs during construction of the concrete bridge deck. Lateral torsional buckling involves a lateral deformation and twist of the cross section. Figure 2.1 depicts the buckled shape of a girder in the LTB mode and also illustrates the concept of the “center of twist”, which is the

location where an axis passing through the web of the unbuckled girder and the buckled girder intersect. Although most publications illustrate the LTB buckling mode as shown in Figure 2.1, depending on the bracing and load position on the cross section, the center of twist can also be located on the cross section of the girder.

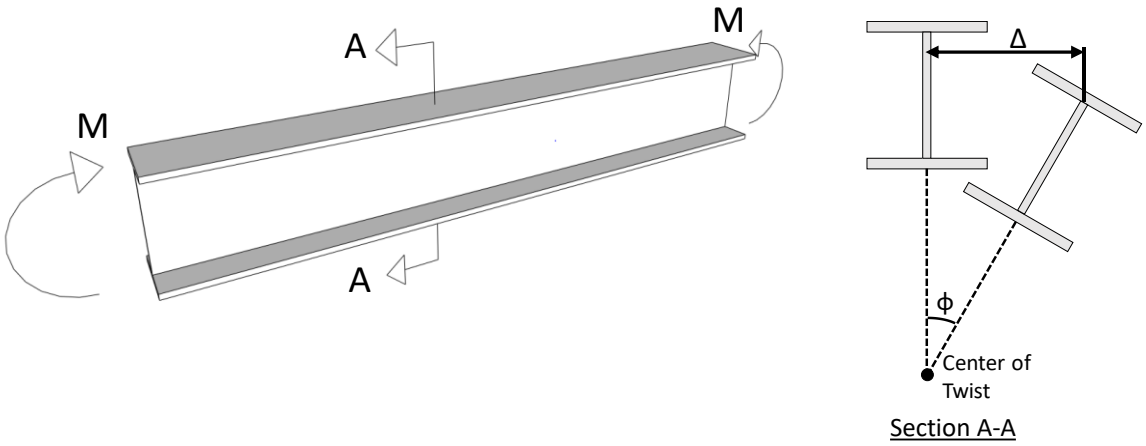

Figure 2.1: Lateral Torsional Buckling of a Typical I-Girder Section

The elastic solution for LTB capacity of a doubly-symmetric I-girder section subjected to uniform moment was developed by Timoshenko and Gere (1961) and is provided in the following expression:

$$M_g = \frac{\pi}{L_b}\sqrt{EI_yGJ + \left(\frac{\pi E}{L_b}\right)^2 I_y C_w} \qquad \text{Equation 2.1}$$

where L_b is the unbraced length, E is Young's modulus of elasticity, I_y is the weak axis moment of inertia, J is the torsional constant, G is the shear modulus, and C_w is the warping constant.

Equation 2.1 is intended for doubly-symmetric sections. In bridge construction, the strength of the composite cross section includes contributions from the steel girder as well as the concrete bridge deck. The strength of the girder is dependent on the location of the plastic neutral axis (PNA) as depicted in Figure 2.2 where the PNA is located in the concrete deck. Because the PNA is often in the bridge deck or very near the top flange, a smaller top flange is sometimes chosen relative the bottom flange, thereby resulting in a single axis of symmetry, which requires a different solution than Eq. 2.1. Solutions for singly-symmetric sections sometimes make use of a single-symmetry ratio is that is defined by the expression $\rho = I_{yc} / I_y$, where I_{yc} and I_y are the weak axis moment of inertias for the compression flange and the tension flange, respectively. With equal flange sizes, the $\rho = 0.5$. The American Association of State Highway and Transportation Officials (AASHTO) Bridge Specification limits this ratio to $0.1 < \rho < 0.9$, which allows engineers to consider top flanges that are significantly smaller than the bottom flange.

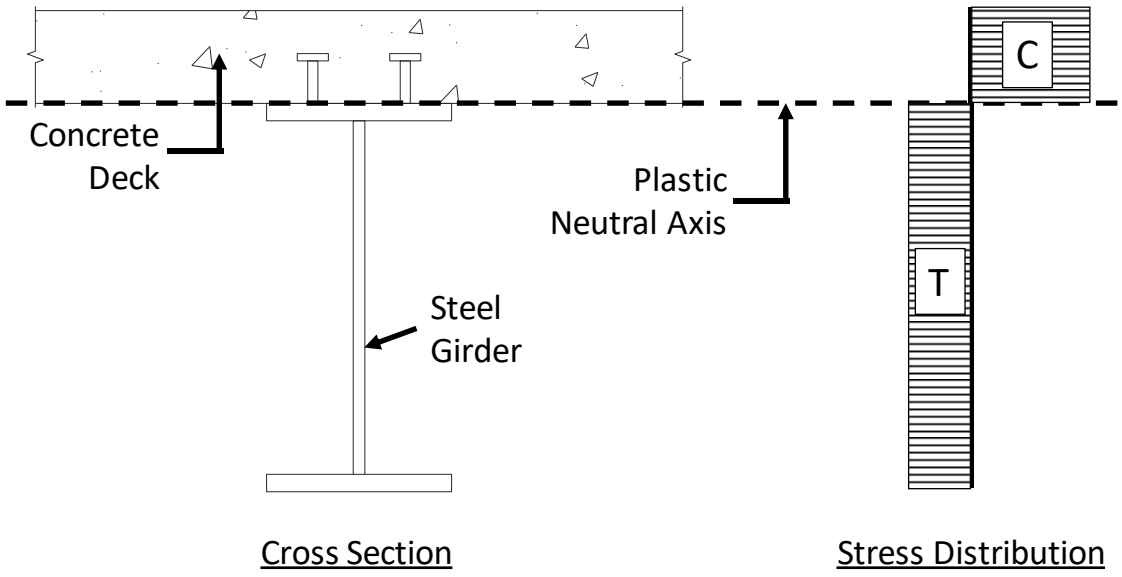

Figure 2.2: Composite Action of a Typical Steel Girder

This reduction does significantly decrease the amount of steel in the girder cross section, however it also makes the girder more susceptible to LTB. Thus, the moment capacity solution must reflect the different inertial effects of each flange. AASHTO (2014) provides an approximate solution for the buckling capacity of singly-symmetric sections subjected to a uniform moment, which can be seen below in Equation 2.2.

$$M_g = \pi E \left(\frac{I_{yc}}{L_b}\right) \sqrt{0.772 \left(\frac{J}{I_{yc}}\right) + 9.87 \left(\frac{d}{L_b}\right)^2} \qquad \text{Equation 2.2}$$

In this equation, L_b is the unbraced length, E is Young's modulus, I_{yc} is the weak axis moment of inertia of the compression flange, J is the torsional constant, and d is the depth of the girder cross section.

Equations 2.1 and 2.2 are applicable for beams subjected to uniform moment loading; however most practical applications typically result in girders having a variable moment along the length. Most design specifications include solutions developed for uniform moment loading (such as Eq. 2.1 and 2.2) and then use a moment gradient modifier, C_b, to account for moment gradient effects. There are a variety of Cb factor expressions that are available to the designer. The AASHTO specification utilizes a Cb factor that is similar to a long-used expression that is a function of the first order moment diagram; however the AASHTO equation is expressed in terms of stresses. The AASHTO expression includes several limits in an attempt to make the expression applicable to a wide variety of problems. However, many of these limits make the expression difficult to use and in some cases overly-conservative. The American Institute of Steel Construction (AISC) specification utilizes a relatively simple expression that is intended for use in doubly-symmetric sections and has been shown to provide reasonably accurate solutions

for most practical cases. Although the expression is intended for doubly-symmetric sections, a modifier was developed and presented in Helwig et al (1997) to include singly-symmetric sections. The modified expression is given as follows:

$$C_b = \frac{12.5M_{max}}{2.5M_{max} + 3M_A + 4M_B + 3M_C} R_m \leq 3.0 \qquad \text{Equation 2.3}$$

In this equation, M_{max} is the maximum moment experienced in the unbraced length, M_A, M_B, and M_C are the moments at the quarter points of the unbraced length, and R_m is a parameter accounting for singly-symmetric sections. In cases of single curvature bending, $R_m = 1.0$; in cases where reverse curvature bending is present, $R_m = 0.5 + 2\rho^2$.

The location of the load application can have a significant impact on the buckling capacity of the girder. For example, a load applied above the shear center causes an additional overturning torque as the girder displaces, while a load applied below the shear center causes a restoring torque that prevents the girder from twisting. Thus, Equation 2.4 was developed to account for load height in the moment modification factor (Helwig et. al, 1997; Galambos, 1998). In this equation C_b is the moment modification factor from Equation 2.3, y is the location of the load relative to the midheight of the cross section (positive measured downward), and h is the height of the girder. The parameters used to calculate this adjusted moment gradient, denoted as C_b^*, are depicted below in Figure 2.3.

$$C_b^* = 1.4^{\left(\frac{2y}{h}\right)} C_b \qquad \text{Equation 2.4}$$

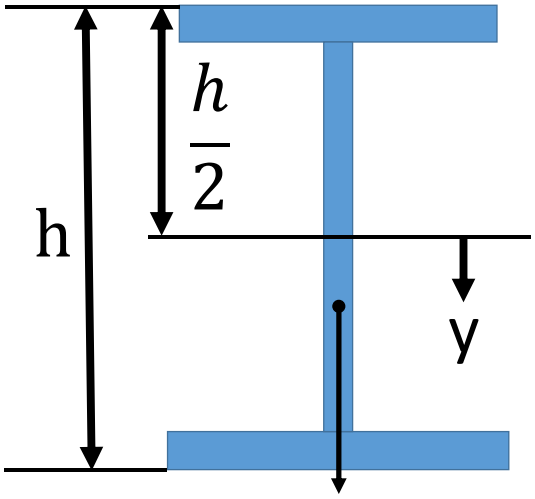

Figure 2.3: Parameters for Calculating Moment Gradient Accounting for Load Height

In an effort to increase the buckling capacity of noncomposite steel girders during construction, several methods of bracing have been utilized that allow the members to exceed the limits derived from the aforementioned section. These braces, in addition to an explanation into their effectiveness, are discussed in detail in the next section.

2.2.2 Methods of Beam Bracing

In general, there are four different categories of bracing systems: discrete (nodal), lean-on, continuous, and relative. Provided in this section is a brief description of each bracing method, as well as coinciding examples. A more thorough explanation into the types of beam bracing, including factors that impact their effectiveness, is presented by Yura (2001).

Discrete, or nodal, braces can be visually represented by a number of springs along the length of the girder. These braces can be effective either by the restraining of lateral displacement of the compression flange or twist. Some examples of discrete bracing are temporary guy cables (lateral restraint) or cross-frames (twist restraint). Lean-on bracing

consists of multiple girders being connected, requiring them to buckle as a system rather than individually. This type of bracing allows heavily loaded members to rely on adjacent girders below their capacity for strength. An example of a lean-on brace is a twin girder system connected laterally at the top flange with only one girder loaded past its buckling capacity. Continuous and relative bracing systems rely on similar behavior, where both restrain the relative moment of two points at different distances along the girder span. Continuous bracing restricts the flanges from displacing different amounts at all points along the span, preventing lateral buckling of the brace flange at any location. An example of a continuous brace is the installation of a metal deck over the entire span. Likewise, relative bracing prevents differential displacement between two points on adjacent girders. Unlike continuous bracing, however, lateral buckling can still occur between the discrete brace points. For example, a lateral truss between two girder flanges constrains the braced points so that they must move the same distance laterally. Since the truss diagonal prevents the flanges from displacing different amounts, lateral buckling can only occur within the span of the diagonal member. Figure 2.4 below shows a visual representation of the aforementioned bracing methods.

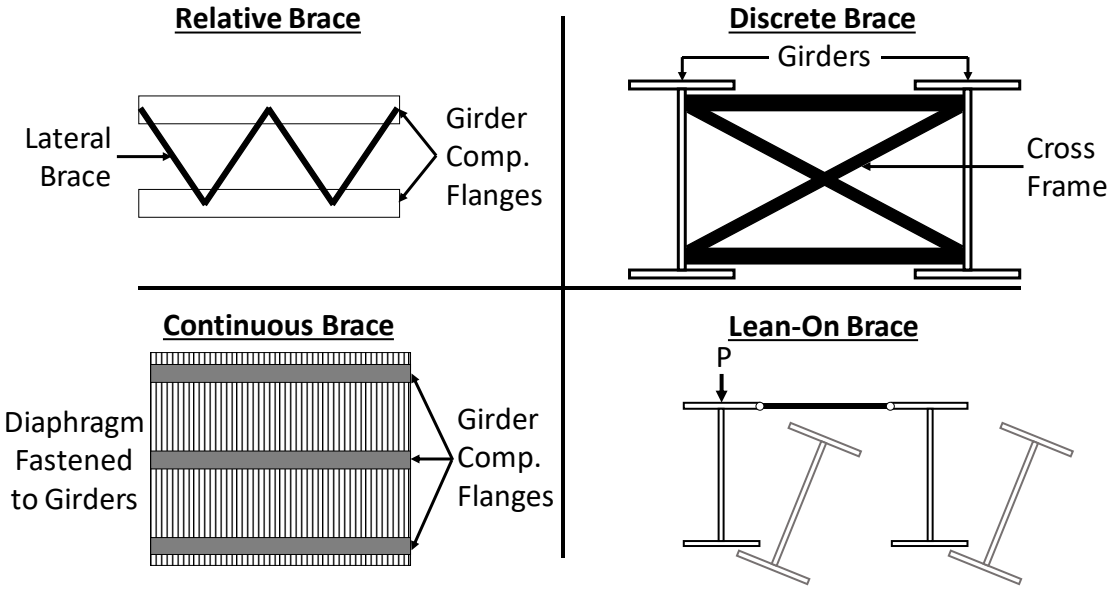

Figure 2.4: Examples of Different Bracing Methods; Adapted from (Yura & Helwig, 2014)

2.3 STRENGTH AND STIFFNESS REQUIREMENTS OF BRACING

Brace effectiveness is a function of both the brace stiffness and strength. If one parameter is insufficient, the actual buckling capacity of the member will be significantly less than the expected capacity of the braced system. This was first understood by Winter, who explained the concept using a simply-supported rigid column with a hinge and restoring spring (the brace) at midheight (Winter, 1960). Figure 2.5 shows an example of Winter's bracing model, from which Winter was able to derive the ideal brace stiffness required for a perfectly straight system to buckle between the brace points.

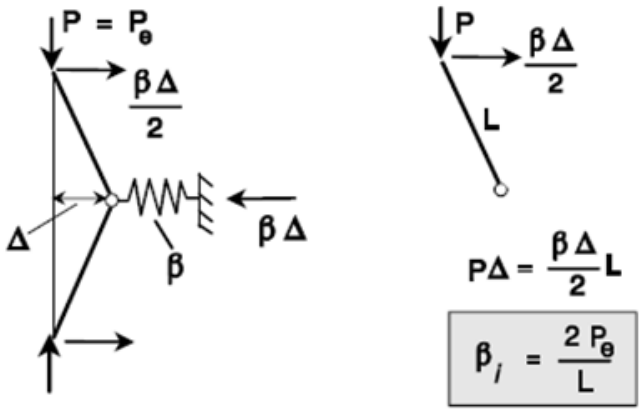

Figure 2.5: Winter's Rigid Column Bracing Model (Yura & Helwig, 2014)

Perfectly straight members, however, are not realistic in practice and the ideal stiffness has proven to be unconservative in systems with initial out-of-straightness. This is illustrated in Figure 2.6, where the column is assigned a reasonable initial imperfection and the buckling capacity is graphed for different brace stiffnesses. It can be seen that using the ideal stiffness on a member with initial imperfection will cause the member to buckle prior to reaching the Euler load.

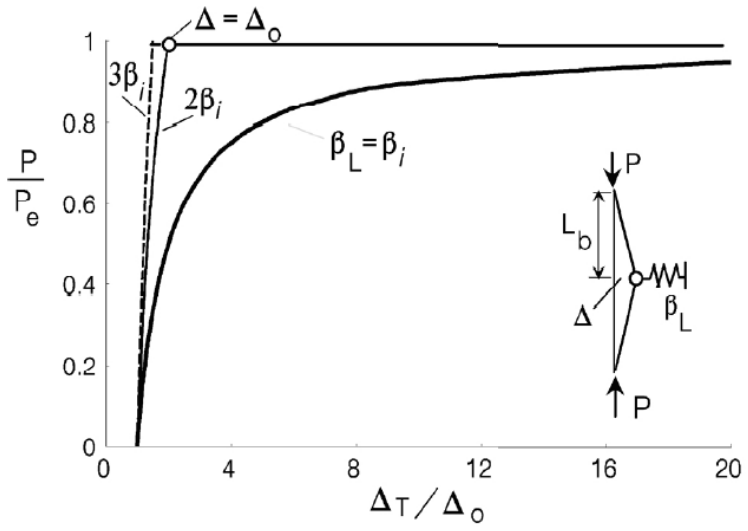

Figure 2.6: Normalized Buckling Capacity of Winter's Column with Varying Stiffness and Initial Imperfection (Yura, 2001)

As mentioned previously, the effectiveness of bracing systems is dependent not only on stiffness but also on brace strength. Returning to the example in Figure 2.5, the force in the brace can be expressed by $F_{br} = (\Delta - \Delta_o)\beta_{br}$, where Δ is the total lateral displacement at midheight, Δ_o is the initial out-of-straightness at midheight, and β_{br} is the stiffness of the brace. Figure 2.6 shows that for an initial imperfection of $L_b/500$ and a brace stiffness equal to the ideal stiffness, the total deflection increases greatly as load is applied. Since the force in the brace is directly related to the midheight displacement, the brace forces also increase substantially as the load increases. Conversely, the total displacement is decreased if a larger brace stiffness is implemented, thus decreasing the forces in the brace. The effects of bracing stiffness on reducing brace forces can be seen below in Figure 2.7, which when considered with Figure 2.6 shows that a brace with two times the ideal stiffness adequately controls both deformation and brace forces. This relationship between brace stiffness and strength eventually led to the AISC LRFD Specification recommending at least twice the ideal stiffness for bracing elements (AISC, 2011).

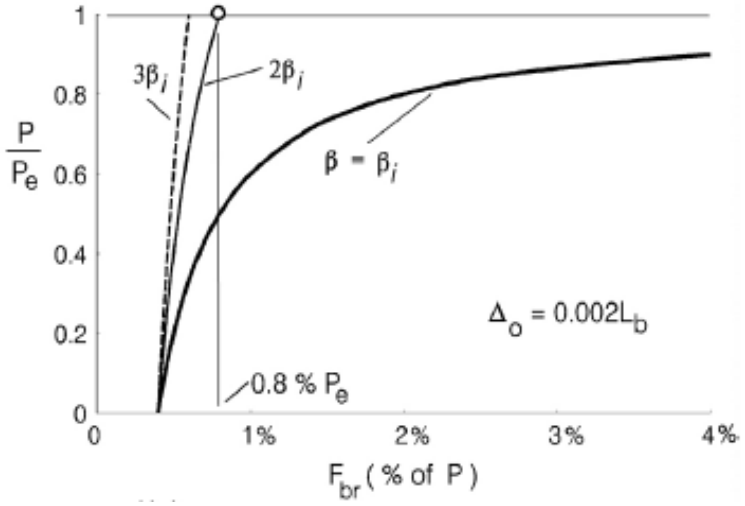

Figure 2.7: Brace Forces Induced for Winter's Column with L_b/500 Initial Imperfection and Varying Stiffness (Yura, 2001)

Winter's work focused on the bracing of column members, which succumb to primarily flexural buckling modes. This concept can be applied to beam buckling, however beam braces must also restrain the torsional buckling component. The factors that impact beam buckling behavior were discussed in Section 2.2.1, including concepts such as moment gradient, load height, and singly-symmetric behavior. Yura (2001) provides an in-depth exploration into the factors that affect beam bracing behavior. The next section of this report will apply the concepts discussed in this section and relate them to shear diaphragm bracing applications.

2.4 DIAPHRAGM BRACING OF BEAM SYSTEMS

For the remainder of this chapter, focus will be placed on shear diaphragm bracing and its impact on the buckling capacity of girder systems. Shear diaphragms, classified as either a relative or continuous-type brace based on their connection to the girders, are

effective by controlling relative lateral deformations of the top flange that contribute to LTB. These diaphragms extend along the length of the girders, and provide significant warping restraint to the girders. Warping occurs when a slender section, such as a steel I-girder, experiences a lateral displacement of the top and bottom flanges in opposite directions. When warping is permitted, these flanges are able to displace without inducing additional stresses in the flanges and the girder is more prone to buckling. If warping is restrained, bending stresses are induced in the flanges to resist the out of plane movement. An example of an I-girder with warping permitted (left) and restrained (right) is shown below in Figure 2.8.

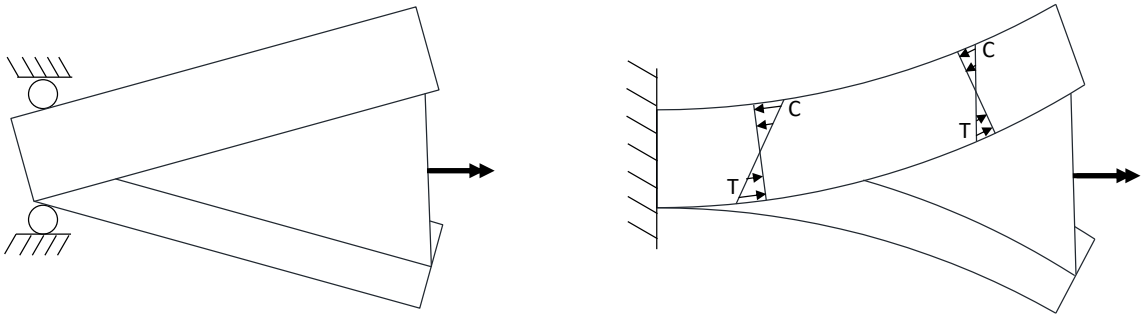

Figure 2.8: I-Girder Section Supported at the Top with Warping Permitted (left) and Warping Restrained (right)

As a girder system buckles, typically the top flanges of the girders will buckle out of plane in a half-sine curve with the largest deflection being at the midspan of the unsupported length. A plan view of this buckling behavior, with shear diaphragm attached, is shown below in Figure 2.9. As the girders begin to buckle, the shear stiffness of the diaphragms provide warping restraint to the top flanges. This restoring moment is induced along the total diaphragm-braced length, though it can also be seen from the figure that the maximum warping of the flanges occurs near the ends of the girder length while the flanges

are relatively unwarped near midspan. Thus the largest restoring moment, and subsequently the most effective diaphragm brace position, is located near the ends of the span.

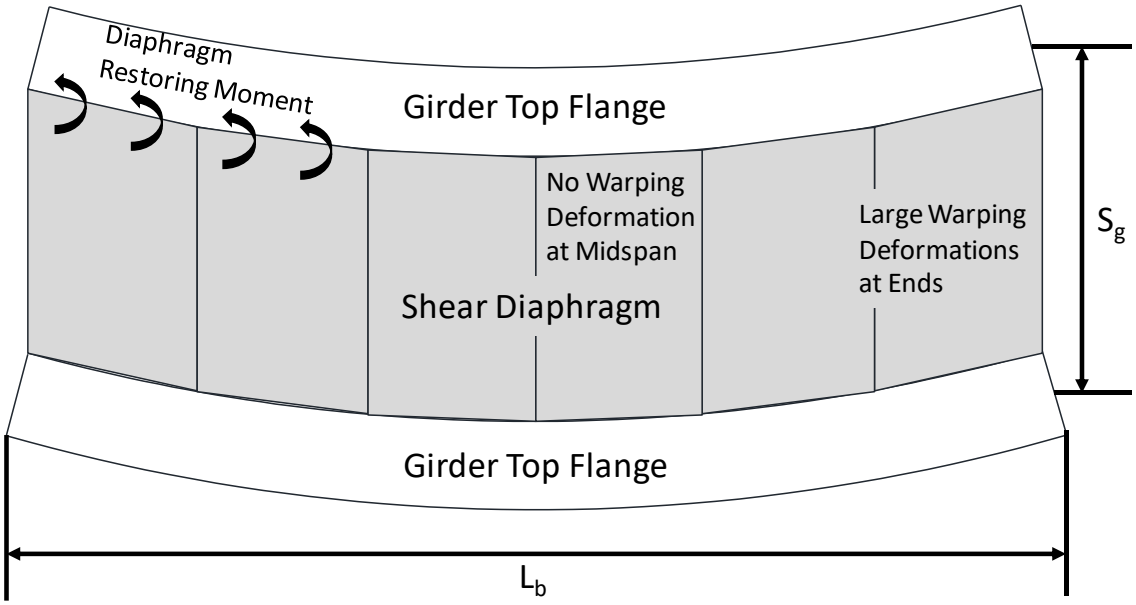

Figure 2.9: Shear Diaphragm Bracing Behavior as Top Flange Warping Restraint; Adapted from (Helwig & Yura, 2008a)

Design equations to quantify shear diaphragm bracing stiffness behavior were first developed in two independent studies by Errera & Apparao (1976) and Nethercot & Trahair (1975). Errera & Apparao derived a closed-form solution for diaphragm braced beams subjected to a uniform moment, which assumed a sinusoidal lateral displacement and girder twist along the span. This solution is seen below in Equation 2.5, where M_{cr} is the moment buckling capacity of the diaphragm braced girder, L is the spacing between points of zero twist, E is the modulus of elasticity, I_y is the weak axis moment of inertia, G is the shear modulus, C_w is the warping coefficient, J is the torsional constant, Q is the shear rigidity of the diaphragm, and e is the distance from the girder's center of gravity to the shear diaphragm plane.

$$M_{cr} = \sqrt{\frac{\pi^2 EI_y}{L^2}\left(\frac{\pi^2 EC_w}{L^2} + GJ + Qe^2\right)} + Qe$$ Equation 2.5

A simple approximation of this equation, determined by both Errera & Apparao and Nethercot & Trahair, expressed the buckling capacity of a diaphragm braced beam under uniform moment as:

$$M_{cr} = M_g + 2Qe$$ Equation 2.6

Where M_g is the moment capacity of the girder without diaphragm bracing and the other parameters are as defined for Equation 2.5. Work done by Helwig & Frank (1999) to investigate these equations using a W30x90 rolled section showed that the simplified Equation 2.6 provided a very accurate representation of the Equation 2.5 closed-form solution. The expressions were also validated with comparisons of three-dimensional finite element solutions for twin-girder systems with shear diaphragm bracing.

While Equation 2.5 and Equation 2.6 are only applicable for uniform moment load cases, Lawson & Nethercot (1985) developed a solution for girders subject to transverse loading and is shown below in Equation 2.7.

$$M_{cr} = C_b d\left[\frac{-P_e g}{2} + \frac{Q(1-g)}{2} + \sqrt{\left(\frac{-P_e g}{2} + \frac{Q(1-g)}{2}\right)^2 - \frac{Q^2}{4} + \left(\frac{P_e}{2} + \frac{Q}{2}\right)\left(\frac{P_e}{2} + 2P_T + \frac{Q}{2}\right)}\right]$$

Equation 2.7

In Lawson & Nethercot's equation d is the depth of the girder, P_e is the Euler weak axis buckling capacity or $P_e = (\pi^2 EI_y/L^2)$, $P_T = GJ/d^2$, g is defined as the load height factor, and all other variables are as previously defined. This equation also incorporated the moment gradient coefficient, C_b, to account for non-uniform moment. However, later studies done by Helwig concluded that Equation 2.7 overestimated the shear diaphragm bracing behavior for these systems (1994).

To determine a more accurate and simplified solution, Helwig and Frank (1999) conducted an in-depth finite element analysis study and proposed Equation 2.8:

$$M_{cr} = C_b^* M_g + mQd \qquad \text{Equation 2.8}$$

Where C_b^* is the moment gradient coefficient accounting for load height (previously defined in Equation 2.4), m is a constant between 0.375 and 1.0 relating to web slenderness ratio and torsional bracing conditions, and all other variables are as previously defined. A detailed list of m values for different cases is shown below in Table 2.1 Table 2.1: m Values for Equation 2.8 for Different Slenderness Ratios, Load Heights and Bracing Conditions .

Table 2.1: m Values for Equation 2.8 for Different Slenderness Ratios, Load Heights and Bracing Conditions (Helwig & Yura, 2008a)

	$h/t_w < 60$		$h/t_w > 60$	
Bracing Condition	Centroid Loading	Top Flange Loading	Centroid Loading	Top Flange Loading
No Intermediate Discrete Bracing	0.85	0.5	0.5	0.375
With Intermediate Discrete Bracing	0.85	0.85	0.5	0.375

Equation 2.8 can be rearranged to solve for the ideal effective shear modulus of the diaphragm bracing, shown below in Equation 2.9:

$$G'_{ideal} = \frac{\left(M_u - C_b^* M_g\right)}{mds_d} \qquad \text{Equation 2.9}$$

Where M_u is defined as the maximum moment and s_d is the tributary width of deck bracing each beam. This expression represents the required stiffness given ideal conditions, however as discussed previously with Winter's model the ideal stiffness is not sufficient for members with initial imperfections. Helwig & Yura (2008b) suggested that for girders with an initial twist of $\theta = L/(500d)$, the required shear stiffness of diaphragm bracing must be four times the ideal stiffness demands in order to adequately control forces and deformations. This proposed design stiffness is shown in Equation 2.10.

$$G'_{req'd} = \frac{4\left(M_u - C_b^* M_g\right)}{mds_d} \qquad \text{Equation 2.10}$$

For similarly imperfect girders, Helwig & Yura specified the expected brace strength requirement if the stiffness calculated from Equation 2.10 was used for diaphragm bracing design. This strength requirement was specified as the effective moment induced in the diaphragm and is shown below in Equation 2.11. In this equation all variables are as defined previously.

$$M'_{br} = 0.001 \frac{M_u L}{d^2} \qquad \text{Equation 2.11}$$

This section provided a discussion of past research related to the buckling capacity of both unbraced and diaphragm-braced girder systems. Also explained in this section were the design requirements for diaphragms in girder bracing applications. The following section provides the background on determining the stiffness and strength of shear diaphragm systems in an experimental test procedure, as well as a discussion on the behavior of diaphragms when subjected to shear loading.

2.5 STIFFNESS AND STRENGTH OF SHEAR DIAPHRAGM SYSTEMS

The shear stiffness and strength of a diaphragm can be found experimentally by connecting the diaphragm to a testing frame similar to the one show in Figure 3.1. The diaphragm provides all of the lateral strength and stiffness to the system since the frame is a mechanism on its own. The frame experiences a lateral deflection as the load in the system is increased. The parameters shown in Figure 3.1 are as follows: P = lateral load; Δ = lateral displacement; γ = shear strain; f = spacing between loading beams; L = length of the test frame; w = diaphragm width; S_d = diaphragm tributary width; h = diaphragm width; V = panel shear; R_L = left horizontal reaction; R_R = right horizontal reaction.

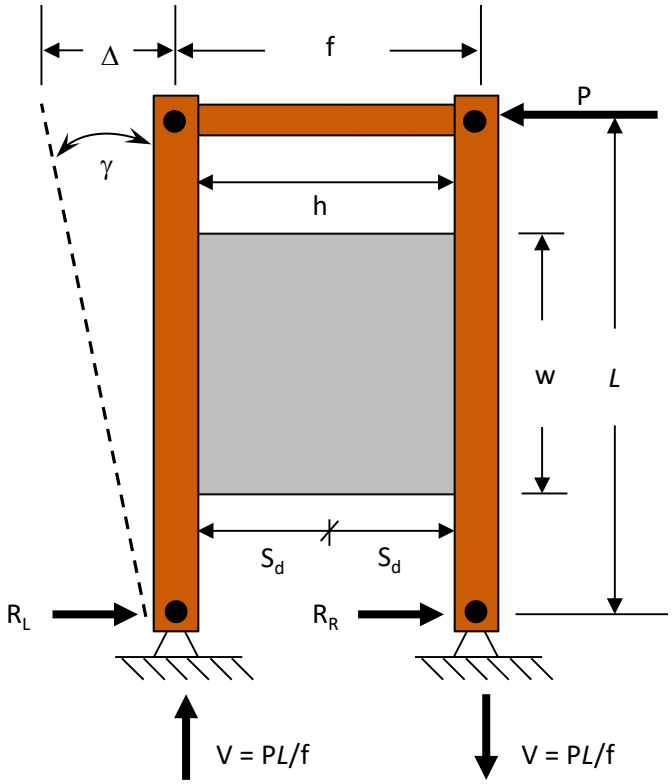

Figure 2.10: Shear Test Frame with Diaphragm

The shear force on the diaphragm can be found from statics by taking a cut through the system and summing the forces in the vertical direction as shown in Figure 3.2. Therefore, the internal shear force on the diaphragm must be V = PL/f and the corresponding average shear stress on the diaphragm must be τ' = V/w with units of force per unit length (k/in). Traditionally, shear modulus, G, is defined as shear stress divided by shear strain. For the purposes of this report, the effective shear modulus will be defined as G' = τ'/γ. Thus, for the system shown in Figure 3.1, the expression for G' will be:

$$G' = \frac{PL}{fw\gamma} \qquad \text{(k/in)} \qquad \text{Equation 2.12}$$

Furthermore, the diaphragm shear rigidity, Q, is expressed as follows:

$$Q = G' s_d \qquad \text{(k/rad)} \qquad \text{Equation 2.13}$$

For the test frame, the diaphragm tributary width is simply s_d = h/2, but for a bridge the following expression must be used (Egilmez, 2005):

$$s_d = \frac{(S_g - b_{tf})(n-1)}{n} \qquad \text{(ft)} \qquad \text{Equation 2.14}$$

Where, S_g = center to center spacing of girders; b_{tf} = girder top flange width; n = number of girders.

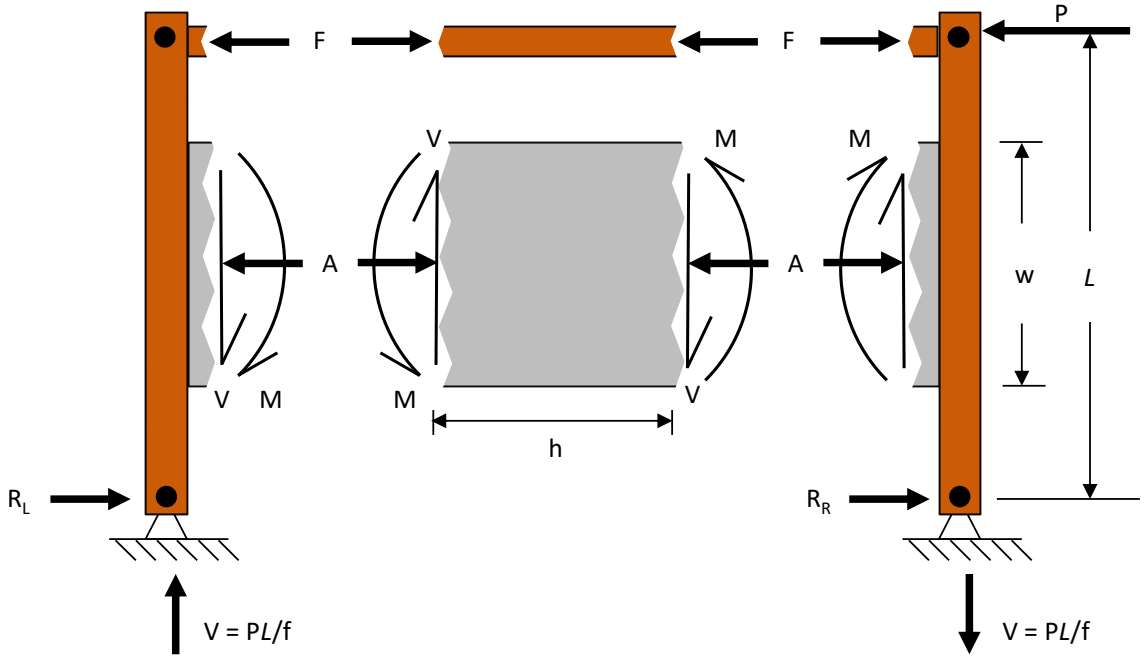

Figure 2.11: Internal Reactions of Shear Diaphragm

In addition to shear, the diaphragm experiences a moment, M, and can potentially experience an axial load, A, to satisfy equilibrium. From statics, M = Vh/2 and the moment on the left side of the diaphragm equals the moment on the right side of the diaphragm due to symmetry. The axial load on the panel depends on the stiffness properties of the diaphragm. For simplicity, the diaphragm can be visualized as a cross-frame with a tension tie and a compression strut as shown in Figure 2.12. If the diaphragm has the same stiffness in compression and in tension, then A = 0, F = P/2 (compression), and $R_L = R_R = P/2$. If the diaphragm is stiffer in compression than it is in tension, then A > 0 (compression), F < P/2 (compression), and $R_L > R_R$. This is the case for reinforced concrete diaphragms after tension cracks have formed. If the diaphragm compression stiffness is much greater than the diaphragm tension stiffness, the diaphragm behaves as a compression brace.

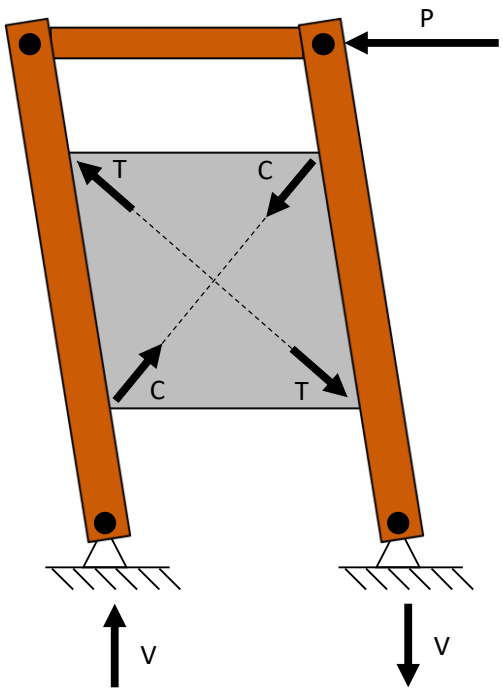

Figure 2.12: Diaphragm Shear Behavior

The ultimate shear strength of the diaphragm is simply taken as $V_{ult} = P_{ult}L/f$. Thus, the ultimate effective shear capacity of the diaphragm is calculated as:

$$S_{ult}' = \frac{P_{ult}L}{fw} \qquad \text{(k/in)} \qquad \text{Equation 2.15}$$

The ultimate shear capacity of the diaphragm can be governed by the strength of the diaphragm itself or by the strength of the connection from the diaphragm to the test frame or by a combination of the two. The following section provides a summary of past research on shear diaphragm bracing capabilities of permanent metal deck forms (PMDFs), as well as the findings from these experiments.

2.6 PERMANENT METAL DECK FORMS AS SHEAR DIAPHRAGM BRACES

This section focuses on the results from previous studies regarding permanent metal deck forms and their performance as a shear diaphragm. Extensive research has been conducted on the viability of permanent metal deck forms, or PMDFs, as diaphragm bracing elements. PMDFs are widely used on steel bridge systems as formwork for the concrete deck, however researchers have investigated if they could be relied on as braces during the construction phase where stability presents the greatest concern. A study conducted by Currah (1993) considered the shear stiffness and strength capacities of different types of open profile and flat soffit PMDFs. Results from this experiment illustrated that the stiffness of the diaphragm was not the only parameter for ensuring brace effectiveness, but that flexibility in the diaphragm-girder connection could greatly decrease the system stiffness and strength. Diaphragm bracing by profiled sheeting is commonly relied upon in the building industry when the sheeting is fastened directly to the

beams/girders. However, PMDF in the bridge industry is typically supported on cold-formed angles that allow the contractor to vary the elevation of the forms to account for changes in the flange thickness along the length as well as differential camber between adjacent girders. As the eccentricity of the welded deck support angle increases with the support angle, the connection to the girders introduces significant flexibility that impacts the bracing behavior of the shear diaphragm. An example of this can be seen in Table 2.2, where four different flat soffit (LSM) PMDFs were loaded in shear and the system stiffness was determined. The table shows the stiffness of the diaphragm as well as the effect of the connection stiffness.

Table 2.2: Flat Soffit Shear Stiffnesses for Various Connection Methods. Rigid vs. Eccentric Support Angle is shown as Boxed (Currah, 1993)

Deck Type	Rigid Support $G'_{.4Pult}$ (kips/inch)	Welded Angle Eccentric Support $G'_{.4Pult}$ (kips/inch)	Strap Angle Eccentric Support $G'_{.4Pult}$ (kips/inch)	Welded Angle Eccentric Support S_{avg} at Ultimate (kips/inch)	Welded Angle Eccentric Support S_{avg}/Fastener (kips/in./fast.)
LSM1516	59	6[a]		0.069	0.0058
LSM1524	41	7		0.054	0.0068
LSM2216	26	12	10	0.075[b]	0.0063
LSM2224	21	11		0.049	0.0061

a - average of two tests
b - value is 0.075 for both welded angle and strap angle tests

Later work completed by Jetann (2003) and Egilmez (2005) coincided with Currah's observation that increased eccentricity in the support angles decreased the stiffness and strength of the PMDF system. However, these eccentricities could not be avoided in most applications due to changes in flange thickness or differential camber between girder lines. To counter the effect of support angle eccentricity, Egilmez utilized a stiffening angle at the overlap of the metal decking sheets (or each end for a single sheet) as shown in Figure 2.13. This angle was attached to the girder via a welded connection plate, and the PMDF was directly fastened to the angle. Figure 2.14 shows the shear stress-strain curves for an 18-gauge, 8 foot wide PMDF with both stiffened and unstiffened connection details. As can be seen in the figure, the addition of the stiffening angle provided a significant increase in the stiffness and strength of the PMDF specimens.

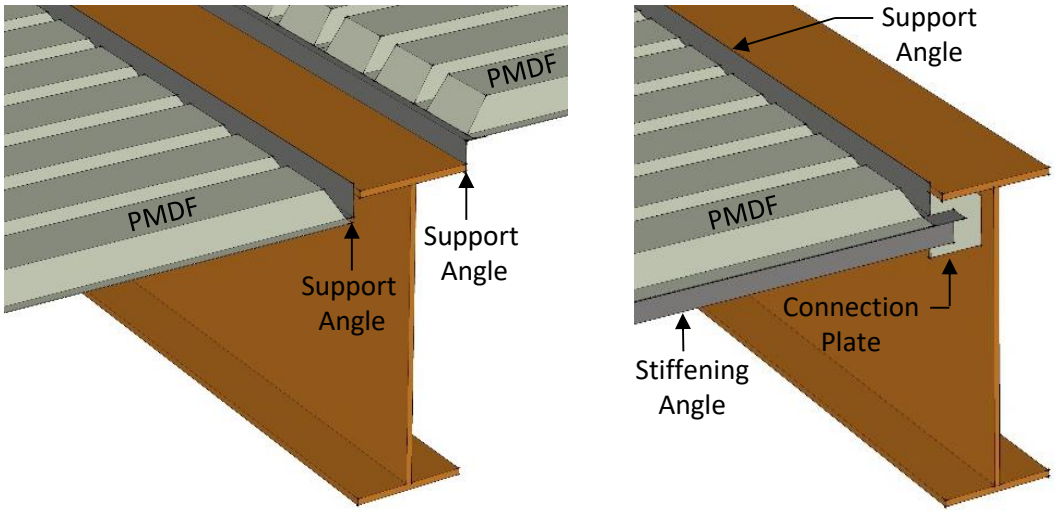

Figure 2.13: Unstiffened PMDF Connection (left) and PMDF Connection with Stiffening Angle/Connection Plate (right) (Roskos et al., 2017)

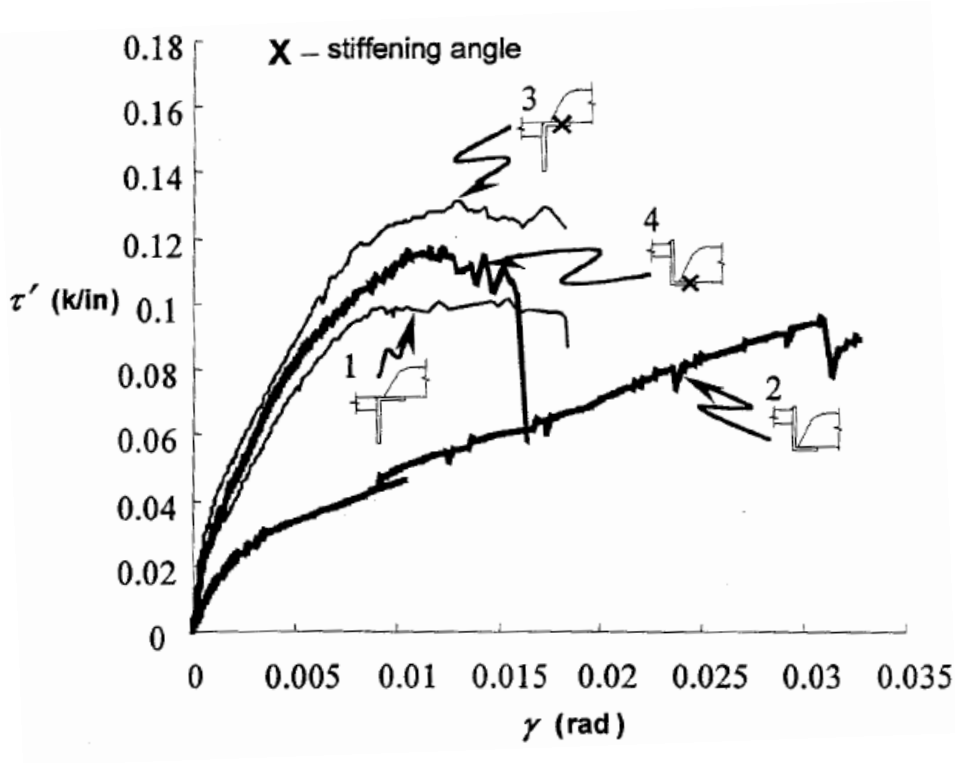

Figure 2.14: Shear Stress-Strain Curve for an 18ga PMDF with Stiffened (X) and Unstiffened Connections (Jetann, 2003)

This purpose of this chapter was to provide a detailed summary into the fundamental concepts of girder buckling and bracing. This chapter primarily focused on the idea of shear diaphragm bracing, including the evolution of previous research regarding the use of PMDFs as a bracing element. The ensuing chapters of this thesis will discuss the experimental procedure and findings of current research stemming from the concepts discussed in this chapter.

Although the focus of this research is on the bracing behavior of precast concrete panels, there are some similarities with the PMDF bracing. The PCPs are typically supported on a bedding strip to adjust the elevation of the panels and the bedding strip can have a similar effect as the cold-formed support angle for the PMDF.

CHAPTER 3: SHEAR FRAME EXPERIMENTAL PROCEDURE

3.1 OVERVIEW

This chapter discusses the experimental procedure for the full-scale PCP shear frame tests. The purpose of these tests were to develop an effective connection between the PCPs and the top flanges of steel girder systems, as well as to empirically determine the structural behavior of these modified PCPs when subjected to in-plane shear loading. The fabrication of the test assembly, as well as the setup and instrumentation for each of the PCP connection details considered, are explained within this chapter.

3.2 SHEAR FRAME FABRICATION

It should be noted that this section is abridged and is included to provide clarity for proceeding sections. The thesis work published by McCammon discusses in detail additional parameters considered in the behavior of the shear frame assembly (2015).

3.2.1 Shear Frame Test Setup

The shear frame was designed and fabricated with the intent to primarily subject the PCP/connection system to pure shear deformations. To ensure accurate measurements, the members of the test frame were designed to have large axial, flexural, and torsional stiffness to minimize the elastic deformations of the frame during the tests. Furthermore, the frame was designed and detailed to minimize internal friction so that the measurements correctly reflected the strength and stiffness of the PCP/connection system.

The test apparatus was constructed at the Ferguson Structural Engineering Laboratory (FSEL) in an orientation consistent with reality (i.e. the PCPs were placed parallel to the earth's surface). The frame was anchored to the FSEL reaction floor that has

anchors at 4 ft on center. For the purpose of discussion, the frame has been broken down into six main parts: two reaction blocks, two loading beams, one adjustable connection strap, one hydraulic actuator, and four tie-down beams. Figure 3.1 shows a plan view drawing of the testing frame with the major components identified. A picture of the assembled frame is shown in Figure 3.2.

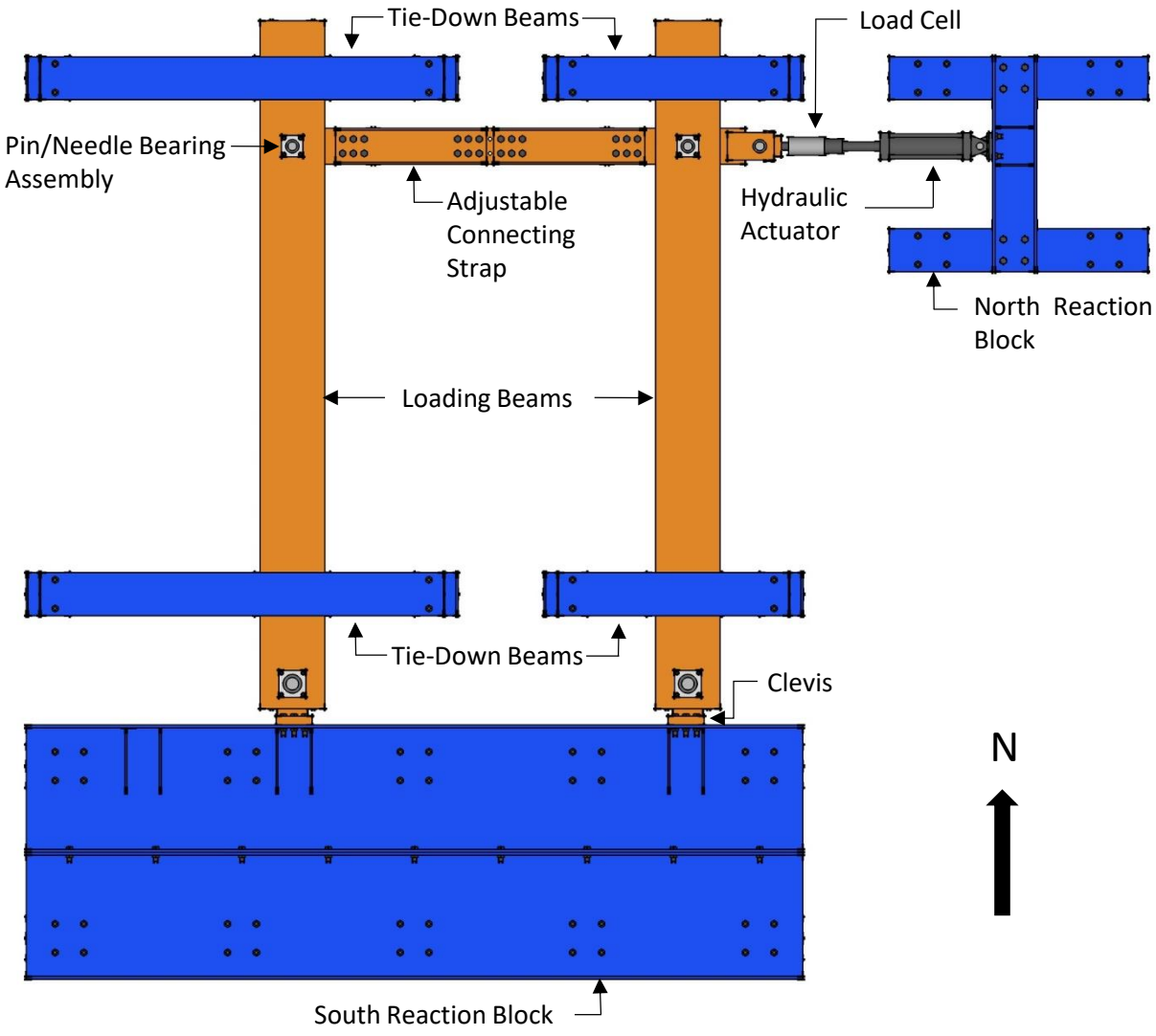

Figure 3.1: Plan View of Test Setup

Figure 3.2: Isometric View of Test Setup

The south reaction block consisted of two 18 ft long W36x135 beams bolted together at the flanges and supported vertically by two 18 ft long W12x65 beams located directly above the anchors in the strong floor. A total of 40 threaded 1 inch diameter rods pass through the webs of the W36x135 beams and both flanges of the W12x65 beams. Each threaded rod was post-tensioned to a force of approximately 30 kips, resulting in a total clamping force in excess of 1000 kips between the south reaction block and the strong floor. This large force was required to keep the reaction block from sliding and/or spinning due to the shear force and moment couple from the frame. The north reaction block consisted of two W12x65 beams that were post-tensioned to approximately 500 kips to the strong floor by 16 threaded 1 inch diameter rods. The W12x65s were connected by a W12x79 spreader beam that directly resisted load from the actuator.

The two loading beams were each fabricated from a 16 ft long W12x79 rolled section and a 16 ft long 18x1 inch steel plate that simulated the top flange of a bridge girder. The W12x79 beams were oriented with the webs parallel to the strong floor and the 18x1 inch plates rested on top of the edge of the two flanges. These two sections were stitch welded together, forming a closed section that had a large torsional and flexural stiffness. The loading beams were each supported vertically by three heavy duty casters that reacted on a ½ inch thick plate which was leveled with hydrostone and supported by the strong floor. Figure 3.3 shows a cross-section of the loading beam assembly.

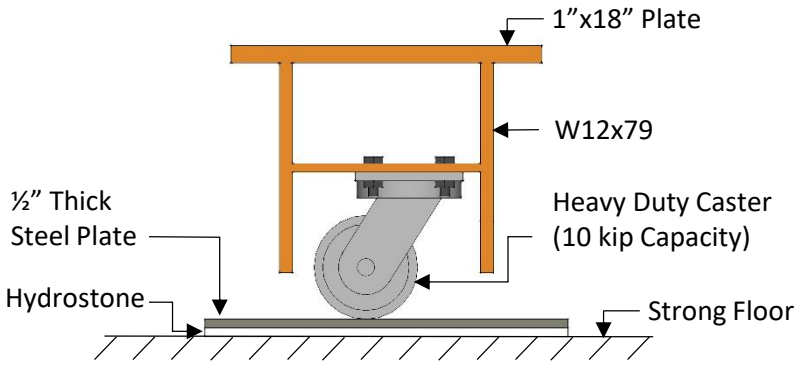

Figure 3.3: Loading Beam Cross-Section

Each loading beam connected to the south reaction block via a clevis and two needle bearings that accepted a 3.5 inch diameter pin as shown in Figure 3.4. The needle bearings were seated inside two manufactured bearing housings that mounted to the beam across from one another (one in the 18x1 inch plate and the other in the web of the W12x79). A portion of the bearing housing projected through the flame-cut holes in the loading beam and a steel-filled epoxy was used to fill the gap between the two which allowed load to be transferred through bearing. To increase the bearing area of the epoxy, doubler plates were welded to the web of the W12x79 and the 18x1 inch plate. To achieve equal thickness values a 1 inch plate was welded to the web of the wide flange and a ½ inch plate was welded to the 1”x18” plate. A similar but smaller needle bearing and 2-½” diameter pin assembly was used to connect the north end of the loading beams to the adjustable connection strap.

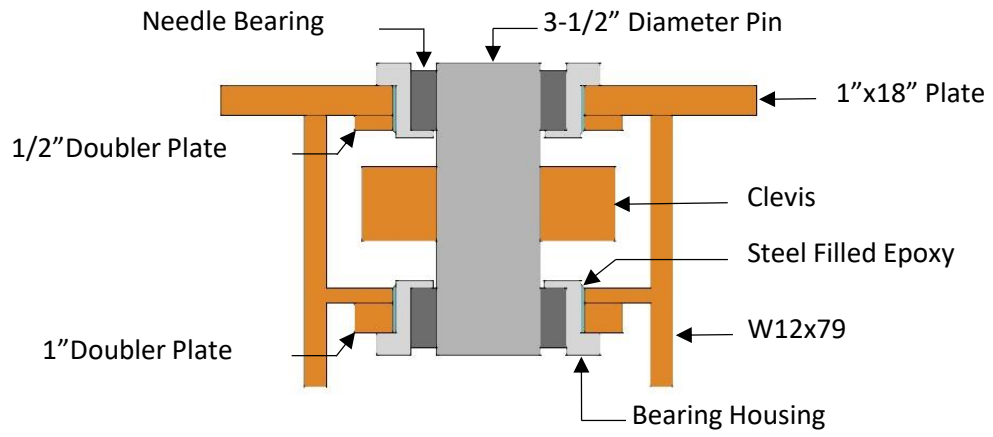

Figure 3.4: Pin/Needle Bearing Cross-Section

The same adjustable connection strap fabricated for Currah's test frame (Currah, 1993) was used in this test setup. The strap consisted of three 10x2-½ inch steel plates and four C10x25 steel channels bolted together with 24 A325 1 inch diameter bolts (4 groups of 6 bolts each). The structural bolts in this assembly were fully tightened to ensure no slippage occurred between the members. The strap could be assembled so that the center of the loading beams were spaced as close as 9'-2" and as far as 12'-8" to allow panels with different spans to be tested. The far end of the connection strap was joined to the hydraulic actuator via two needle bearings and a 2-½ inch diameter pin. Two heavy duty casters were used to vertically support the adjustable connection strap.

A 200 kip double-acting hydraulic actuator with an 18-inch stroke was used to load the system. The loading beams were square with the reaction block when the actuator was at half stroke (9 inches) which allowed a maximum shear strain of 0.06 radians to be applied to the system in each direction. A variable speed pneumatic hydraulic pump was used to power the hydraulic actuator which allowed the load rate to be controlled by the operator.

Since the PCPs were located on or above the simulated top flanges (18x1 inch plates) of the test frame and not in the same plane at which the load was applied, one of the loading beams was subjected to forces that tended to lift off of the strong floor while the other loading beam experienced forces that reacted against the strong floor. Therefore, four tie-down beams (one at each end of the two loading beams) were used to restrain the vertical movement of the loading beams (see Figure 3.5). Teflon with chemical etching on one side was epoxied to the bottom of the tie-down beam and the top of the loading beams at their contact point to minimize friction in the system. Three heavy duty casters (rated for 10 kips each) were mounted to the bottom of each loading beam to resist the vertical loads from the test frame and allow the frame to move laterally with minimum resistance. The casters were offset from one another along the length of the beam to help resist torsion and give the loading beams stability during the assembly process.

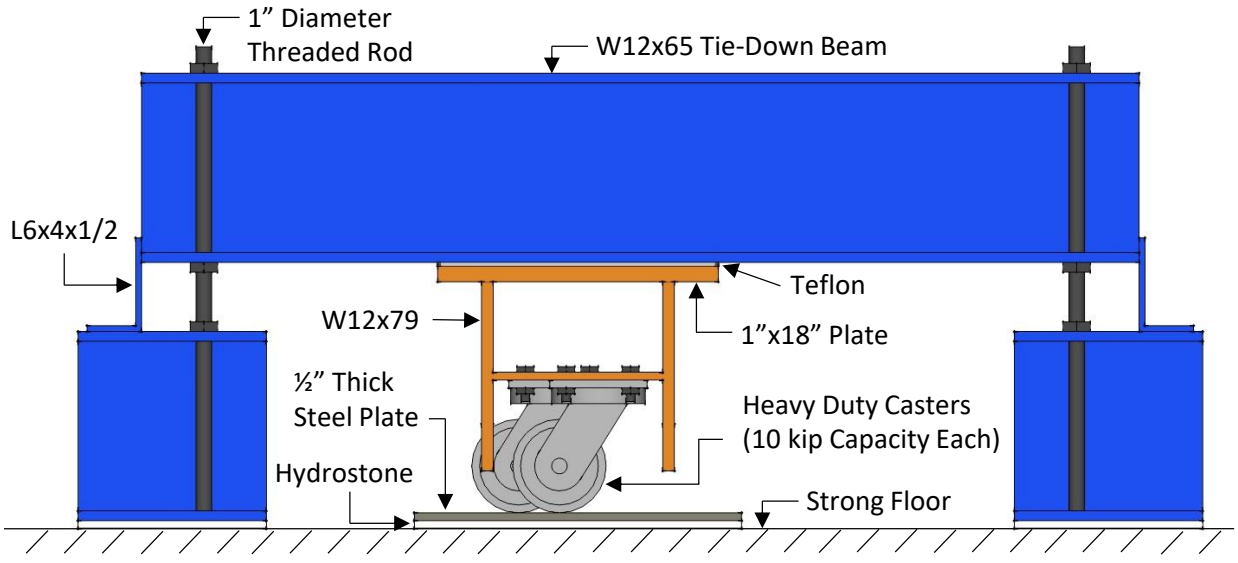

Figure 3.5: Tie-Down Beam Elevation

Care was taken in assembling the test frame in an effort to minimize friction in the system. The loading beams and adjustable connection strap were placed on blocks and leveled. At this point, the casters were located approximately 1 to 1-½ inches above the strong floor (which was not perfectly level in the region of the test setup). Eight ½ inch thick steel plates were placed under the casters and raised with three leveling screws until the plates came into contact with the casters. Hydrostone (quick-setting grout) was then poured between the strong floor and the steel plates and the blocks were removed from the test frame. The result was a level surface on which the leveled test frame could move. The tie-down beams were then placed on top of the loading beams and leveled.

3.3 SPECIMEN DESIGN AND GEOMETRY

Due to the absence of prior research on the bracing capabilities of precast concrete panels, the PCP specimens were designed for a number of different failure modes specified in AISC and ACI standards. These parameters were considered in addition to current TxDOT standards on PCP design. The details of those parameters considered, as well as the geometries selected for experimental testing, are discussed within this section.

3.3.1 Panel Design and Geometry

Typical curved steel I-girder bridges have a girder spacing between six and twelve feet. Given that the PCPs would be required to span this distance, it was important that the panel geometry provide a reasonable representation of what would be expected in field applications. TxDOT standards require that precast deck panels at or exceeding a width of five feet be cast with prestressed strands in the transverse direction, so a local precaster was consulted for casting operations (TxDOT, 2006). Limitations of the shear frame's adjustable connection strap (discussed in Section 3.2.1) required a minimum panel length

of 8’-3”. However, the width of the plant’s standard prestressing bed was eight feet, so the panel dimensions were specified at 8’-0” longitudinally by 8’-3” transversely to achieve an approximately square geometry. Figure 3.6 shows the geometry used to fabricate the PCP test specimens.

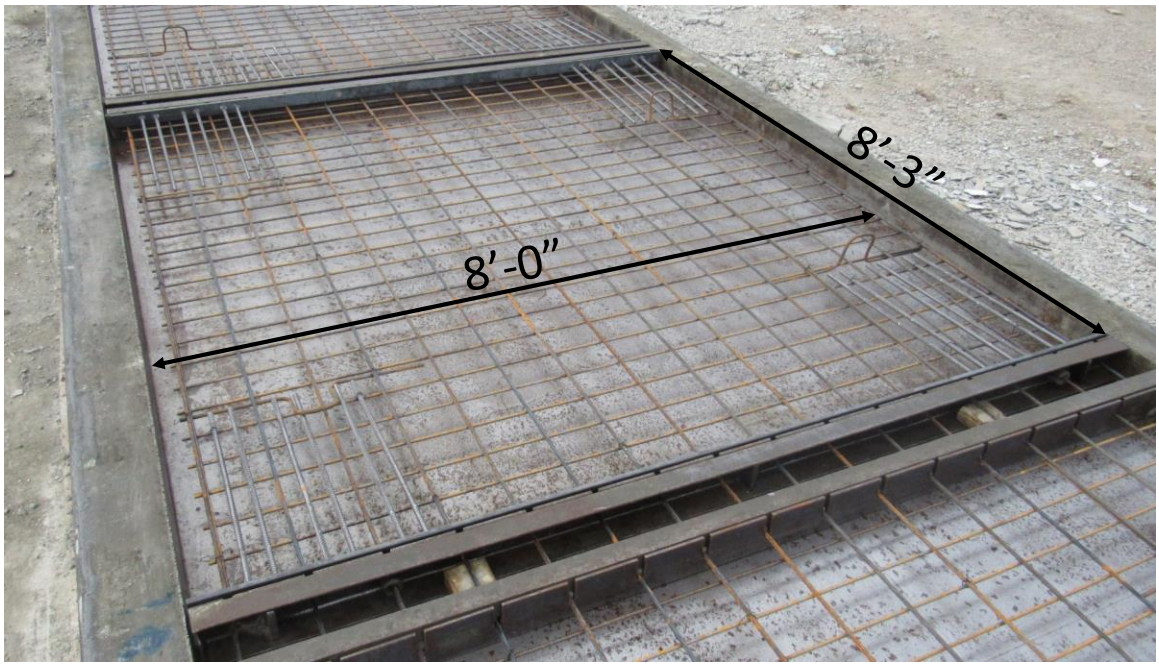

Figure 3.6: PCP Formwork Geometry for Shear Frame Testing

3.3.2 Bedding Strip Geometry

As a method to support the precast concrete panels on the top flanges of girder systems, current practice employs the use of polystyrene bedding strips. These bedding strips extend the length of the PCP and are offset towards the edge of the girder flange to allow concrete to flow underneath the panel during topping slab placement, as shown in Figure 3.7. Differential elevation between girder lines is accommodated by adjusting the height of the bedding strip, with a minimum ½ inch and a maximum 4 inch height for a 2 inch wide strip as specified by TxDOT standards (2010). An epoxy is applied to attach the

bedding strip to the girder flange, and also adheres it to the PCP if the strip height exceeds 2 ½ inches.

Using basic static principles, it was expected that the maximum bedding strip height would produce the most flexible behavior during testing due to the large eccentricity between the shear frame load and the restoring force of the panel. Conversely, the minimum height would reduce that eccentricity, thus an increasingly stiff response would be expected. To achieve a measure of the behavior at the two extremes, 2-inch wide bedding strips at both ½ inch and 4 inch heights (see Figure 3.7) were considered in the experimental program.

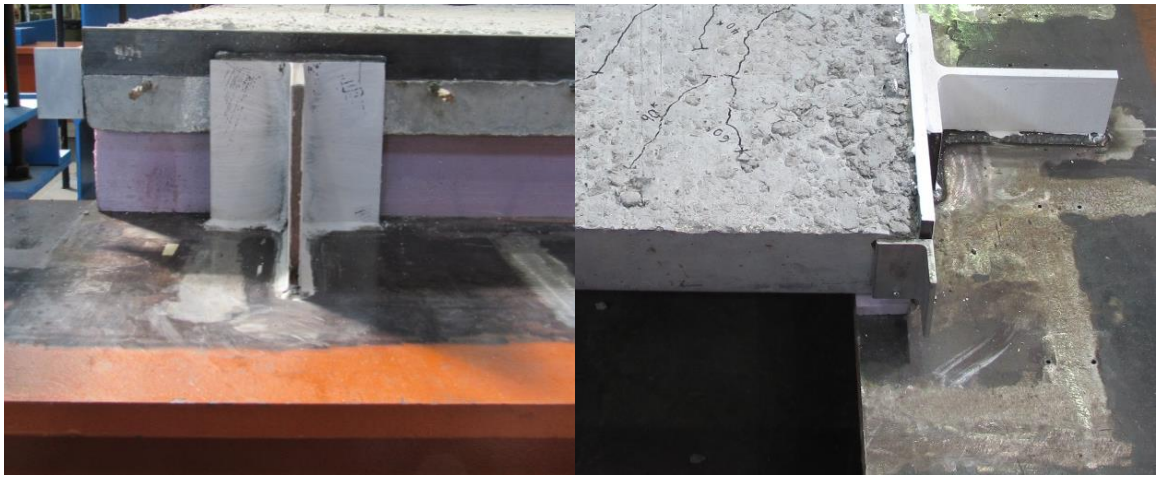

Figure 3.7: PCPs Resting on 4 Inch (left) and ½ inch (right) Polystyrene Bedding Strips

3.3.3 Embed Design Parameters and Geometry

Current TxDOT implementation of PCPs, which entails placing them on epoxied bedding strips as mentioned in Section 3.3.2, provides no significant in-plane shear resistance from the panels to the girders. Thus, a main goal of the experiment was to develop a connection with enough stiffness and strength to utilize the structural capabilities of the PCP. Several connections were developed for experimental testing: a shear stud

connection, an embedded angle connection, and an embed-WT welded connection. The shear stud and embedded angle methodologies are discussed by McCammon (2015). This thesis focuses on the welded WT connection method, and the geometries of the four configurations examined in experimental testing are outlined in the following paragraphs.

The embed-WT connection consisted of a 2 inch wide flat bar extending the full length of the PCP and resting directly above the prestressing strands. This bar was embedded in the concrete by a series of deformed bar anchors (D2Ls), which were stud-welded at a slight angle relative to the face of the flat bar so that they would extend to the welded wire fabric beneath the prestressing strands. The embeds were cast into the PCP at a local precasting facility, and were tied back to the formwork using rebar ties to prevent concrete from covering the outer face. A rolled WT shape welded to the embed and the girder top flange was used to connect the PCP to the girder. Elevation and plan views of the embed-WT connection can be seen in Figure 3.8 and Figure 3.9, respectively.

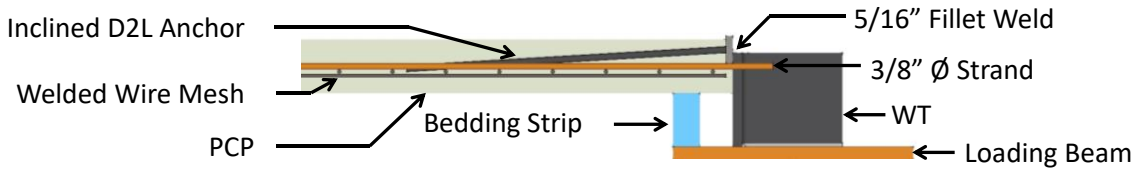

Figure 3.8: Elevation View of the Embed-WT Panel to Girder Connection

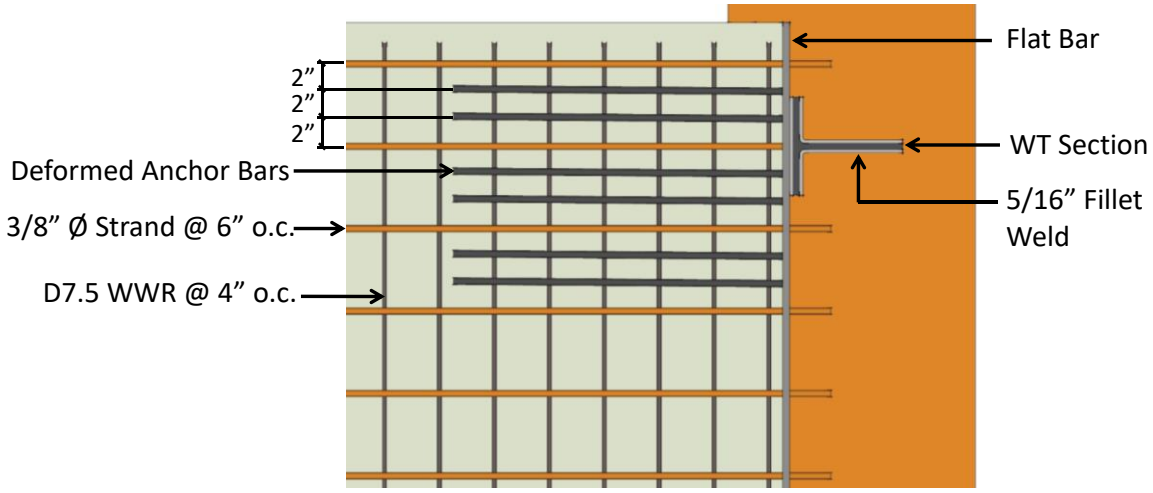

Figure 3.9: General Plan View of the Embed-WT PCP Connection Detail

Each panel configuration was designated with specific nomenclature, an example of which can be seen below in Figure 3.10. Eight total PCP tests were conducted, with four details considered at maximum and minimum bedding strip heights: A.1., B.1., C.2., and D.2. Several parameters were modified to investigate behavioral impacts: the embed thickness, the diameter and length of the deformed anchor bars, and the number of WT shapes in each corner of the PCP. The height of the WTs were also altered to account for the different bedding strip heights specified for testing in Section 3.3.2. Table 3.1 provides a summary of all details considered for experimental testing. Plan and elevation views of each PCP detail can be found in Appendix A.1.

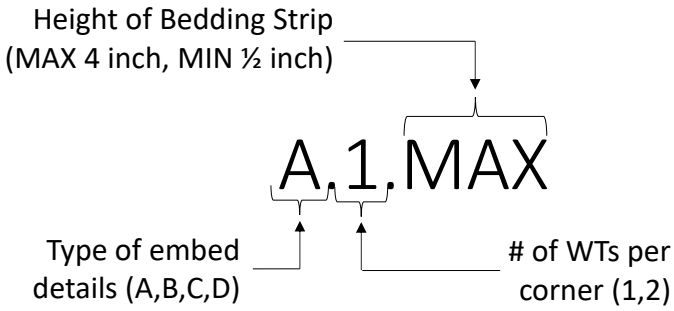

Figure 3.10: PCP Nomenclature Used for Experimental Documentation

Table 3.1: Summary of PCP Design Details Used in Experimental Procedure

Label	Anchors per Corner	Embed Size	WTs per Corner	Bedding Strip Height
A.1.MAX	(6) 1/2" Ø x 2'-0" Long	2"x1/2"	(1) WT8x28.5 x 7"	4"
A.1.MIN	(6) 1/2" Ø x 2'-0" Long	2"x1/2"	(1) WT8x28.5 x 3.5"	1/2"
B.1.MAX	(6) 5/8" Ø x 2'-6" Long	2"x5/8"	(1) WT8x28.5 x 7"	4"
B.1.MIN	(6) 5/8" Ø x 2'-6" Long	2"x5/8"	(1) WT8x28.5 x 3.5"	1/2"
C.2.MAX	(10) 1/2" Ø x 2'-0" Long	2"x5/8"	(2) WT8x28.5 x 7"	4"
C.2.MIN	(10) 1/2" Ø x 2'-0" Long	2"x5/8"	(2) WT8x28.5 x 3.5"	1/2"
D.2.MAX	(8) 5/8" Ø x 2'-6" Long	2"x3/4"	(2) WT8x28.5 x 7"	4"
D.2.MIN	(8) 5/8" Ø x 2'-6" Long	2"x3/4"	(2) WT8x28.5 x 3.5"	1/2"

Each panel was designed according to ACI 318-08 Appendix D and AISC code provisions. Design considerations from ACI included: the concrete breakout strength of the anchors in shear and tension (ACI D.6.2.1 and ACI D.5.2.1, respectively), the anchor shear reinforcement nominal capacity (ACI D.6.2.9), the rupture strength of the anchor in tension and shear (ACI D.5.1.2 and D.6.1, respectively), and the anchor tension reinforcement nominal capacity (ACI D.5.2.9). AISC Section J4.1 was used to design the strength of the embedded flat bar in tension, while Chapter 8 was utilized for weld strength calculations. Detailed calculations for PCP design can be found in Appendix A.2.

3.4 INSTRUMENTATION

In an effort to fully capture the behavior of the test specimen, several methods of instrumentation were utilized to monitor strains and displacements at key points of interest. Locations of these devices included the shear frame assembly, the PCP, the longitudinal surface of the PCP embed, and the WT connection between the PCP and the shear frame. Data from all instrumentation was continuously recorded using a data acquisition system.

3.4.1 Shear Frame Instrumentation

The load in the shear frame was continuously monitored during testing by a 100 kip capacity load cell connected in series between the hydraulic actuator and the frame. This load cell was calibrated prior to testing, and subsequently a calibration factor was applied to accurately measure the load being applied to the system.

Deflections experienced in the shear frame assembly were monitored using eight linear potentiometers, placed in line with the edge of the PCP. At each corner, one potentiometer was located on the outer edge of the 1 inch by 18 inch plate of the loading beam. The second apparatus was precisely placed ten inches below the first, thus measuring the twist experienced in the loading beams. Layout of the linear potentiometers in each corner can be seen in Figure 3.11.

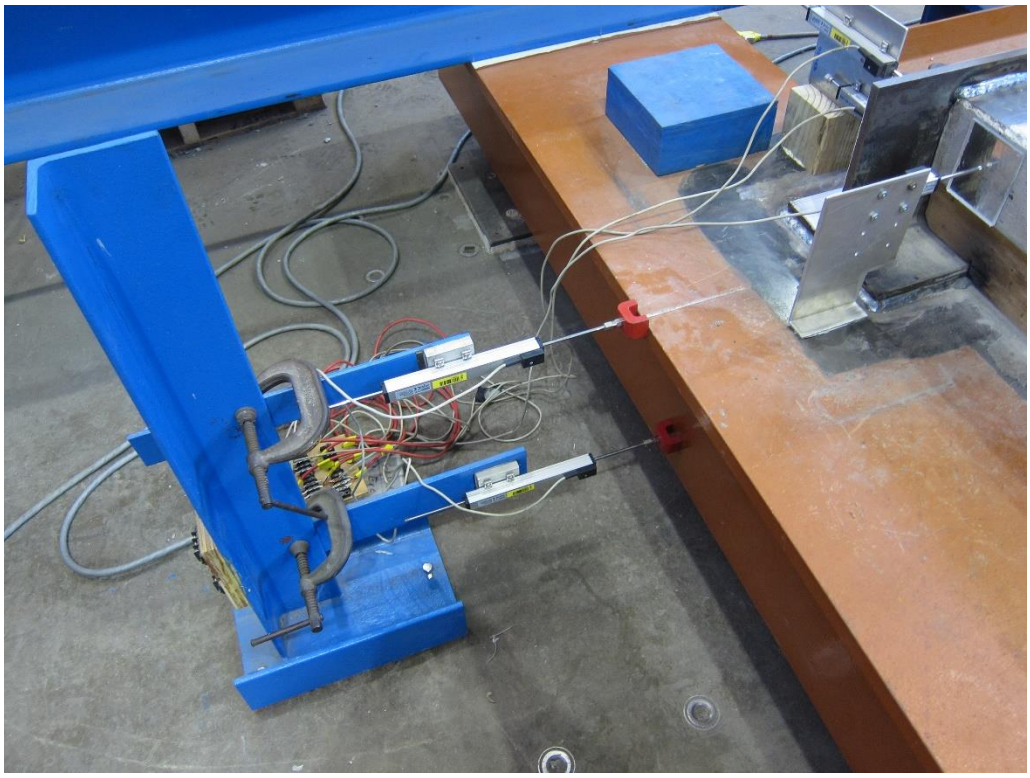

Figure 3.11: Linear Potentiometers Located at Each Corner of the Shear Frame

3.4.2 PCP and Connection Instrumentation

Due to the complex design of the PCP, each component had to be monitored individually to understand the overall behavior during testing. Linear potentiometers were placed on both faces of each corner, which allowed the two-dimensional measurement of lateral displacements of the panel relative to the shear frame. Figure 3.12 below shows the configuration of potentiometers used throughout experimental testing. To avoid friction from the concrete surface, aluminum angles were attached to provide a smooth contact surface. Additional potentiometers were located on the faces of the WT sections, with one on either side of the stem offset one inch from the edge of the flange. The WT shapes and embed corners were coated with a lime-water (whitewash) mixture so as to obtain an indication of inelastic deformation during testing, which can be seen in Figure 3.13. Three

strain gages were applied to the outward face of the embed plate at one foot on-center. This allowed a redundant method of measuring the force induced in the embed, as well as to ability to monitor its ability to transfer the panel forces.

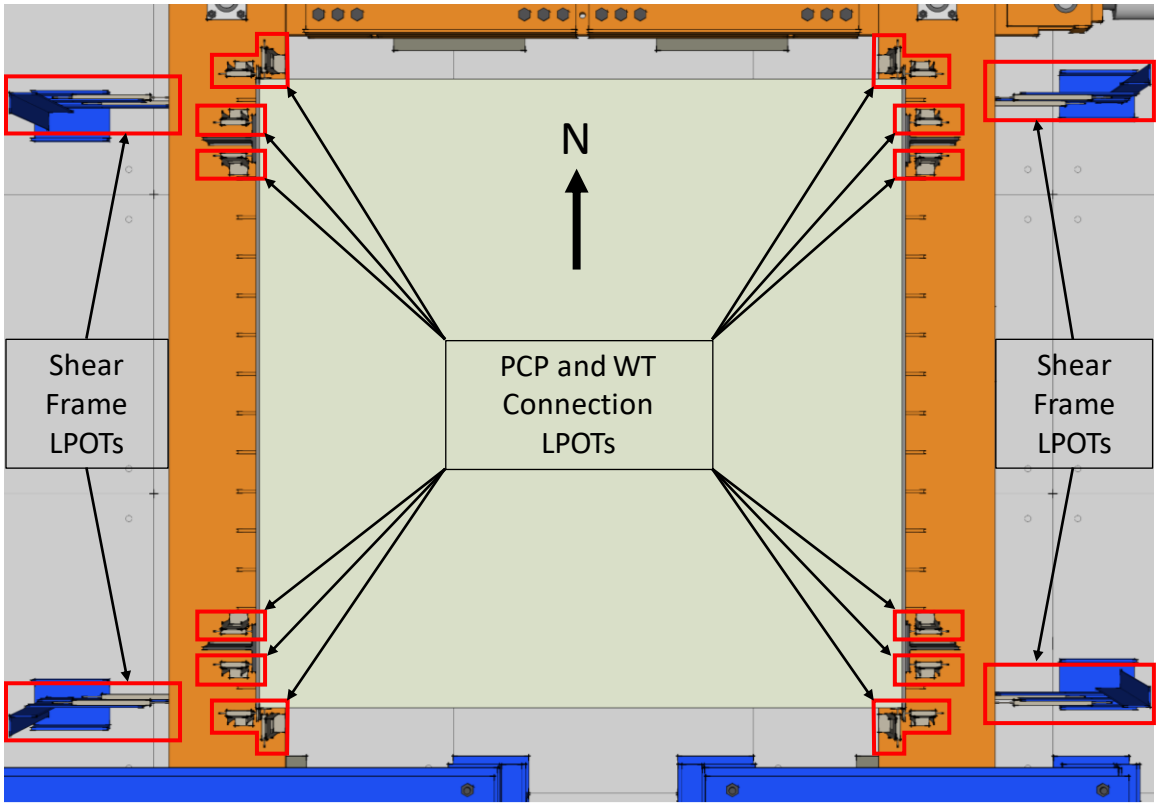

Figure 3.12: Plan View Layout of Linear Potentiometers, Shown as one WT per Corner

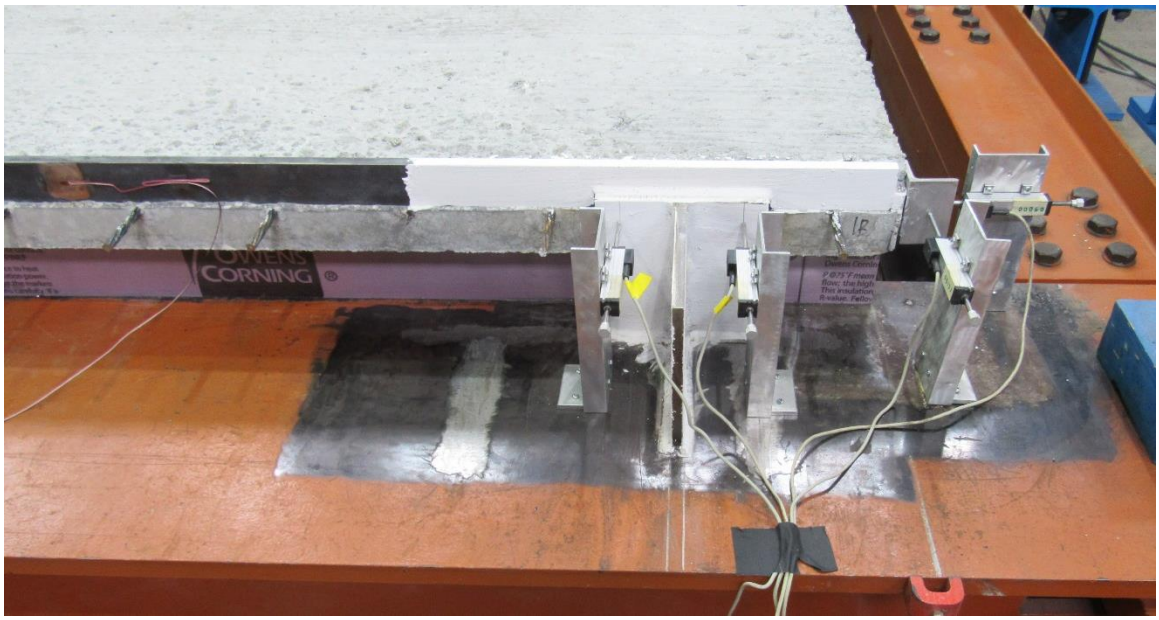

Figure 3.13: Configuration of Corner Potentiometers and Whitewash Application

3.5 TEST PROCEDURE

This section outlines the procedures followed for experimental tests involving the shear frame assembly. A frame friction test was developed to determine if the test setup performed as a pure mechanism, and the experimental method used to examine the in-plane shear properties of the PCPs is discussed in detail within this portion.

3.5.1 Shear Frame Friction Test

To ensure that the load applied to the shear frame was being resisted solely by the attached PCP, it was crucial that the amount of built-in resistance within the system be minimized. This was accomplished by the approach described in Section 3.2.1. Given that the frame was designed to act as a mechanism, a procedure was developed to determine the force required to displace the frame.

A beam clamp was affixed to the northwest corner of the shear frame, in line with the centerline of the actuator and the connection strap. The actuator was disconnected from

the system so as not to attribute to the resistance of the frame. A tension scale was attached to the beam clamp by way of a two foot lifting strap, and load was applied by hand until a shift in the frame was observed. The results of this test showed that less than 25 lbs of force were required to displace to frame, thus it could be reasonably assumed that the built-in resistance of the frame could be neglected.

3.5.2 Panel Shear Tests

Each panel discussed in Table 3.1 was subjected to an ultimate loading test to determine the shear capacity of the proposed PCP details. Prior to testing, the shear frame was squared at each corner and the swivel casters were aligned correctly to minimize unintended restraint. The panels were then connected to the loading beams at all corners and properly instrumented. An isometric view of the connected PCP before loading can be found below in Figure 3.14. Actuator load cell and linear potentiometer readings were tared, and each potentiometer was individually checked for measurement accuracy. The condition of each embed-WT connection and panel corner were visually inspected and photographed for documentation.

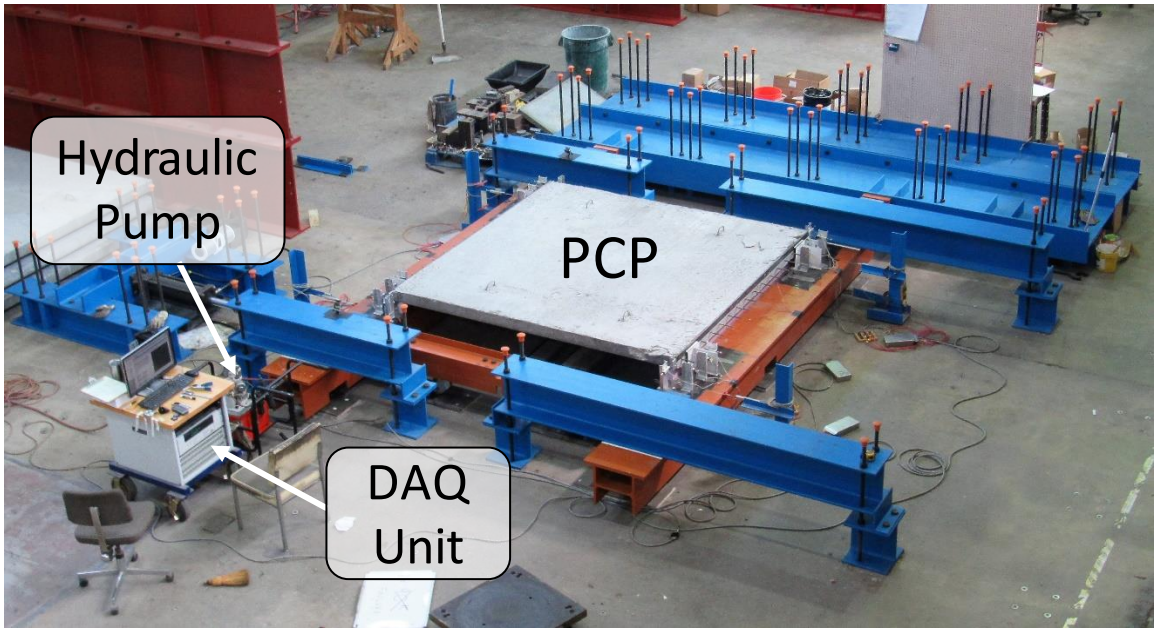

Figure 3.14: Isometric View of Connected PCP During Shear Testing

Load was then carefully applied through the actuator by a hydraulic pump, and was held at 10 kip increments to outline PCP cracking and inspect connections. This process was repeated until failure occurred in the specimen. At this point the mode of failure was observed and documented, all instrumentation was removed, and final photographs were taken. The frame was unloaded, the PCP was removed, and the assembly was re-squared for the subsequent panel test. Examination of the results from these tests are presented in Chapter 4.

CHAPTER 4: EXPERIMENTAL TEST RESULTS

4.1 OVERVIEW

This chapter provides a detailed synopsis of the results gathered from the PCP shear tests following the experimental procedure outlined in Chapter 3. The structural properties of the PCPs tested using the shear frame assembly are highlighted, including the shear stiffness and strength of the panels. Forces developed in the proposed embeds are examined, in addition to crack patterns and modes of failure induced by shear loading. Also discussed within this chapter is the behavior of the shear frame assembly during testing, as proper understanding of frame reaction is necessary for accurate interpretation of the test results.

4.2 PANEL MATERIAL PROPERTIES

All panels tested within the scope of this thesis were cast from the same concrete batch. Cylinders were cast on-site, transported back to the Ferguson Laboratory, and cured according to ASTM C31 standards. The curing period prior to cylinder strength testing was 35 days, at which time compressive strength, modulus of elasticity, and split cylinder tensile tests were performed. Compressive strength tests, modulus of elasticity tests, and split cylinder tests were completed in compliance with ASTM C39, ASTM 469, and ASTM 496, respectively. The results of these material tests are outlined in Table 4.1.

Table 4.1: Concrete Cylinder Strength Test Results for all PCP Specimens

Cure Period	**35 days**
f_c'	**8767 psi**
E	**5020 psi**
f_t	**630 psi**

4.3 SHEAR FRAME BEHAVIOR

The shear testing apparatus, fabricated as specified in Chapter 3, was designed to have relatively little deformation during the PCP tests. However, due to the large stiffness in the PCP diaphragm and connection, it is suspected that elastic deformations such as twist and in-plane bending may have occurred during the tests. Thus it was important to determine the behavior of the loading beams for each test so that meaningful results can be gathered from the tests. Section 3.4.1 outlined the deformation monitoring using two linear potentiometers (LPOTs) that provided a measure of the translation of two points on the test beam at each monitored location. The readings from the linear potentiometer include a combination of translation and twist of the beams. The two linear potentiometers were spaced at 10 inches vertically and placed at each corner of the PCP. As the load was applied, the shear force in the PCP resulted in resultant forces along the diagonal of the panel consisting of compression and tension struts leading to torsional effects of opposite signs along the length of the test frame beams. This can be seen in Figure 4.1 and Figure 4.2, which show the progression of twist at each corner as load is applied for the A.1.MAX and A.1.MIN panel tests, respectively. The nomenclature of the tests was discussed near the end of Chapter 3. The respective MAX and MIN designation refers to the use of the 4 inch thick and ½ inch thick bedding strips.

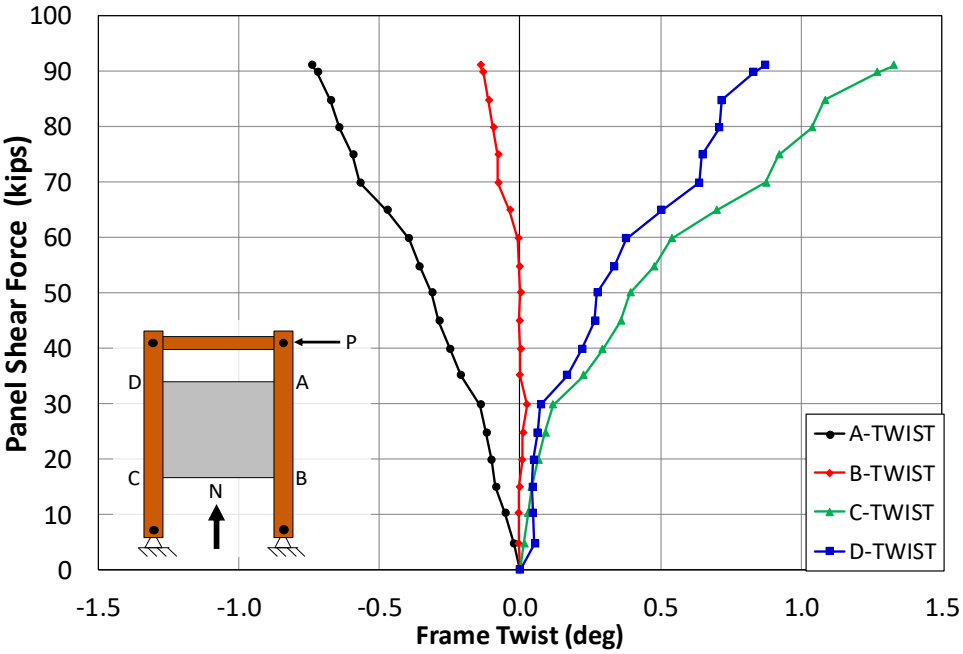

Figure 4.1: Twist Behavior of the Shear Frame for Panel Test A.1.MAX

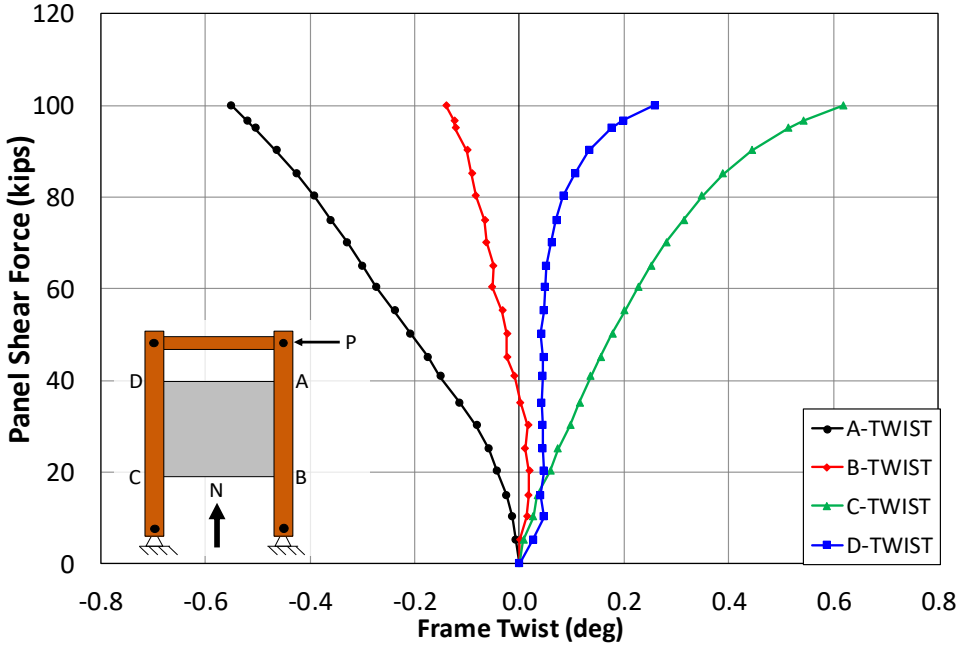

Figure 4.2: Twist Behavior of the Shear Frame for Panel Test A.1.MIN

As would be expected, the A.1.MAX detail resulted in higher rotational magnitudes than the A.1.MIN configuration. This was due to the reaction forces from the panel being applied at a greater eccentricity relative to the loading beam shear center, caused by the larger bedding strip height. Beam twist was also found to be greater in corners A and C relative to corners B and D. When load was applied through the actuator, a compression strut (A to C) and tension tie (B to D) formed in the panel. Rotation was observed at higher loads, where the tension-action created separation between the WT and the face of the PCP while compression-action caused the WT to bear against the panel face. The bearing action in the compression regions created a force couple, which in turn induced additional torque that contributed to a larger twist magnitude. Figure 4.3 provides a visual example of connection behavior in both tension and compression, while Figure 4.4 illustrates the force couple that develops when the WT bears against the panel.

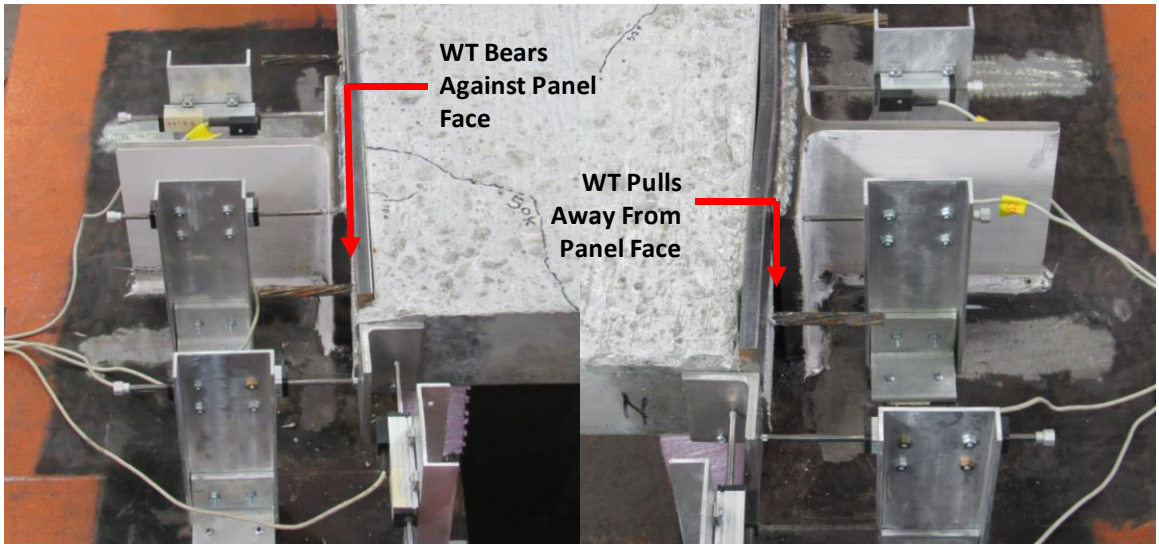

Figure 4.3: PCP to Girder Connection Behavior in Compression (left) and Tension (right) Regions

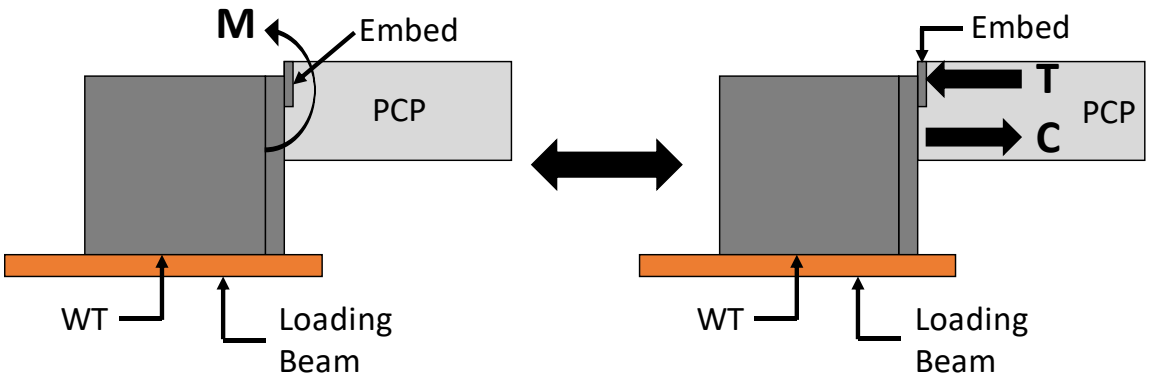

Figure 4.4: Force Couple Developed in the PCP for Compression Region Connections

Similar behavior was observed for connection details B.1, C.2, and D.2 at both the maximum and minimum bedding strip heights. Loading beam twist comparisons for these details can be found within Appendix A.3.1. To confirm that the rotation experienced did not have a substantial effect on the results, lateral displacement measurements were taken at top flange and 10 inches below then were interpolated to the shear center as shown in Figure 4.5.

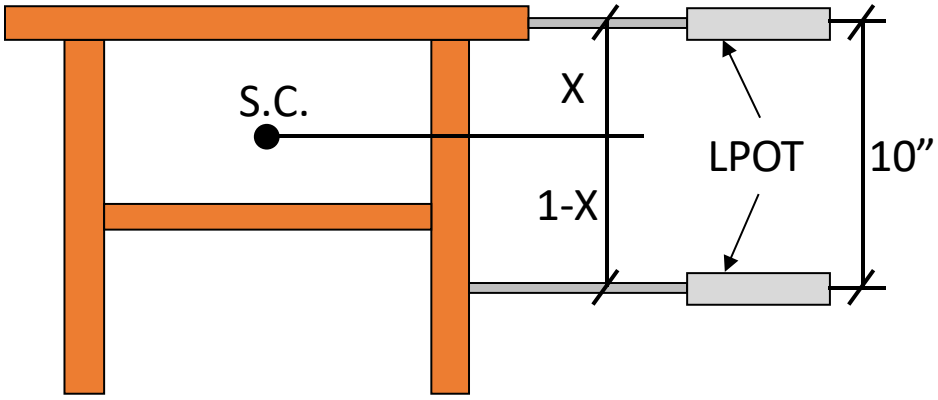

Figure 4.5: Interpolation of Shear Center Displacement and LPOT Configuration

In addition to torsion, in-plane bending of the loading beams also was considered when analyzing the behavior of the PCP diaphragm. Shear strain values were calculated within the width of the PCP where in-plane bending would be minimized in order to avoid underestimating the stiffness of the connected panels. A finite element model showing the in-plane bending and twist behavior of the shear frame with a PCP attached is shown in Figure 4.6. To understand the relative in-plane behavior between the two loading beams, lateral displacements at the beam shear centers were recorded at each panel corner. This allowed the direct comparison of lateral movement at similar points along each girder length. Figure 4.7 and Figure 4.8 show the shear center lateral displacement at each corner for the A.1.MAX and A.1.MIN shear tests, respectively.

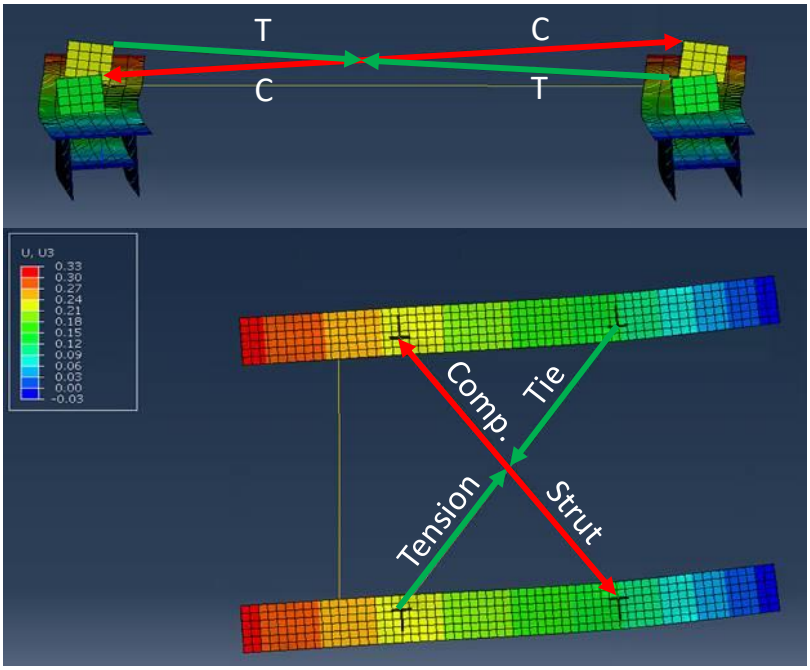

Figure 4.6: Elevation (top) and Plan (bottom) View of Abaqus Finite Element Model Showing Shear Frame Twist and In-Plane Bending

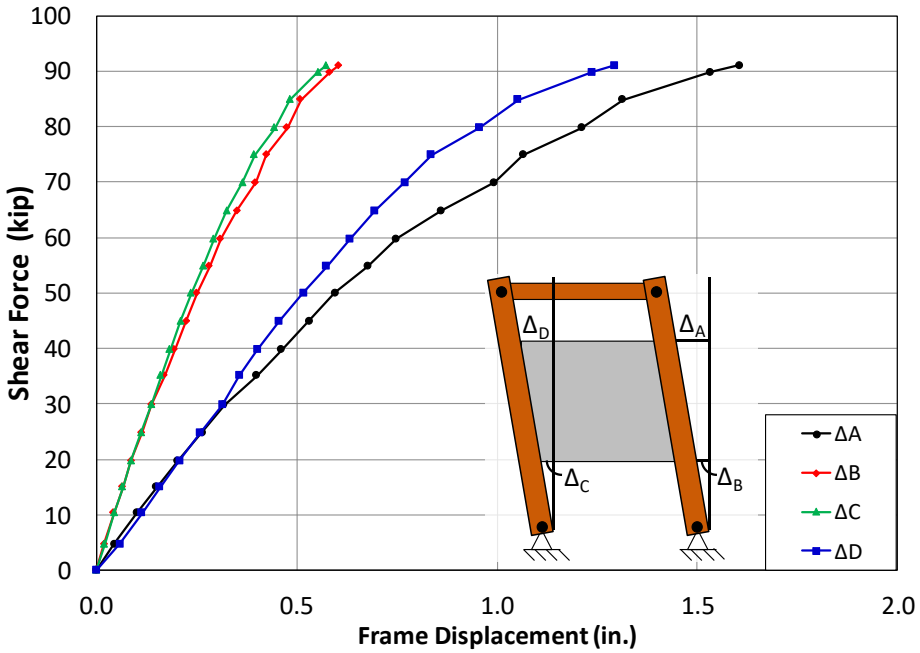

Figure 4.7: Loading Beam Shear Center Lateral Displacement for PCP Detail A.1.MAX

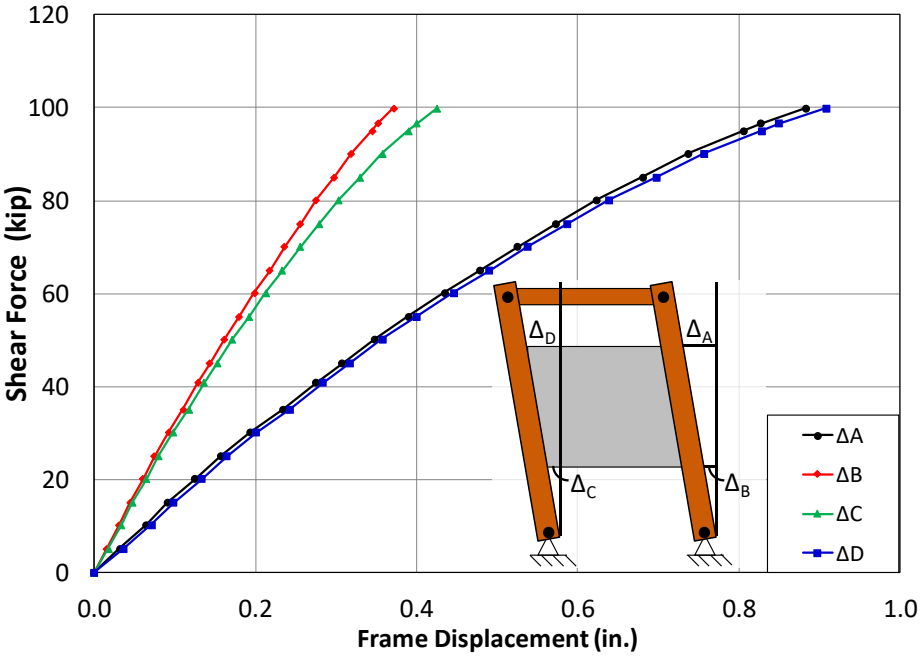

Figure 4.8: Loading Beam Shear Center Lateral Displacement for PCP Detail A.1.MIN

It can be seen from the data that the two beams displace approximately equal amounts for the ½ inch bedding strip detail, however there is a significant displacement differential between points A and D. A possible explanation for this discrepancy is that unequal in-plane bending effects were experienced in each loading beam, caused by the different reaction forces transferred from the connected PCP diaphragm. Experimental methods that can be used in future testing to better understand this behavior are discussed in Chapter 5.

4.4 PANEL ULTIMATE SHEAR STRENGTH

Each PCP was tested according to the procedure outlined in the previous chapter. As loading was applied to the panel, the shear strain and shear force were monitored continuously using a data acquisition system and localized measurement instruments. Data points were taken at 5 kip shear load increments, and each panel was loaded until failure occurred. The tests were conducted using both a 4 inch bedding strip and a ½ inch bedding strip, so that a bound envelope of results could be determined. As noted in Chapter 3, a total of four different anchor details were tested labeled A, B, C, and D. Therefore, 8 total tests were tested on the 4 different details with 2 different bedding strip heights. For the purpose of comparison, curves of the applied shear force versus the shear strain are shown together; however 4 separate graphs are made in which each specific anchor detail is highlighted with a more prominent line color, while the other 3 anchor details utilize a less prominent gray line. This can be understood by the reader by reviewing Figure 4.9 and Figure 4.10 which highlight the behavior of the panels connected to the shear frame using the A.1 and B.1 details, respectively, for both minimum and maximum bedding strip heights. In each plot, results from the other connection details are shown but are shaded for clarity.

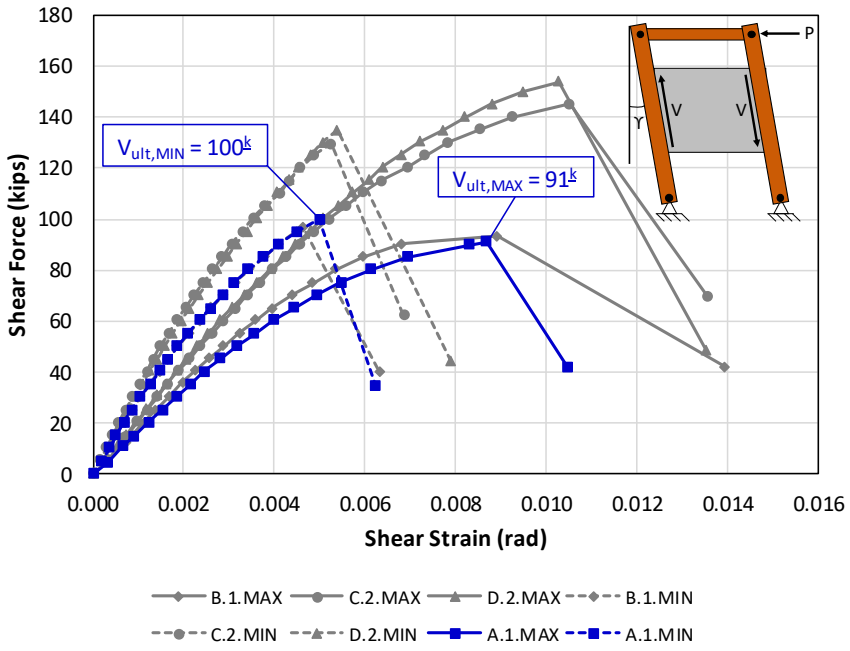

Figure 4.9: Shear Behavior up to Ultimate Load for PCP Detail A.1

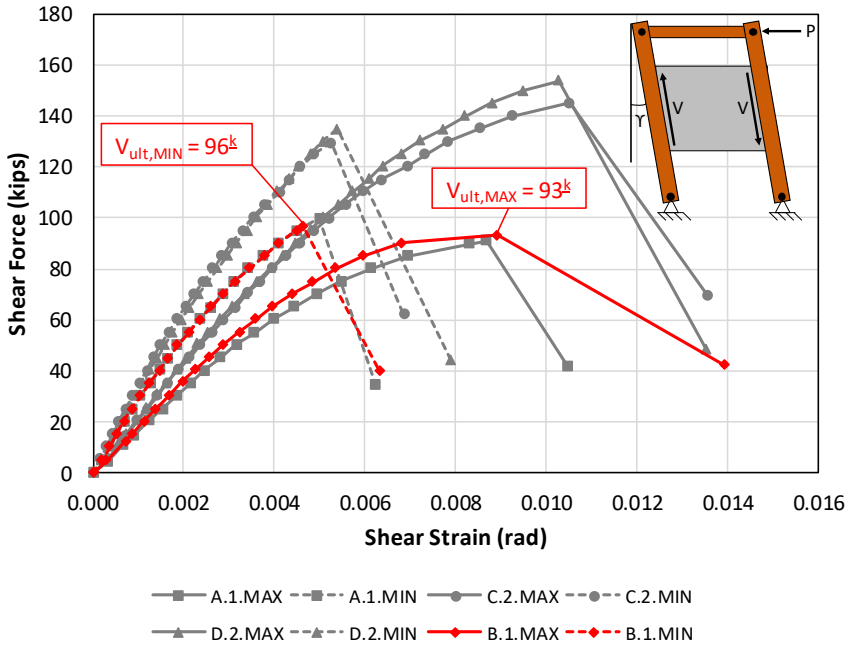

Figure 4.10: Shear Behavior up to Ultimate Load for PCP Detail B.1

As expected, the panels connected at a larger eccentricity (4 inch bedding strip) exhibited a more ductile response prior to failure than the corresponding panels with the smaller eccentricity (½ inch strip). A.1 and B.1 PCPs with maximum bedding strip heights (MAX) experienced a shear strain exceeding 0.008 radians before failure, while the same details placed using minimum bedding strip heights (MIN) failed at or before reaching 0.005 radians of shear strain. From the figures, it can be observed that there was not a significant increase in ultimate shear capacity, V_{ult}, as the bedding strip height was reduced. Details A.1.MAX and A.1.MIN failed at a shear of $91^{\underline{k}}$ and $100^{\underline{k}}$ of shear, respectively, a 9.4% difference. B.1.MAX and B.1.MIN failed at $93^{\underline{k}}$ and $96^{\underline{k}}$, respectively, or a 3.2% difference.

In comparison, panels designed with C.2 and D.2 connection details achieved significantly higher shear loads and strains prior to panel failure than their A.1 and B.2 counterparts. Figure 4.11 and Figure 4.12 show the behavior of the C.2 and D.2 panels during the ultimate load test, respectively.

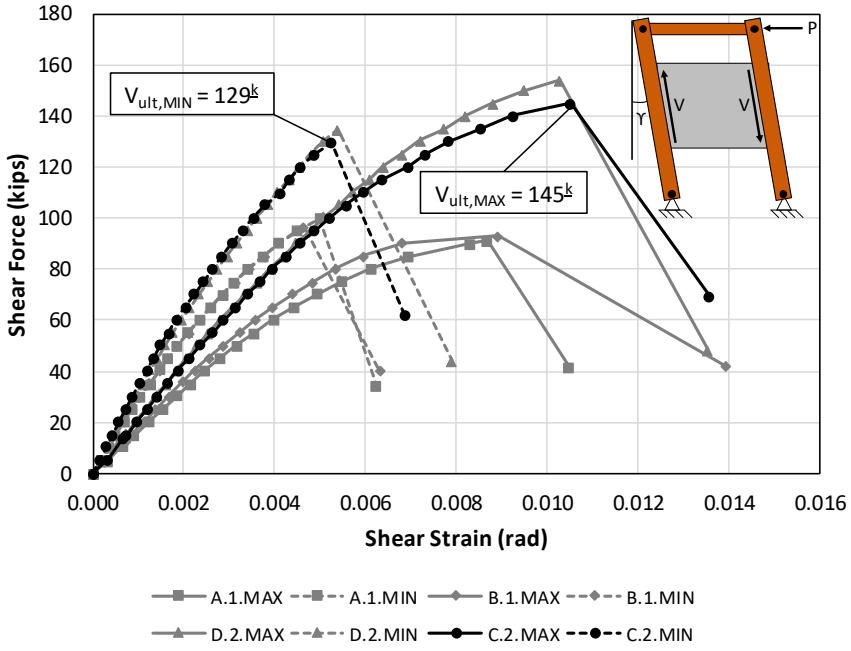

Figure 4.11: Shear Behavior up to Ultimate Load for PCP Detail C.2

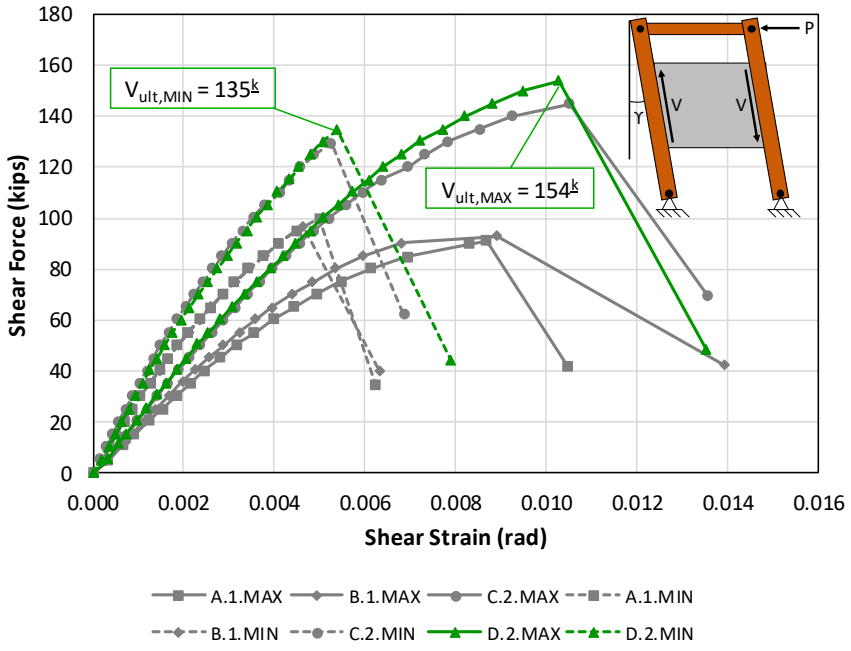

Figure 4.12: Shear Behavior up to Ultimate Load for PCP Detail D.2

For these panels, a more ductile response was again found when a 4 inch bedding strip height was used, with over 0.010 radians of shear strain experienced at failure compared to less than 0.006 radians for the ½ inch strip specimens. The shear load capacity was much greater for the C.2 and D.2 panels than their A.1 and B.1 counterparts, due to the more robust design of the embed connection. One particularly interesting observation to be made, however, is that the ultimate capacities remained relatively the same when the bedding strip height was reduced. This illustrated that the additional prying moment created from an increased connection eccentricity had little effect on the panel's ultimate capacity. The slight variation in ultimate strength between strip heights was most likely due to the high variability of concrete tensile properties. Despite this minor difference, all panels tested well exceeded the expected design strength. The results of the PCP in-plane shear tests when considering ultimate load are summarized below in Table 4.2, while calculations used in determining the expected shear capacity can be found in Appendix A.2.

Table 4.2: Ultimate Load Capacities for PCP Shear Tests

Connection Detail	**Strip Height (in.)**	**γ_{max} (rad x 10^{-3})**	**$V_{expected}$ (kips)**	**V_{max} (kips)**
A.1	4	8.69	24.3	91
	½	4.99		100
B.1	4	8.92	27.1	93
	½	4.64		96
C.2	4	10.52	40.0	145
	½	5.25		129
D.2	4	10.27	35.9	154
	½	5.39		135

4.5 PANEL SHEAR STIFFNESS

Perhaps equally as important as shear strength is the shear stiffness of the PCPs, as both strength and stiffness are required for an effective brace. In determining the stiffness of the PCP connected to the shear frame assembly, ultimate loading test data points were considered within the first 40% of the ultimate load. This stiffness value, denoted as V/γ and expressed in kips per radian, represents the elastic stiffness of the PCP before permanent deformations occur. In addition to specific stiffness values, parameters of interest included the effect of bedding strip height on system stiffness as well as the effect different connection details had on the overall stiffness performance. Figure 4.13 and Figure 4.14 show the stiffness behavior of the A.1 and C.2 details, respectively. Additional figures for PCP details B.1 and D.2 can be found in Appendix A.3.4.

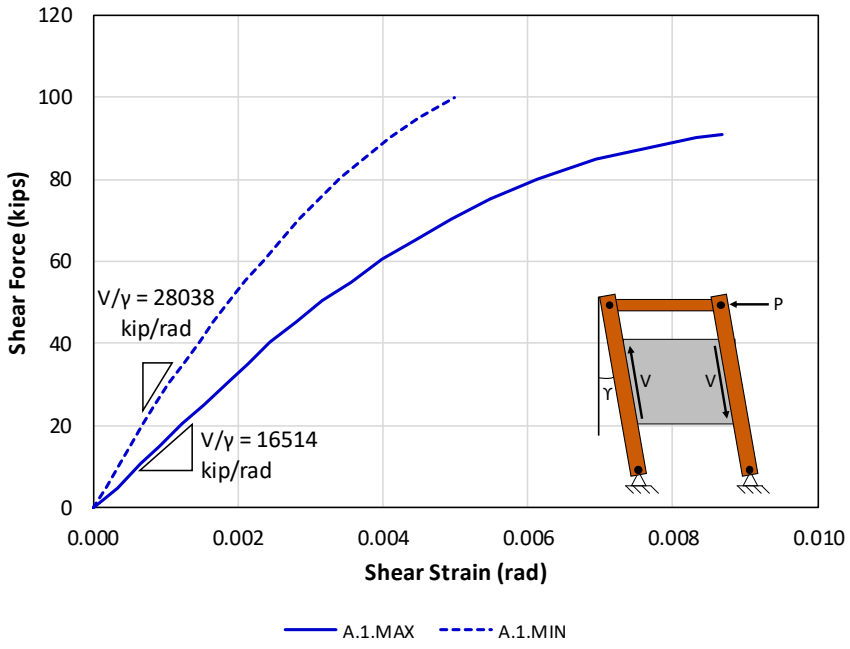

Figure 4.13: Shear Stiffness Behavior for PCP Detail A.1

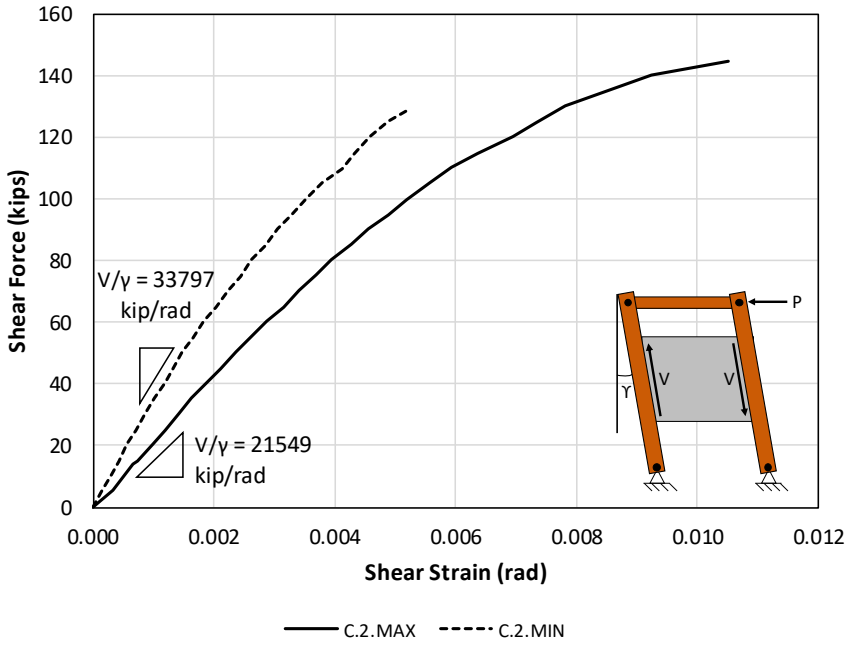

Figure 4.14: Shear Stiffness Behavior for PCP Detail C.2

It can be seen from the figures that the bedding strip height has a large influence on the stiffness of the system, with the minimum strip height resulting in a 70% increase for detail A.1 and a 57% increase for detail C.2 compared to the maximum height. The stiffness increase became slightly less pronounced when stronger connection details were used, as the increased connection stiffness counteracted the vertical eccentricity of the PCP relative to the loading beams. Overall, significant stiffness was achieved from the system when PCPs were attached and results from each tests are summarized below in Table 4.3

Table 4.3: Shear Stiffness Results for PCP Ultimate Load Tests

Connection Detail	Strip Height (in.)	γ_{max} (rad x10^{-3})	V_{max} (kips)	V/γ (kips/rad)
A.1	4	8.69	91	16,514
	½	4.99	100	28,038
B.1	4	8.92	93	18,341
	½	4.64	96	28,101
C.2	4	10.52	145	21,549
	½	5.25	129	33,797
D.2	4	10.27	154	22,047
	½	5.39	135	32,109

4.6 EMBED AXIAL BEHAVIOR

Another parameter that was measured during the PCP shear loading tests was the behavior of the embed flat bar in each panel. The flat bar extended the full length of the PCP specimen, with varying amounts of deformed anchor bars stud welded to each corner to provide sufficient bondage between the embed and the concrete panel. Specific details of each embed design are outlined in Section 3.3.3 of this thesis. To understand how load was being transferred through the embed detail, three strain gages were placed at a spacing of 1 foot on-center on the outer face of the embed. These strain readings were monitored continuously during testing, and an average strain was calculated at 5 kip shear load increments up to PCP failure. Figure 4.15 and Figure 4.16 show the average strain experienced in both the east and west embeds of PCP details A.1.MAX and B.1.MAX, respectively, as load was applied. A36 steel was used in the fabrication of the embeds, however since no coupon tests were conducted on the material the yield line depicted is an illustration of where yield would be expected for this material based upon the nominal strength values (36 ksi yield).

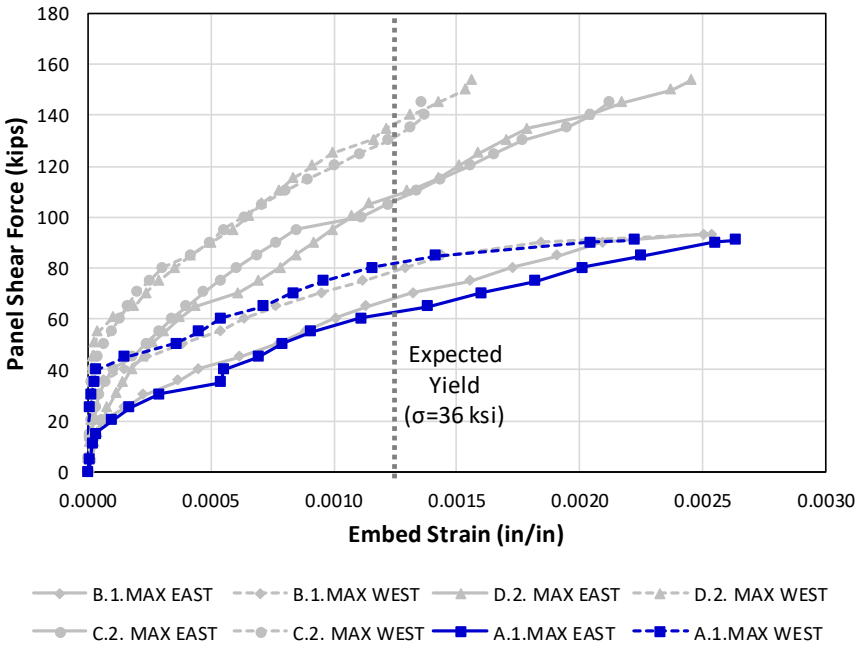

Figure 4.15: Axial Strain Measured in Relation to Panel Shear for PCP Detail A.1.MAX

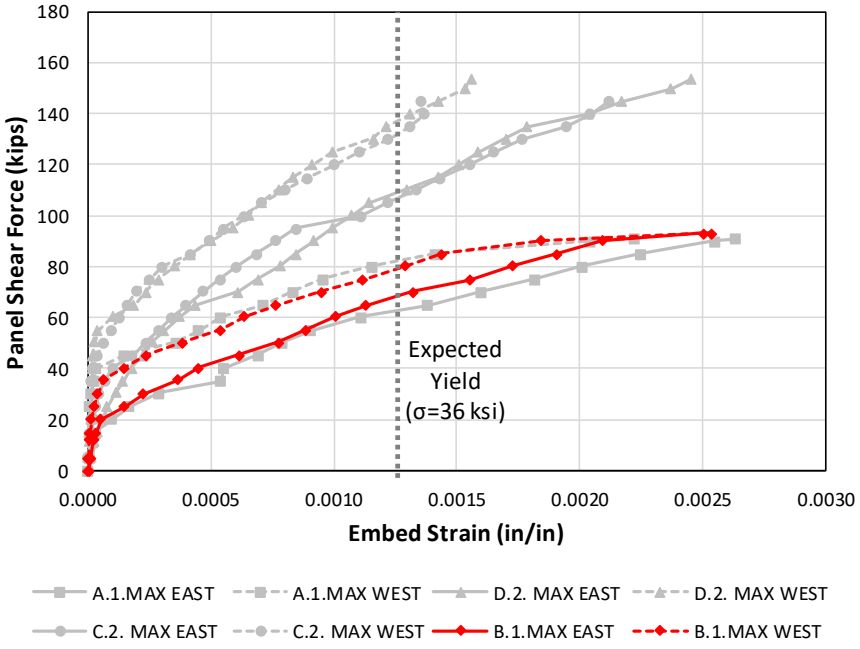

Figure 4.16: Axial Strain Measured in Relation to Panel Shear for PCP Detail B.1.MAX

It can be seen from the figures above that embed details A.1.MAX and B.1.MAX exhibit similar strain behavior as the load was increased in the PCP. Given that the flat bar thickness for detail B.1.MAX is ⅝ inch compared to ½ inch for detail A.1.MAX, the similar strain behavior shows that B.1.MAX attracts more load through the embed flat bar. Both details revealed a very ductile behavior prior to panel failure, achieving strains exceeding 0.0025 in/in. Detail A.1.MAX reached nominal yield strains at 62.5^{k} and 82^{k} of panel shear for the east and west embeds, respectively. For detail B.1.MAX, the nominal yield strains were reached at panel shears of 68^{k} and 78.5^{k} for the east and west embeds, respectively.

As was the case with comparing the A.1.MAX and B.1.MAX details, embed details C.2.MAX and D.2.MAX followed similar strain behavior as load was applied on the shear frame. Thus higher load was induced in the D.2.MAX embed, due to the increased ¾ inch thickness as opposed to the ⅝ inch C.2.MAX flat bar thickness. C.2.MAX and D.2.MAX experienced much higher panel shear loads prior to nominal yield strain than the A.1.MAX and B.1.MAX details previously discussed. Panel shear loads for C.2.MAX at the nominal yield strains of the east and west embeds were 106^{k} and 131^{k}, respectively, while D.2.MAX loads were measured as 108.5^{k} and 136.5^{k} for the east and west embeds. Decreased strain values seen in the figures at the maximum loads are due to these points being considered immediately prior to panel failure, where element failure may have caused load redistribution in the embed. Figure 4.17 and Figure 4.18 show the average strain in both embeds for PCP details C.2.MAX and D.2.MAX, respectively.

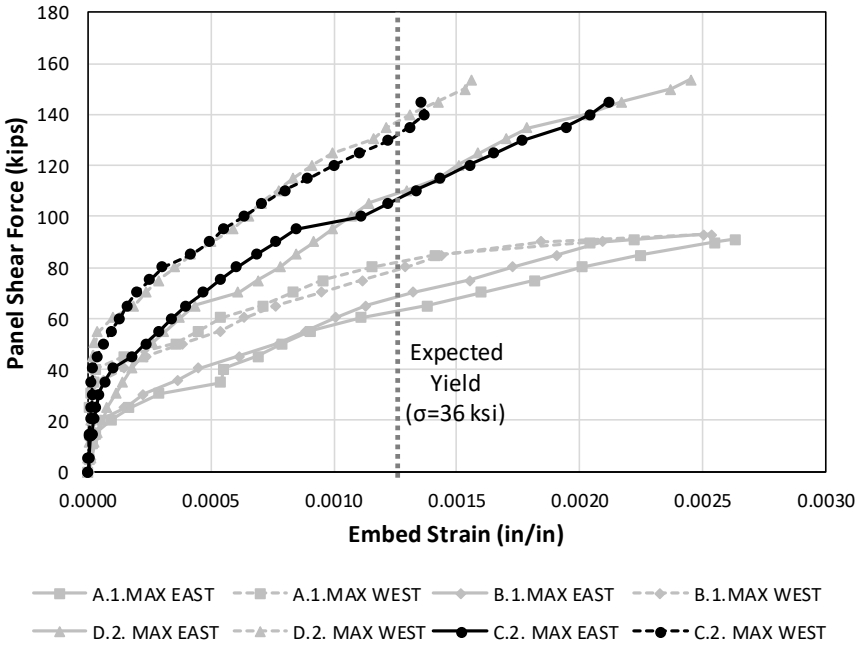

Figure 4.17: Axial Strain Measured in Relation to Panel Shear for PCP Detail C.2.MAX

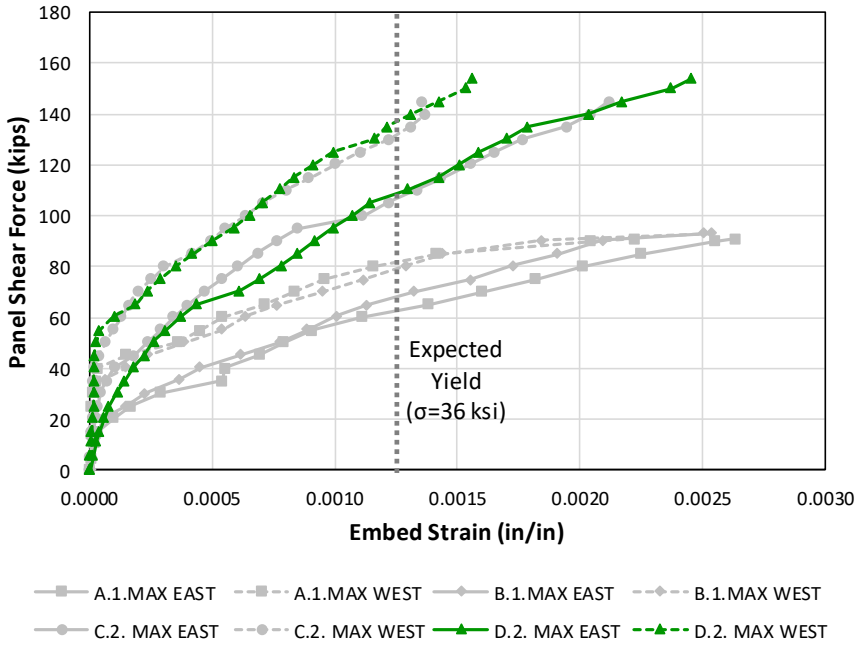

Figure 4.18: Axial Strain Measured in Relation to Panel Shear for PCP Detail D.2.MAX

Overall, it was found during the ultimate shear loading tests that the east embed experienced greater axial strain at the same panel shear load as the west embed. This could be due to unevenly distributed cracking between the west and east corners of the PCP specimens, which would have caused unequal redistribution of loads through the full-length embed. These effects could have been compounded by imbalanced bending and twist effects between the shear frame loading beams, as discussed in Section 4.3. Similar trends were observed in the minimum bedding strip height tests, although for these panels much smaller strains were obtained prior to PCP failure. For the ½-inch strip tests, the nominal yield strain was rarely achieved before panel failure. A comparison between PCP detail A.1 tested at 4 inch and ½ inch bedding strip heights is shown below in Figure 4.19. A summary of the embed behavior observed during this experiment is provided in Table 4.4. Results from all embed strain behavior comparisons is provided in Appendix A.3.5.

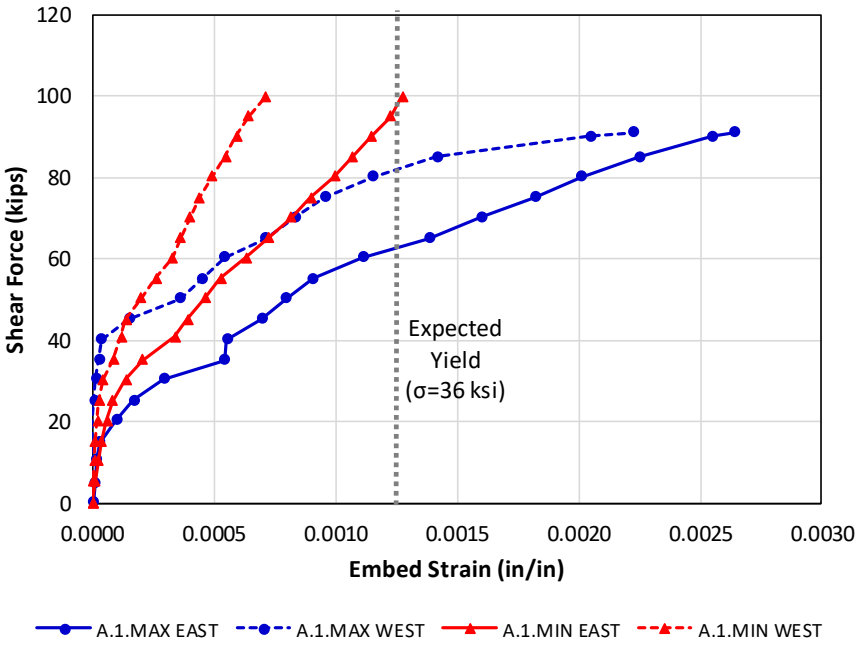

Figure 4.19: Axial Strain Comparison for PCP Details A.1.MAX and A.1.MIN

Table 4.4: Embed Strain Behavior for all PCP Connection Details

Connection Detail	Strip Height (in)	V_{max} (kips)	Embed	V_{panel} @ $(\sigma_y)_{exp}$ (kips)	ε_{max} (in/in x10^{-3})
A.1	4	91	East	62.5	2.64
			West	82	2.22
	½	100	East	97	1.27
			West	$>V_{max}$	0.71
B.1	4	93	East	68	2.51
			West	78.5	2.54
	½	96	East	$>V_{max}$	0.98
			West	$>V_{max}$	0.94
C.2	4	145	East	106	2.12
			West	131	1.36
	½	129	East	125	1.12
			West	$>V_{max}$	0.40
D.2	4	154	East	108.5	2.45
			West	136.5	1.56
	½	135	East	$>V_{max}$	1.16
			West	$>V_{max}$	0.41

4.7 PANEL CRACK BEHAVIOR AND CONNECTION YIELDING

Physical behavior of the PCP specimen was visually observed and documented throughout testing. To understand how the connected panels would behave when used as construction bracing on girder systems, the cracking behavior of the specimen when subjected to in-plane shear needed to be monitored. Cracks that developed were outlined directly on the specimen with a black marker at each load step. As the actuator applied load to the system, tensile and compressive forces were induced at approximately a 45 degree angle through the panel. A visual representation of this was shown previously in this chapter in Figure 4.6. This resulted in crack patterns forming perpendicular to the force resultants, and much more significant cracking in the tension regions of the PCP (corners

B and D). As expected, very little cracking was observed in the compression regions of the specimens (corners A and C). Figure 4.20 and Figure 4.21 show the cracking behavior for panels A.1.MAX and C.2.MAX immediately prior to failure. PCPs B.1.MAX and D.2.MAX exhibited very similar behavior to the figures included here, and crack patterns for these specimens are provided in the Appendix.

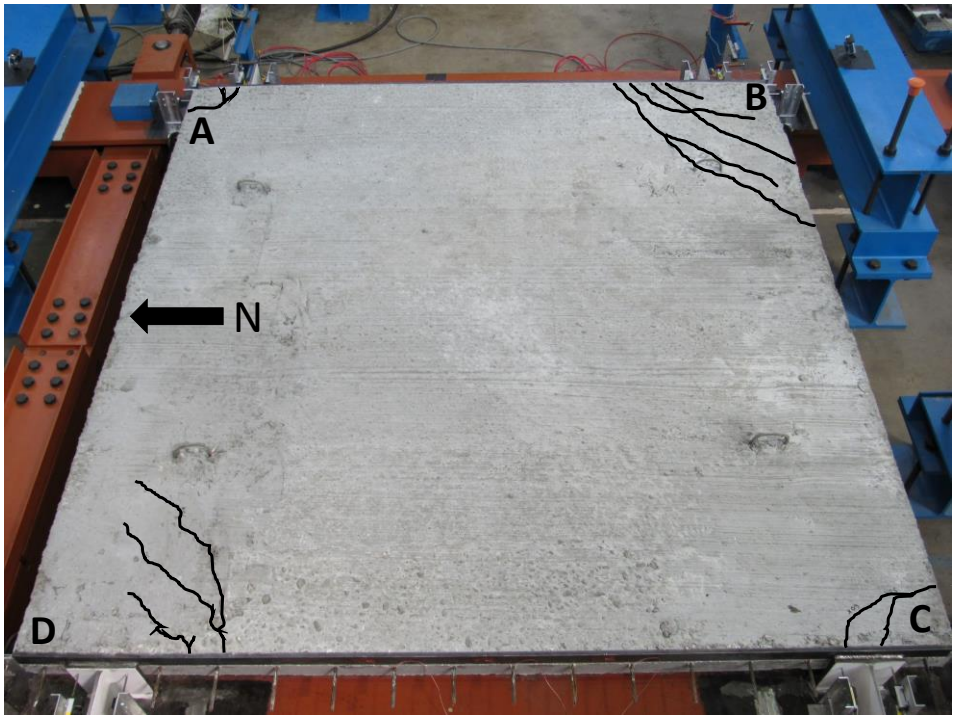

Figure 4.20: Cracking Behavior at Ultimate Load for PCP Detail A.1.MAX

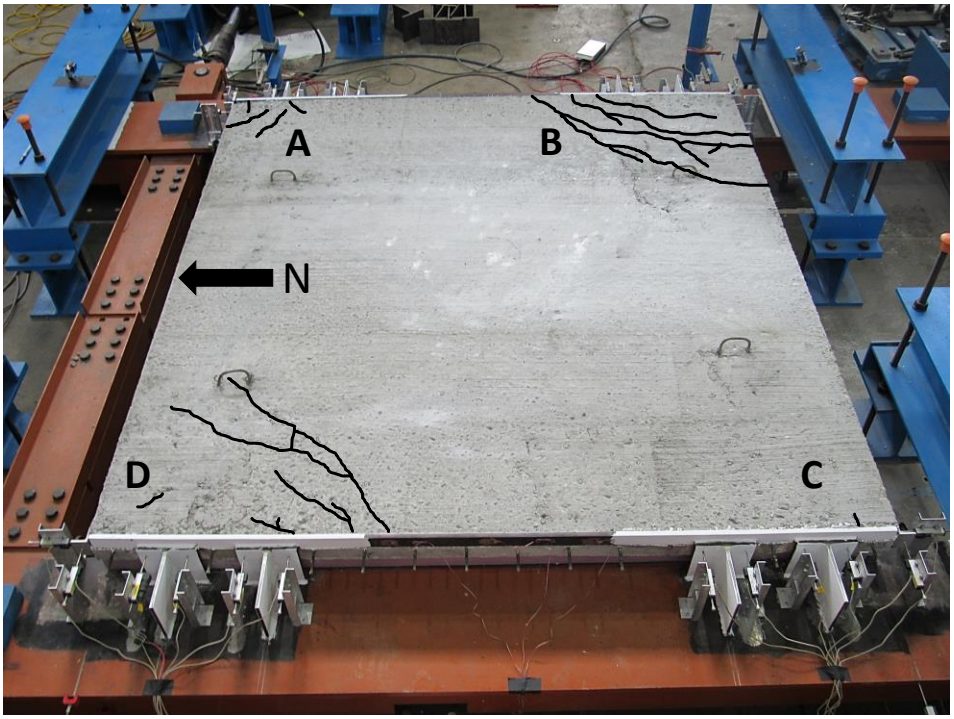

Figure 4.21: Cracking Behavior at Ultimate Load for PCP Detail C.2.MAX

The PCPs tested using a ½-inch bedding strip height behaved similarly to the maximum height panels. However, for the minimum strip details there was little-to-no cracking observed in the compression regions of each panel, and somewhat reduced cracking in the tension regions of the two-WT configurations. The absence of compression cracks was most likely due to the smaller bending moment effects from the WT bearing on the face of the panel within those regions, a concept that was discussed in Section 4.3. Given that the eccentricity (and thus the moment) was smaller for the minimum strip details, the tension component of the force couple was reduced resulting in less cracking behavior. A crack running the length of panel A.1.MIN occurred during the casting and shipping process, however this crack did not seem to impact overall panel behavior. The cracking patterns for details A.1.MIN and C.2.MIN are shown in in Figure 4.22 and Figure

4.23, while the corresponding patterns for details B.1.MIN and D.2.MIN are provided in the Appendix.

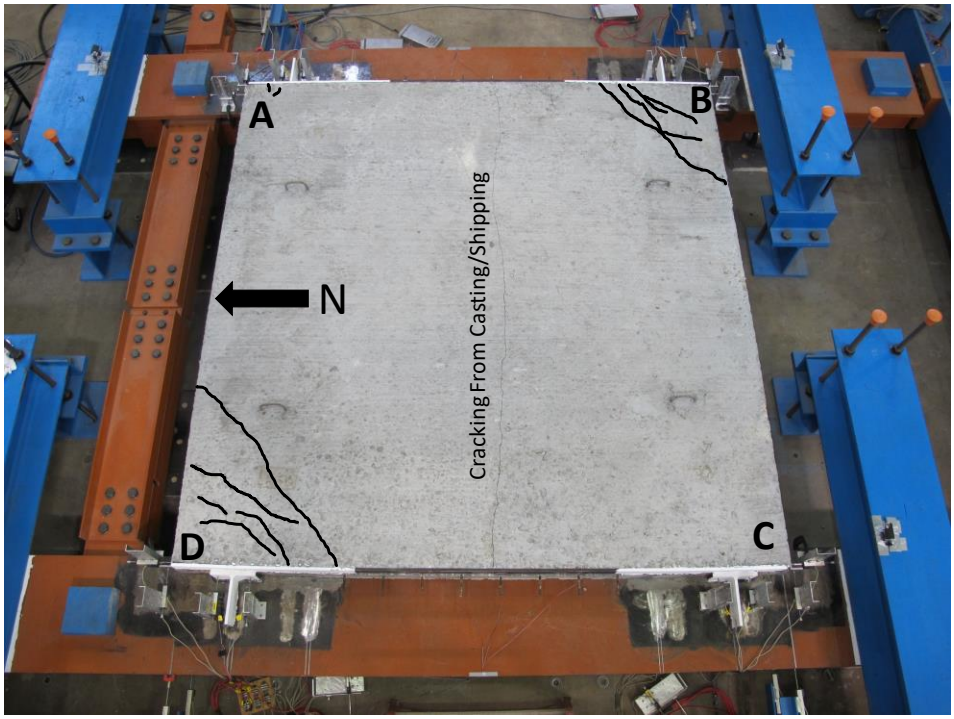

Figure 4.22: Cracking Behavior at Ultimate Load for PCP Detail A.1.MIN

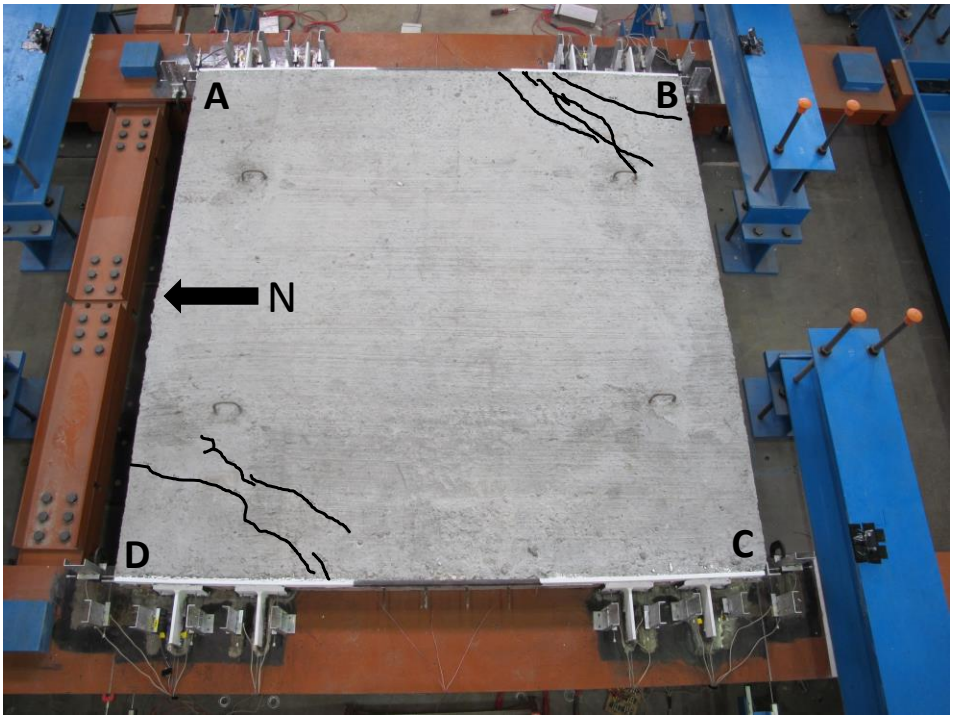

Figure 4.23: Cracking Behavior at Ultimate Load for PCP Detail C.2.MIN

The connection detail and bedding strip height also appeared to have an effect on the load at which cracking was first observed. The stronger connection details achieved a higher load before first visible cracking. Reducing the bedding strip height from 4 inches to ½ inches also correlated with an increased load before first visible cracking. This led to the ½ inch PCPs reaching a higher percentage of ultimate load before the panel began showing signs of distress. The load at which each PCP configuration showed signs of cracking is summarized in Table 4.5.

Table 4.5: Cracking Shear Load for Each PCP Detail

Connection Detail	Strip Height (in.)	Load Step Cracking Was First Observed (kips)
A.1.MAX	4	30
B.1.MAX	4	40
C.2.MAX	4	50
D.2.MAX	4	50
A.1.MIN	½	40
B.1.MIN	½	40
C.2.MIN	½	50
D.2.MIN	½	60

In addition to concrete cracking, yielding occurred in the WTs prior to PCP failure. Whitewashing techniques discussed in Chapter 3 allowed for visual inspection of yielding, as inelasticity caused the mill scale and corresponding whitewash to fleck off of the steel surface. Yielding was observed in all specimens, however it was more predominately present in connections utilizing the 4 inch bedding strip. Minimal yielding was experienced in the WTs at the ½ inch configuration. Figure 4.24 and Figure 4.25 show the yielding behavior of WTs used at the maximum and minimum bedding strip heights, respectively.

Figure 4.24: WT Yielding for PCP Details A.1.MAX (left) and D.2.MAX (right)

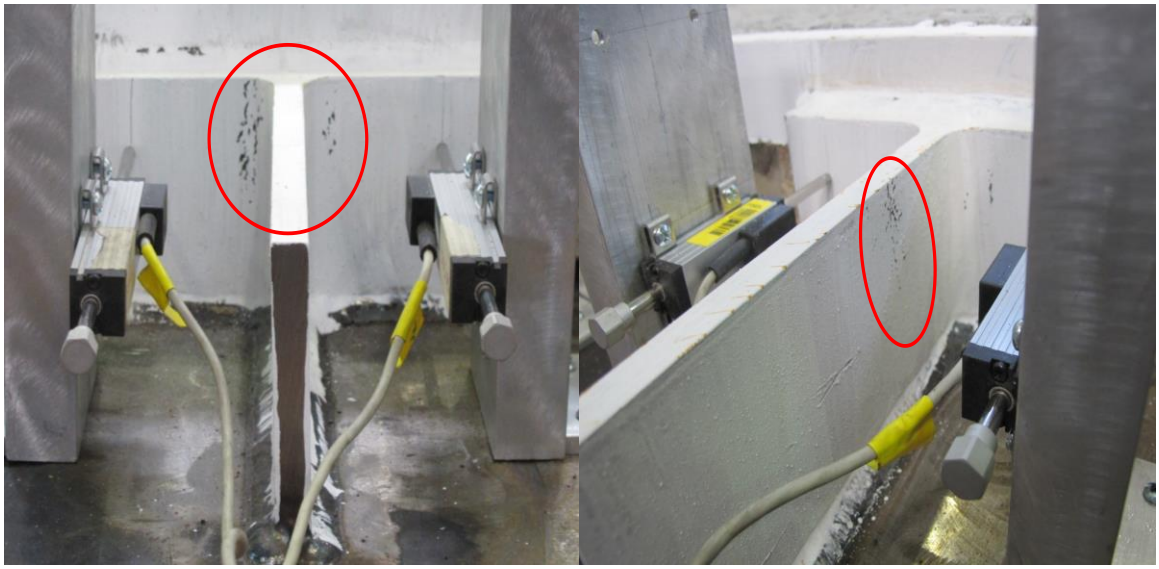

Figure 4.25: WT Yielding for PCP Details A.1.MIN (left) and D.2.MIN (right)

Overall, it was found that the PCPs exhibited several signs of distress prior to failure. Yielding at the base and within the k-region of the WT shapes was observed in all specimens. Significant cracking was also observed in each specimen prior to shear load failure. One other indication of the PCP nearing its capacity was a bulging, or debonding,

behavior between the embed and the concrete. In this scenario, the embed would display bowing away from the concrete panel, usually resulting in a visible gap between the embed and the concrete. This behavior would occur either at the center of the panel width or at the connection between the WT and the PCP. An example of this bulging behavior can be seen in Figure 4.26.

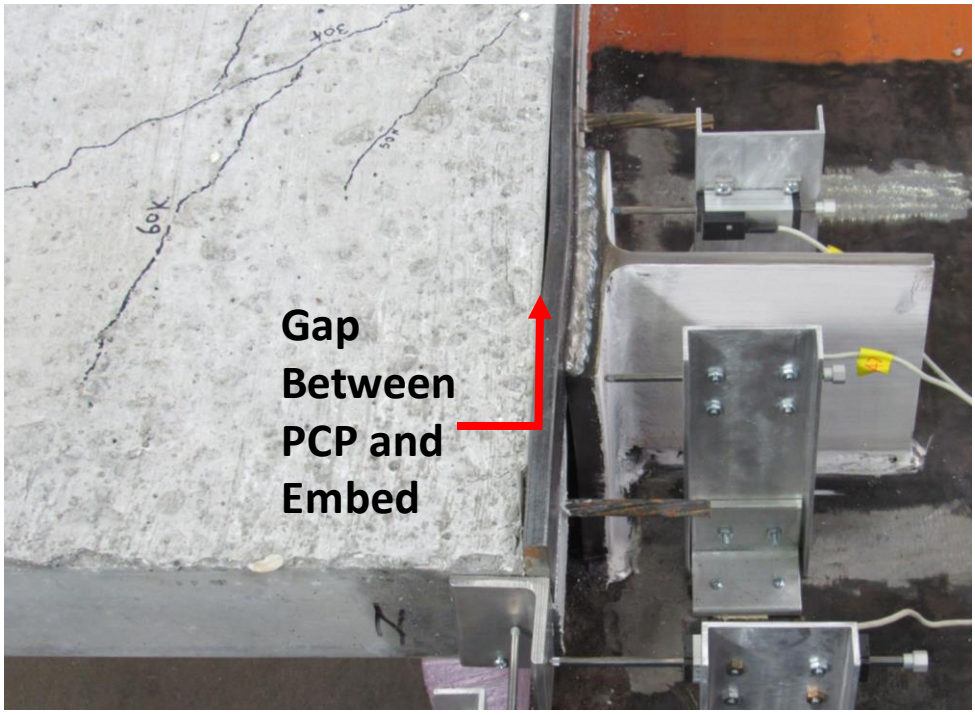

Figure 4.26: Bulging Behavior at WT-PCP Connection Near Failure Capacity

4.8 FAILURE MODES

Each PCP was loaded on the shear frame assembly until failure occurred. There were two primary causes of failure observed during the test procedure: concrete side face breakout and weld rupture. Concrete side face breakout as applicable to this experiment is a failure mode that consisted of major spalling of the outer face concrete as the shear load was applied through the embed/PCP connection. Although the deformed anchor bars were

designed to reside at the center of the panel thickness, the relatively thin geometry of the PCPs led to this failure mode controlling capacity in all specimens other than B.1.MAX. When the spalled concrete on the top face of the panel was removed, it was revealed that significant bending was experienced in the deformed anchors bars of the embed. An example of side face breakout failure experienced in the specimens is shown in Figure 4.27.

Figure 4.27: Concrete Side Face Breakout Failure and Corresponding Anchor Bar Bending shown for PCP Detail A.1.MAX

PCP connection detail B.1.MAX reached failure by means of a rupture in the weld connecting the WT flange to the loading beam. This rupture occurred in both WT sections on the west side of the shear frame, first taking place at the northwest corner then subsequently the southwest WT. Specimen B.1.MAX may have been susceptible to this type of failure due to a combination of factors. The embed was designed to a higher capacity than its A.1.MAX counterpart, thus it may have attracted a larger load with only one WT per corner to connect the PCP to the loading beam. The 4 inch bedding strip detail most likely also contributed to weld rupture due to the increased moment induced in the weld from a larger load eccentricity. Upon further inspection, it was also found that the

weld at the base of the WT was not wrapped around the corner to extend the full width of the flange, which made the weld more vulnerable to rupture by unzipping. The expected strength capacity of the welded connections was calculated to be slightly greater than that of the side face breakout failure mode, and was designed considering the elastic method. Thus, like the side face breakout provisions, it was found to be highly conservative. Detailed calculations for weld strength capacity can be found in Appendix A.2. The weld rupture failure mode observed in experimental testing is shown below in Figure 4.28.

Figure 4.28: WT to Loading Beam Weld Rupture at Northwest (left) and Southwest (right) Corners for PCP Detail B.1.MAX

This chapter provided a detailed overview of the PCP in-plane shear test results, including observations and interpretation of the data collected. A discussion of the holistic conclusions gathered from these experimental tests is provided in Chapter 5, as well as future work to be completed using the results of this study. Chapter 5 also provides insight into methods that can be used to better understand the behavior of the shear frame assembly should further tests be executed.

CHAPTER 5: CONCLUSIONS AND FUTURE RESEARCH

5.1 OVERVIEW

Horizontally curved bridge systems are often utilized to navigate restricted right-of-way situations or for highway flyovers due to the tight radius of curvature that are necessary. The large torsional demands on these systems can lead to significant bracing requirements to increase the stiffness and control lateral torsional buckling. Typical cross frame bracing can be expensive to fabricate and can result in fatigue concerns during the life of the bridge. Partial depth precast concrete deck panels, or PCPS, are frequently used on straight-girder systems but have not generally been used on horizontally curved girder systems by the Texas Department of Transportation (TxDOT). If properly engaged, the PCPs have the potential to provide significant bracing to the girders during construction.

The primary purpose of the research outlined in this thesis is to determine the capabilities of PCPs as shear-diaphragm bracing on straight and horizontally curved girder systems during the construction phase. Four different connection details for attaching the PCP to the girders were introduced and tested within this study, with consideration given to the effect of bedding strip height on PCP behavior.

5.2 SHEAR LOADING EXPERIMENTS

An investigation into the in-plane shear stiffness and strength of the connected diaphragm was conducted by means of full-scale ultimate shear capacity tests. These tests were carried out using a fabricated shear frame assembly, examining the behavior of each of the different PCP details discussed within this thesis. Results were presented on the

stiffness and strength behaviors of each PCP. Individual elements of the PCP system were also monitored throughout testing, such as panel cracking and embed behaviors.

5.2.1 Stiffness and Strength Behavior

All PCP connection details tested were found to provide substantial stiffness and strength as a shear-diaphragm brace. It was also observed that, as the design strength of individual connection elements was increased, the panels were able to achieve a higher overall shear capacity and stiffness. The connection parameters modified throughout testing were: the number of WT shapes per PCP corner, the embed flat bar thickness, and the number and thickness of deformed anchor bars cast into the concrete at each corner. Such design modifications could be incorporated as a method to accommodate systems with more substantial brace loads. However, further study must be conducted before recommendations can be made for bracing design. Additionally, it should be noted that bedding strip height had a significant impact on the PCP system stiffness, with a ½ inch PCP bedding strip providing at least a 46 percent increase in stiffness compared to when a 4 inch bedding strip was used.

5.2.2 Connection Detail Considerations

The design of the PCP connection detail had a direct impact on the behavior of the embed during shear loading. Connection details designed to withstand higher capacity experienced less axial strain in the embed prior to panel failure, indicating a less ductile overall response. Higher capacity connections also, as expected, reached higher shear loads before the nominal yielding stresses of A36 steel were exceeded. The bedding strip height also affected the strain in the embed. Panels connected at a 4 inch strip height all exceeded the nominal yield strain of the embed, while panels connected using the ½ inch strip height often did not reach nominal yield strain before panel failure.

Failure in all but one specimen was governed by shear anchor breakout from the side of the concrete, where shear parallel to the failure surface caused major spalling (in this case at the top face of the panel). Although it was the controlling failure mode, ultimate shear capacities calculated in the laboratory experiments were greater than 3 times the predicted capacity calculated using ACI 318. Thus, it was determined that the code is quite conservative in predicting this failure mode, which relies on the tensile properties of the concrete. One approach that could be utilized to increase the side-face breakout capacity of the PCP is to extend the deformed anchor bars across the entire panel width rather than simply in the corners. This would increase the concrete breakout area, thus increasing required shear for side face breakout.

The PCP specimen that did not succumb to concrete side face breakout failed by weld rupture at the base of the WTs on the west side of the panel. Further inspection of the failed connection revealed that the weld was only placed on the stem-side face of the WT for this test, thus leaving it vulnerable to rupture by unzipping. To inhibit this failure mode, it is important that the weld connecting the WT to the loading beam be wrapped around the corners at the outer faces of the WT flanges.

5.2.3 Additional Considerations

It should be noted that the experimental tests discussed within this thesis focus on the use of PCPs as a stability brace during the construction phase. Consideration was not given to the composite deck behavior in the completed bridge, although this could be the subject of future study. Specific cases with exceptionally high deck demands, such as instances where the demands require depths exceeding normal provisions, may also warrant additional consideration in future study.

5.3 FUTURE RESEARCH

Research is currently being conducted on the effectiveness of PCP shear diaphragm bracing on steel twin I-girder and steel tub girder systems. These girders are subjected to lateral load and gravity load buckling tests, which will be used to validate finite element models. Upon validation, these models will be used for parametric studies on a range of expected field applications to develop design recommendations for PCP stability bracing. The results from the panel tests outlined in this thesis will provide the strength of the panels for comparison of panel forces from parametric FEA studies.

One of the unknowns in the panel tests is the exact magnitude of the torsional and lateral deformations that occurred during the tests. The researchers were not aware of these deformations until comparisons were made with stiffness measurements from the twin I-girder and tub girder tests. Assumptions were made in Chapter 4 about the twist of the girders relative to the theoretical shear center of the beams in the test frame. To fully understand the extent of bending and twist of the loading beams along the frame length, it is recommended that an additional shear test be carried out using a steel X-brace of known stiffness. The members of this proposed brace could consist of square HSS tubes, using knife plate connections to keep the member forces concentric and attaching to the loading beams at designated heights of interest by means of removable bolted plates. It is recommended to add increased instrumentation in these tests, including: strain gages on the diagonal members, vertically stacked LPOTs (similar to those used at the panel corners in this thesis) at multiple points along the loading beam length, and vision system targets on both loading beams to monitor local and global displacements in real time. This data will provide a better indication of how frame bending and twist effects may influence the PCP behavior observed within the scope of this thesis. An isometric model view of the proposed shear frame test setup can be seen in Figure 5.1.

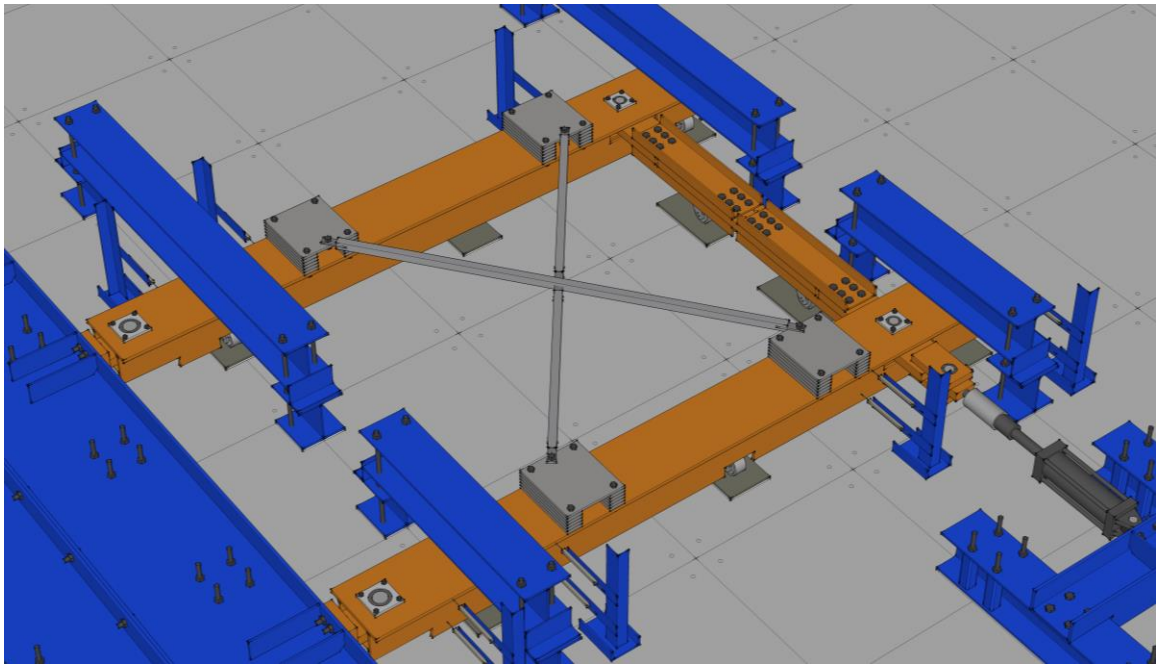

Figure 5.1: Isometric View of HSS X-Brace Model for Shear Frame Behavioral Tests

Further experiments are also to be completed using the shear frame assembly in an effort to optimize the PCP closure pour for curved post-tensioned concrete U-beams. Although these girders have been considered as alternate proposals in the state of Texas, they have not been selected for design due to constructability concerns such as extensive closure pour reinforcement requirements. These tests will examine the structural behavior of the current detail, as well as develop alternative connections that improve the feasibility of these systems.

APPENDIX A

A.1 PCP CONNECTION DETAIL GEOMETRIES

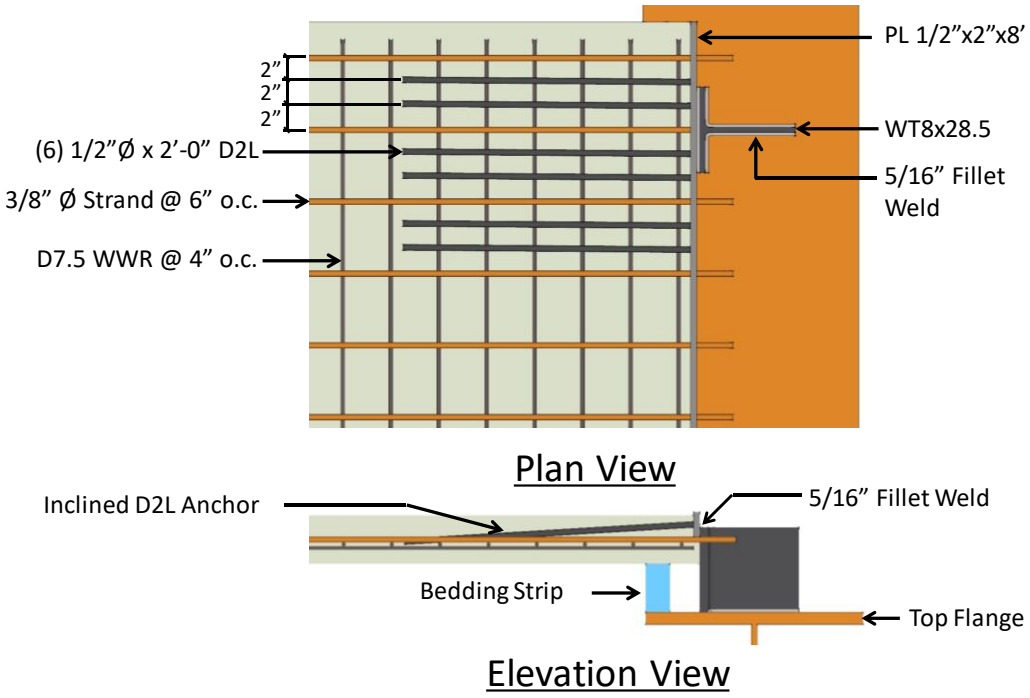

Figure A.1: Plan and Elevation Views of Embed-WT PCP Connection Detail A.1

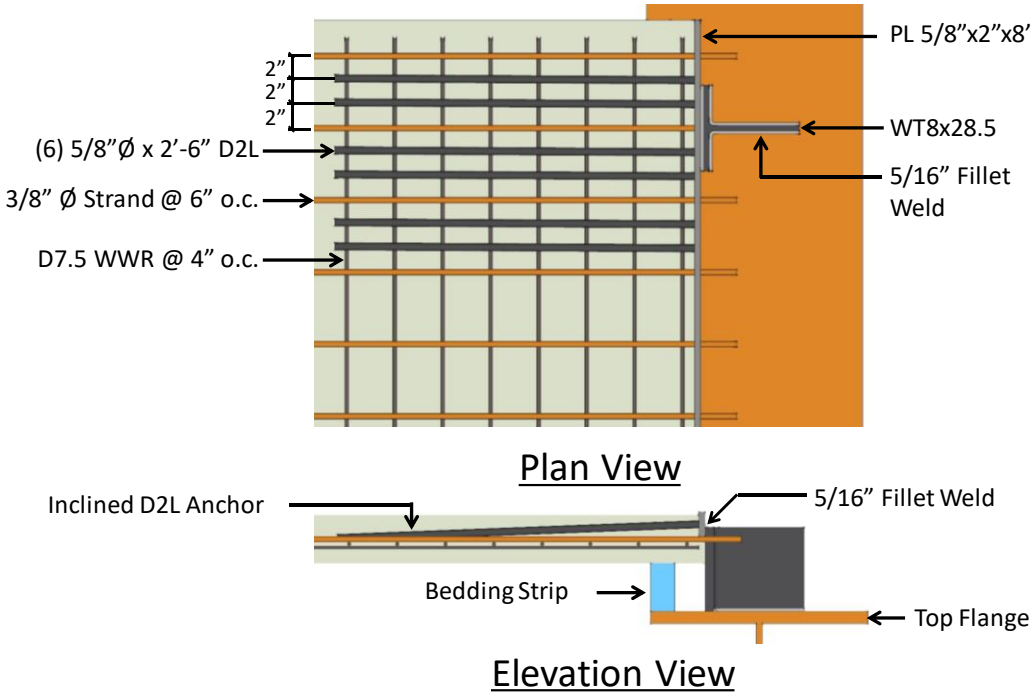

Figure A.2: Plan and Elevation Views of Embed-WT PCP Connection Detail B.1

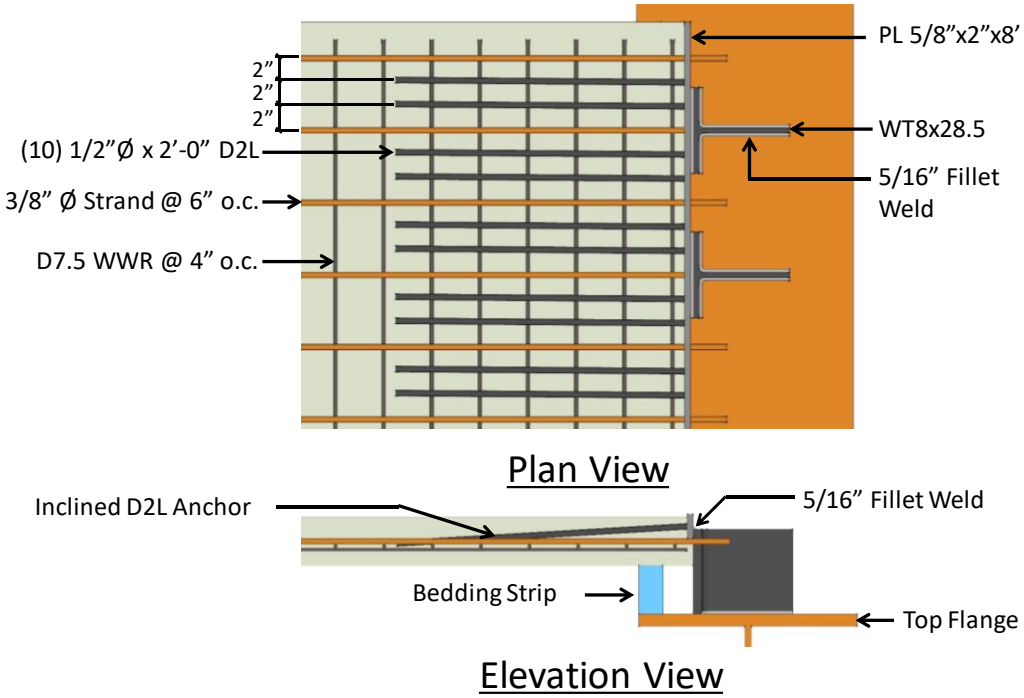

Figure A.3 Plan and Elevation Views of Embed-WT PCP Connection Detail C.2

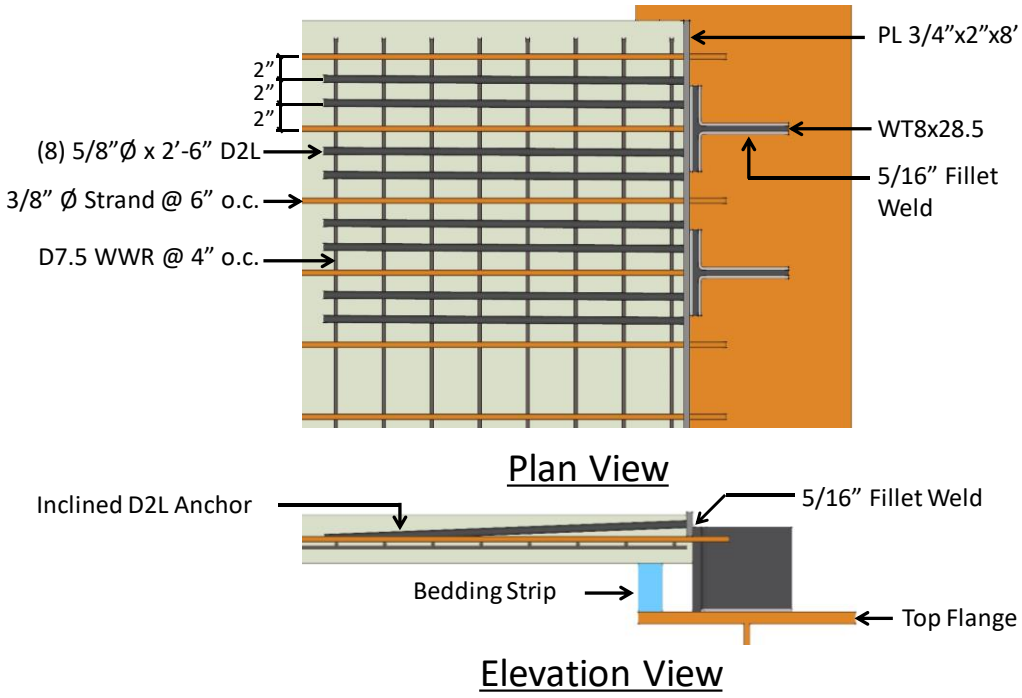

Figure A.4: Plan and Elevation Views of Embed-WT PCP Connection Detail D.2

A.2 PCP Design Capacity Calculations

A.2.1 Panel Reaction Figures

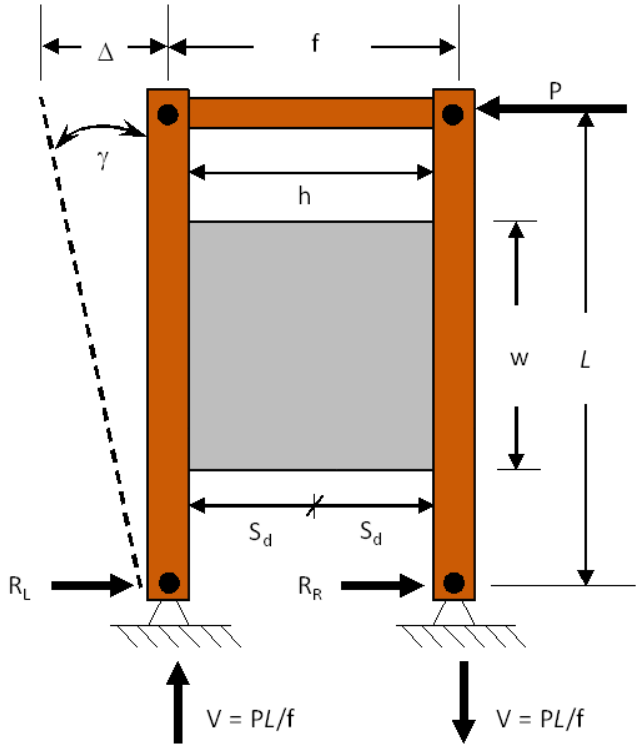

Figure A.5: PCP Geometry Parameters

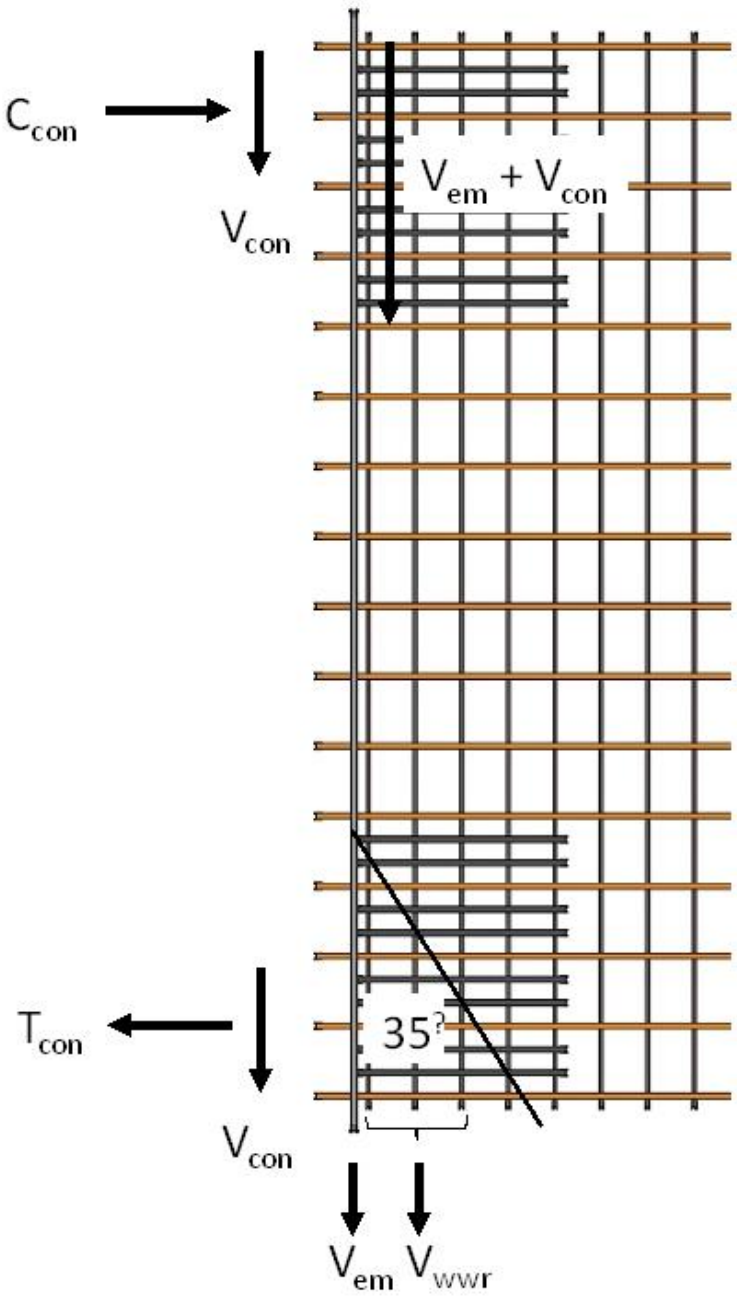

Figure A.6: PCP Embed Connection Reactions

A.2.2 PCP Detail A.1 Capacity Calculations

A.2.2.1 Detail A.1 Panel Capacity

PCP REINFORCEMENT

PCP Information

Shear Frame: **Geometry**

$P_{ram} := 36kip$ (Load in Actuator) $w := 78in$ (Connection Spacing)

$L := 150in$ (Loading Beam Length) $h := 99in$ (PCP Span Length)

$f := 110in$ (Loading Beam Spacing)

Embeds Members: **2"x1/2" Plates**

$F_{y\_em} := 36ksi$ (Embed Yield) $d_{em} := 2in$ (Embed Depth)

$F_{u\_em} := 50ksi$ (Embed Fracture) $t_{em} := 0.5in$ (Embed Thickness)

$A_{em} := d_{em} \cdot t_{em} = 1.0 \cdot in^2$

Concrete Anchors: **1/2" Diameter D2L**

$d_{d2l} := 0.5in$ (Anchor Diameter) $N_{d2l\_T} := 4$ (Tension Anchors per Corner)

$f_{uta\_d2l} := 61ksi$ (Anchor Tensile Strengt $N_{d2l\_V} := 6$ (Shear Anchors per Corner)

Concrete Anchor Tension Reinforcement: **3/8" Diameter Prestressing Strands**

$d_{ps} := 0.375in$ (Strand Diameter) $A_{ps} := 0.085in^2$ (Strand Area)

$f_{ps} := 270ksi$ (Strand Strength) $N_{ps} := 3$ (Number of Strands)

Concrete Anchor Shear Reinforcement: **D7.5 WWR**

$d_{wwr} := 0.3055in$ (WWR Diameter) $A_{wwr} := 0.0733in^2$ (WWR Area)

$f_{y\_wwr} := 60ksi$ (WWR Yield) $N_{wwr} := 2$ (Number of WWR)

Phi & Omega Safety Factors

$\phi_1 := 0.75$ $\phi_2 := 0.90$ $\phi_3 := 1$ $\phi_4 := 0.65$

Shear Frame and PCP Dimensions

$V_{pcp} := \frac{P_{ram} \cdot L}{f} = 49.1 \cdot kip$ $T_{con} := \frac{P_{ram} \cdot L \cdot h}{2f \cdot w} = 31.2 \cdot kip$

$M_{pcp} := V_{pcp} \cdot h = 405.0 \cdot kip \cdot ft$ $V_{con} := \frac{P_{ram} \cdot L}{2f} = 24.5 \cdot kip$

$V_{em} := \frac{A_{em}}{A_{em} + A_{wwr}} \cdot V_{con} = 22.9 \cdot kip$ $V_{wwr} := \frac{A_{wwr}}{A_{em} + A_{wwr}} \cdot V_{con} = 1.7 \cdot kip$

Strength of Embeds and Anchors

Embed Tension Yield (AISC J4.1)

$V_1 := F_{y\_em} \cdot A_{em} \cdot \phi_2$

$V_1 = 32.4 \cdot kip$

Anchor Shear Reinforcement Instead of Concrete Breakout (ACI D.6.2.9)

$V_2 := N_{wwr} \cdot A_{wwr} \cdot f_{y\_wwr} \cdot \phi_1$

$V_2 = 6.6 \cdot kip$

D2L Anchor Tension Rupture (ACI D.5.1)

$A_{d21} := \pi \cdot (0.5 \cdot d_{d21})^2 = 0.20 \cdot in^2$

$T_1 := N_{d21\_T} \cdot f_{uta\_d21} \cdot A_{d21} \cdot \phi_1$

$T_1 = 35.9 \cdot kip$

Anchor Tension Reinforcement Instead of Concrete Breakout (ACI D.5.2.9)

$T_2 := N_{ps} \cdot A_{ps} \cdot f_{ps} \cdot \phi_1$

$T_2 = 51.6 \cdot kip$

D2L Anchor Shear Rupture (ACI D.6.1)

$V_3 := N_{d21\_V} \cdot f_{uta\_d21} \cdot A_{d21} \cdot \phi_4$

$V_3 = 46.7 \cdot kip$

Concrete Side Face Anchor Shear Breakout (ACI D.6.2)

$c_{a1} := 1.5in$ $\phi_{ed\_V} := 1$ $\phi_{c\_V} := 1.0$ $c_{a2} := 14in + 2 \cdot 1.5 \cdot c_{a1} = 18.5 \cdot in$ $l_e := 8 \cdot d_{d21} = 4.0 \cdot in$

$\phi_{ec\_V} := 1.0$ $\phi_p := 2.0$ $\phi_{h\_V} := 1.0$ $f_c := 8767 \cdot psi^2$

$A_{vc} := c_{a2} \cdot 1.5 \cdot c_{a1} = 41.6 \cdot in^2$

$A_{vco} := 4.5 \cdot (c_{a1})^2 = 10.1 \cdot in^2$

$V_b := \left[8 \cdot \left(\frac{l_e}{d_{d21}} \right)^{0.2} \cdot \sqrt{d_{d21}} \right] \cdot 1 \cdot \sqrt{f_c} \cdot (c_{a1})^{1.5} = 1.5 \cdot kip$

$V_{cbg} := \frac{A_{vc}}{A_{vco}} \cdot \phi_{ec\_V} \cdot \phi_{ed\_V} \cdot \phi_{c\_V} \cdot \phi_{h\_V} \cdot V_b \cdot \phi_p = 12.1 \cdot kip$ (Shear Capacity per Corner)

$2 \cdot V_{cbg} = 24.3 \cdot kip$ (Shear Capacity per Embed)

Unity Check

$\frac{T_{con}}{T_1} = 0.867$ $\frac{T_{con}}{T_2} = 0.603$ $\frac{V_{em}}{V_1} = 0.706$ $\frac{V_{wwr}}{V_2} = 0.25$ $\frac{V_{em} + V_{con}}{V_3} = 1.02$ $\frac{T_{con}}{T_1} + \frac{V_{wwr}}{V_3} = 0.90$

A.2.2.2 Detail A.1 Weld Capacity

Frame Load, Frame Geometry, and Connection Geometry			Loads at Corners of Connections			Weld Strength		
P =	17.8	kip	T_{con} =	15.4	kip	ΦR_n =	5.6	kip/in
V =	24.3	kip	V_{con} =	12.1	kip			
L =	150	in						
f =	110	in	**Fillet Weld and Base Metal Parameters**			**Base Metal Check**		
w =	78	in						
h =	99	in						
b_f =	7.64	in	D =	4	Size	t_{f_min} =	0.19	in
t_f =	0.81	in	F_{exx} =	70.0	ksi	t_{w_min} =	0.38	in
d =	9	in	Φ =	0.75				
t_w =	0.495	in	F_y =	50.0	ksi	Unity = 0.23		
h_w =	3	in	F_u =	65.0	ksi	Unity = 0.77		
h_{bs} =	4	in						

WT to PCP Connection in the Plane of the Faying Surface			WT to Girder Connection in the Plane of the Faying Surface				WT to Girder Connection in the Plane of the Faying Surface			
L =	7.64	in	L =	23.525	in					
I_x =	0.00	in^4/in	$\bar{y}$ =	2.85	in					
I_y =	37.16	in^4/in	I_x =	174.98	in^4/in					
I_p =	37.16	in^4/in	I_y =	38.17	in^4/in					
e =	3.50	in	I_p =	213.15	in^4/in					
c_x =	3.82	in	e =	2.85	in					
c_y =	0.00	in	c_x =	3.82	in	CG to A	c_x =	0.25	in	CG to B
			c_y =	2.85	in	CG to A	c_y =	5.34	in	CG to B
R_{px} =	1.59	kip/in								
R_{py} =	0.00	kip/in	R_{px} =	0.52	kip/in		R_{px} =	0.52	kip/in	
R_{mx} =	0.00	kip/in	R_{py} =	0.65	kip/in		R_{py} =	0.65	kip/in	
R_{my} =	4.37	kip/in	R_{mx} =	0.46	kip/in		R_{mx} =	0.87	kip/in	
			R_{my} =	0.62	kip/in		R_{my} =	0.04	kip/in	
R_{xy} =	4.65	kip/in								
			R_{xy} =	1.61	kip/in		R_{xy} =	1.55	kip/in	

WT to Girder Connection Normal to Plane of the Faying Surface			WT to Girder Connection Normal to Plane of the Faying Surface				WT to Girder Connection Normal to Plane of Faying Surface			
R_{pz} =	2.0	kip/in	R_{mz} =	4.3	kip/in	CG to A	R_{mz} =	0.3	kip/in	CG to B
R_{mz} =	0.0	kip/in	R_{mz} =	1.8	kip/in	CG to A	R_{mz} =	3.3	kip/in	CG to B
R_z =	2.0	kip/in	R_z =	6.0	kip/in		R_z =	3.6	kip/in	

WT to PCP Connection Max Load on Weld			WT to Girder Connection Max Load on Weld			WT to Girder Connection Max Load on Weld		
R_{max} =	5.1	kip/in	R_{max} =	6.2	kip/in	R_{max} =	3.9	kip/in
Unity = 0.91			Unity = 1.12			Unity = 0.70		

A.2.3 PCP Detail B.1 Capacity Calculations

A.2.3.1 Detail B.1 Panel Capacity

PCP REINFORCEMENT

PCP Information

Shear Frame: **Geometry**

$P_{ram} := 56kip$ (Load in Actuator) $w := 78in$ (Connection Spacing)

$L := 150in$ (Loading Beam Length) $h := 99in$ (PCP Span Length)

$f := 110in$ (Loading Beam Spacing)

Embeds Members: **2"x5/8" Plates**

$F_{y\_em} := 36ksi$ (Embed Yield) $d_{em} := 2in$ (Embed Depth)

$F_{u\_em} := 50ksi$ (Embed Fracture) $t_{em} := 0.625in$ (Embed Thickness)

$A_{em} := d_{em} \cdot t_{em} = 1.3 \cdot in^2$

Concrete Anchors: **5/8" Diameter D2L**

$d_{d21} := 0.625in$ (Anchor Diameter) $N_{d21\_T} := 4$ (Tension Anchors per Corner)

$f_{uta\_d21} := 61ksi$ (Anchor Tensile Streng $N_{d21\_V} := 6$ (Shear Anchors per Corner)

Concrete Anchor Tension Reinforcement: **3/8" Diameter Prestressing Strands**

$d_{ps} := 0.375in$ (Strand Diameter) $A_{ps} := 0.085in^2$ (Strand Area)

$f_{ps} := 270ksi$ (Strand Strength) $N_{ps} := 3$ (Number of Strands)

Concrete Anchor Shear Reinforcement: **D7.5 WWR**

$d_{wwr} := 0.3055in$ (WWR Diameter) $A_{wwr} := 0.0733in^2$ (WWR Area)

$f_{y\_wwr} := 60ksi$ (WWR Yield) $N_{wwr} := 2$ (Number of WWR)

Phi & Omega Safety Factors

$\phi_1 := 0.75$ $\phi_2 := 0.90$ $\phi_3 := 1$ $\phi_4 := 0.65$

Shear Frame and PCP Dimensions

$V_{pcp} := \frac{P_{ram} \cdot L}{f} = 76.4 \cdot kip$ $T_{con} := \frac{P_{ram} \cdot L \cdot h}{2f \cdot w} = 48.5 \cdot kip$

$M_{pcp} := V_{pcp} \cdot h = 630.0 \cdot kip \cdot ft$ $V_{con} := \frac{P_{ram} \cdot L}{2f} = 38.2 \cdot kip$

$V_{em} := \frac{A_{em}}{A_{em} + A_{wwr}} \cdot V_{con} = 36.1 \cdot kip$ $V_{wwr} := \frac{A_{wwr}}{A_{em} + A_{wwr}} \cdot V_{con} = 2.1 \cdot kip$

Strength of Embeds and Anchors

Embed Tension Yield (AISC J4.1)

$V_1 := F_{y\_em} \cdot A_{em} \cdot \phi_2$

$V_1 = 40.5 \cdot kip$

Anchor Shear Reinforcement Instead of Concrete Breakout (ACI D.6.2.9)

$V_2 := N_{wwr} \cdot A_{wwr} \cdot f_{y\_wwr} \cdot \phi_1$

$V_2 = 6.6 \cdot kip$

D2L Anchor Tension Rupture (ACI D.5.1)

$A_{d21} := \pi \cdot (0.5 \cdot d_{d21})^2 = 0.31 \cdot in^2$

$T_1 := N_{d21\_T} \cdot f_{uta\_d21} \cdot A_{d21} \cdot \phi_1$

$T_1 = 56.1 \cdot kip$

Anchor Tension Reinforcement Instead of Concrete Breakout (ACI D.5.2.9)

$T_2 := N_{ps} \cdot A_{ps} \cdot f_{ps} \cdot \phi_1$

$T_2 = 51.6 \cdot kip$

D2L Anchor Shear Rupture (ACI D.6.1)

$V_3 := N_{d21\_V} \cdot f_{uta\_d21} \cdot A_{d21} \cdot \phi_4$

$V_3 = 73 \cdot kip$

Concrete Side Face Anchor Shear Breakout (ACI D.6.2)

$c_{a1} := 1.5in$ $\quad \phi_{ed\_V} := 1$ $\quad \phi_{c\_V} := 1.0$ $\quad c_{a2} := 14in + 2 \cdot 1.5 \cdot c_{a1} = 18.5 \cdot in$ $\quad l_e := 8 \cdot d_{d21} = 5.0 \cdot in$

$\phi_{ec\_V} := 1.0$ $\quad \phi_p := 2$ $\quad \phi_{h\_V} := 1.0$ $\quad f_c := 8767 \cdot psi^2$

$A_{vc} := c_{a2} \cdot 1.5 \cdot c_{a1} = 41.6 \cdot in^2$

$A_{vco} := 4.5 \cdot (c_{a1})^2 = 10.1 \cdot in^2$

$V_b := \left[8 \cdot \left(\frac{l_e}{d_{d21}} \right)^{0.2} \cdot \sqrt{d_{d21}} \right] \cdot 1 \cdot \sqrt{f_c} \cdot (c_{a1})^{1.5} = 1.6 \cdot kip$

$V_{cbg} := \frac{A_{vc}}{A_{vco}} \cdot \phi_{ec\_V} \cdot \phi_{ed\_V} \cdot \phi_{c\_V} \cdot \phi_{h\_V} \cdot V_b \cdot \phi_p = 13.6 \cdot kip$ (Shear Capacity per Corner)

$2 \cdot V_{cbg} = 27.1 \cdot kip$ (Shear Capacity per Embed)

Unity Check

$\frac{T_{con}}{T_1} = 0.863$	$\frac{T_{con}}{T_2} = 0.938$	$\frac{V_{em}}{V_1} = 0.891$	$\frac{V_{wwr}}{V_2} = 0.32$	$\frac{V_{em} + V_{con}}{V_3} = 1.02$	$\frac{T_{con}}{T_1} + \frac{V_{wwr}}{V_3} = 0.89$

A.2.3.2 Detail B.1 Weld Capacity

Frame Load, Frame Geometry, and Connection Geometry			Loads at Corners of Connections			Weld Strength		
P =	19.9	kip	T_{con} =	17.2	kip	ΦR_n =	5.6	kip/in
V =	27.1	kip	V_{con} =	13.6	kip			
L =	150	in						
f =	110	in	**Fillet Weld and Base Metal Parameters**			**Base Metal Check**		
w =	78	in						
h =	99	in						
b_f =	7.64	in	D =	4	Size	t_{f_min} =	0.19	in
t_f =	0.81	in	F_{exx} =	70.0	ksi	t_{w_min} =	0.38	in
d =	9	in	Φ =	0.75				
t_w =	0.495	in	F_y =	50.0	ksi	Unity = 0.23		
h_w =	3	in	F_u =	65.0	ksi	Unity = 0.77		
h_{bs} =	4	in						

WT to PCP Connection in the Plane of the Faying Surface			WT to Girder Connection in the Plane of the Faying Surface				WT to Girder Connection in the Plane of the Faying Surface			
L =	7.64	in	L =	23.525	in					
I_x =	0.00	in^4/in	$\bar{y}$ =	2.85	in					
I_y =	37.16	in^4/in	I_x =	174.98	in^4/in					
I_p =	37.16	in^4/in	I_y =	38.17	in^4/in					
e =	3.50	in	I_p =	213.15	in^4/in					
c_x =	3.82	in	e =	2.85	in					
c_y =	0.00	in	c_x =	3.82	in	CG to A	c_x =	0.25	in	CG to B
			c_y =	2.85	in	CG to A	c_y =	5.34	in	CG to B
R_{px} =	1.78	kip/in								
R_{py} =	0.00	kip/in	R_{px} =	0.58	kip/in		R_{px} =	0.58	kip/in	
R_{mx} =	0.00	kip/in	R_{py} =	0.73	kip/in		R_{py} =	0.73	kip/in	
R_{my} =	4.88	kip/in	R_{mx} =	0.52	kip/in		R_{mx} =	0.97	kip/in	
			R_{my} =	0.69	kip/in		R_{my} =	0.04	kip/in	
R_{xy} =	5.19	kip/in								
			R_{xy} =	1.80	kip/in		R_{xy} =	1.73	kip/in	

WT to Girder Connection Normal to Plane of the Faying Surface			WT to Girder Connection Normal to Plane of the Faying Surface				WT to Girder Connection Normal to Plane of Faying Surface			
R_{pz} =	2.3	kip/in	R_{mz} =	4.8	kip/in	CG to A	R_{mz} =	0.3	kip/in	CG to B
R_{mz} =	0.0	kip/in	R_{mz} =	2.0	kip/in	CG to A	R_{mz} =	3.7	kip/in	CG to B
R_z =	2.3	kip/in	R_z =	6.7	kip/in		R_z =	4.0	kip/in	

WT to PCP Connection Max Load on Weld			WT to Girder Connection Max Load on Weld			WT to Girder Connection Max Load on Weld		
R_{max} =	5.7	kip/in	R_{max} =	7.0	kip/in	R_{max} =	4.3	kip/in
Unity = 1.02			Unity = 1.25			Unity = 0.78		

A.2.4 PCP Detail C.2 Capacity Calculations

A.2.4.1 Detail C.2 Panel Capacity

PCP REINFORCEMENT

PCP Information

Shear Frame: **Geometry**

$P_{ram} := 58kip$	(Load in Actuator)	$w_o := 78in$	(Outter Connection Spacing)
$L := 150in$	(Loading Beam Length)	$w_i := 54in$	(Inner Connection Spacing)
$f := 110in$	(Loading Beam Spacing)	$h := 99in$	(PCP Span Length)

Embeds Members: **2"x5/8" Plates**

$F_{y\_em} := 36ksi$	(Embed Yield)	$d_{em} := 2in$	(Embed Depth)
$F_{u\_em} := 50ksi$	(Embed Fracture)	$t_{em} := 0.625in$	(Embed Thickness)

$A_{em} := d_{em} \cdot t_{em} = 1.3 \cdot in^2$

Concrete Anchors: **1/2" Diameter D2L**

$d_{d2l} := 0.5in$	(Anchor Diameter)	$N_{d2l\_T} := 4$	(Tension Anchors per Connection)
$f_{uta\_d2l} := 61ksi$	(Anchor Tensile Strength)	$N_{d2l\_V} := 10$	(Shear Anchors per Corner)

Concrete Anchor Tension Reinforcement: **3/8" Diameter Prestressing Strands**

$d_{ps} := 0.375in$	(Strand Diameter)	$A_{ps} := 0.085in^2$	(Strand Area)
$f_{ps} := 270ksi$	(Strand Strength)	$N_{ps} := 2.5$	(Strands per Connection)

Concrete Anchor Shear Reinforcement: **D7.5 WWR**

$d_{wwr} := 0.3055in$	(WWR Diameter)	$A_{wwr} := 0.0733in^2$	(WWR Area)
$f_{y\_wwr} := 60ksi$	(WWR Yield)	$N_{wwr} := 3$	(Number of WWR)

Phi & Omega Safety Factors

$\phi_1 := 0.75 \quad \phi_2 := 0.90 \quad \phi_3 := 1 \quad \phi_4 := 0.65$

Shear Frame and PCP Dimensions

$$V_{pcp} := \frac{P_{ram} \cdot L}{f} = 79.1 \cdot kip \qquad M_{pcp} := V_{pcp} \cdot h = 7830.0 \cdot kip \cdot in$$

$$V_{corner} := \frac{P_{ram} \cdot L}{2f} = 39.5 \cdot kip \qquad T_{con\_o} := \frac{M_{pcp}}{2\left(w_o + \frac{w_i^2}{w_o}\right)} = 33.9 \cdot kip \qquad T_{con\_i} := \frac{T_{con\_o} \cdot w_i}{w_o} = 23.5 \cdot kip$$

$$V_{em} := \frac{A_{em}}{A_{em} + A_{wwr}} \cdot V_{corner} = 37.4 \cdot kip \qquad V_{wwr} := \frac{A_{wwr}}{A_{em} + A_{wwr}} \cdot V_{corner} = 2.2 \cdot kip$$

Strength of Embeds and Anchors

Embed Tension Yield (AISC J4.1)

$V_1 := F_{y\_em} \cdot A_{em} \cdot \phi_2$

$V_1 = 40.5 \cdot kip$

Anchor Shear Reinforcement Instead of Concrete Breakout (ACI D.6.2.9)

$V_2 := N_{wwr} \cdot A_{wwr} \cdot f_{y\_wwr} \cdot \phi_1$

$V_2 = 9.9 \cdot kip$

D2L Anchor Tension Rupture (ACI D.5.1)

$A_{d21} := \pi \cdot (0.5 \cdot d_{d21})^2 = 0.20 \cdot in^2$

$T_1 := N_{d21\_T} \cdot f_{uta\_d21} \cdot A_{d21} \cdot \phi_1$

$T_1 = 35.9 \cdot kip$

Anchor Tension Reinforcement Instead of Concrete Breakout (ACI D.5.2.9)

$T_2 := N_{ps} \cdot A_{ps} \cdot f_{ps} \cdot \phi_1$

$T_2 = 43 \cdot kip$

D2L Anchor Shear Rupture (ACI D.6.1)

$V_3 := N_{d21\_V} \cdot f_{uta\_d21} \cdot A_{d21} \cdot \phi_4$

$V_3 = 77.9 \cdot kip$

Concrete Side Face Anchor Shear Breakout (ACI D.6.2)

$c_{a1} := 1.5in$ $\quad \phi_{ed\_V} := 1$ $\quad \phi_{c\_V} := 1.0$ $\quad c_{a2} := 26in + 2 \cdot 1.5 \cdot c_{a1} = 30.5 \cdot in$ $\quad l_e := 8 \cdot d_{d21} = 4.0 \cdot in$

$\phi_{ec\_V} := 1.0$ $\quad \phi_p := 2$ $\quad \phi_{h\_V} := 1.0$ $\quad f_c := 8767 \cdot psi^2$

$A_{vc} := c_{a2} \cdot 1.5 \cdot c_{a1} = 68.6 \cdot in^2$

$A_{vco} := 4.5 \cdot (c_{a1})^2 = 10.1 \cdot in^2$

$V_b := \left[8 \cdot \left(\frac{l_e}{d_{d21}} \right)^{0.2} \cdot \sqrt{d_{d21}} \right] \cdot 1 \cdot \sqrt{f_c} \cdot (c_{a1})^{1.5} = 1.5 \cdot kip$

$V_{cbg} := \frac{A_{vc}}{A_{vco}} \cdot \phi_{ec\_V} \cdot \phi_{ed\_V} \cdot \phi_{c\_V} \cdot \phi_{h\_V} \cdot V_b \cdot \phi_p = 20.0 \cdot kip$ (Shear Capacity per Corner)

$2 \cdot V_{cbg} = 40.0 \cdot kip$ (Shear Capacity per Embed)

Unity Check

$\frac{T_{con\_o}}{T_1} = 0.944$	$\frac{T_{con\_o}}{T_2} = 0.788$	$\frac{V_{em}}{V_1} = 0.922$	$\frac{V_{wwr}}{V_2} = 0.22$	$\frac{V_{em} + V_{corner}}{V_3} = 0.99$	$\frac{T_{con\_o}}{T_1} + \frac{V_{wwr}}{V_3} = 0.97$

A.2.4.2 Detail C.2 Weld Capacity

Frame Load, Frame Geometry, and Connection Geometry			
P =	29.3	kip	
V =	40.0	kip	
M =	3955.5	kip*in	
L =	150	in	
f =	110	in	
w_o =	78	in	
w_i =	54	in	
h =	99	in	WT9x35.5
b_f =	7.64	in	
t_f =	0.81	in	
d =	9	in	
t_w =	0.495	in	
h_w =	3	in	
h_{bs} =	4	in	

Loads at Corners of Connections		
T_{con_o} =	17.1	kip
V_{con_o} =	10.0	kip
T_{con_i} =	11.9	kip
V_{con_i} =	10.0	kip

Fillet Weld and Base Metal Parameters		
D =	4	Size
F_{exx} =	70.0	ksi
Φ =	0.75	
F_y =	50.0	ksi
F_u =	65.0	ksi

Weld Strength		
$ΦR_n$ =	5.6	kip/in

Base Metal Check		
t_{f_min} =	0.19	in
t_{w_min} =	0.38	in
Unity = 0.23		
Unity = 0.77		

WT to PCP Connection in the Plane of the Faying Surface		
L =	7.64	in
I_x =	0.00	in^4/in
I_y =	37.16	in^4/in
I_p =	37.16	in^4/in
e =	3.50	in
c_x =	3.82	in
c_y =	0.00	in
R_{px} =	1.31	kip/in
R_{py} =	0.00	kip/in
R_{mx} =	0.00	kip/in
R_{my} =	3.59	kip/in
R_{xy} =	3.82	kip/in

WT to Girder Connection in the Plane of the Faying Surface			
L =	23.525	in	
$\bar{y}$ =	2.85	in	
I_x =	174.98	in^4/in	
I_y =	38.17	in^4/in	
I_p =	213.15	in^4/in	
e =	2.85	in	
c_x =	3.82	in	CG to A
c_y =	2.85	in	CG to A
R_{px} =	0.42	kip/in	
R_{py} =	0.73	kip/in	
R_{mx} =	0.38	kip/in	
R_{my} =	0.51	kip/in	
R_{xy} =	1.48	kip/in	

WT to Girder Connection in the Plane of the Faying Surface			
c_x =	0.25	in	CG to B
c_y =	5.34	in	CG to B
R_{px} =	0.42	kip/in	
R_{py} =	0.73	kip/in	
R_{mx} =	0.71	kip/in	
R_{my} =	0.03	kip/in	
R_{xy} =	1.37	kip/in	

WT to Girder Connection Normal to Plane of the Faying Surface			
R_{pz} =	2.2	kip/in	
R_{mz} =	0.0	kip/in	
R_z =	2.2	kip/in	

WT to Girder Connection Normal to Plane of the Faying Surface			
R_{mz} =	3.5	kip/in	CG to A
R_{mz} =	2.0	kip/in	CG to A
R_z =	5.5	kip/in	

WT to Girder Connection Normal to Plane of Faying Surface			
R_{mz} =	0.2	kip/in	CG to B
R_{mz} =	3.7	kip/in	CG to B
R_z =	3.9	kip/in	

WT to PCP Connection Max Load on Weld		
R_{max} =	4.4	kip/in
Unity = 0.80		

WT to Girder Connection Max Load on Weld		
R_{max} =	5.7	kip/in
Unity = 1.01		

WT to Girder Connection Max Load on Weld		
R_{max} =	4.1	kip/in
Unity = 0.74		

A.2.5 PCP Detail D.2 Capacity Calculations

A.2.5.1 Detail D.2 Panel Capacity

PCP REINFORCEMENT

PCP Information

Shear Frame: **Geometry**

$P_{ram} := 74kip$	(Load in Actuator)	$w_o := 78in$	(Outter Connection Spacing)
$L := 150in$	(Loading Beam Length)	$w_i := 54in$	(Inner Connection Spacing)
$f := 110in$	(Loading Beam Spacing)	$h := 99in$	(PCP Span Length)

Embeds Members: **2"x3/4" Plates**

$F_{y\_em} := 36ksi$	(Embed Yield)	$d_{em} := 2in$	(Embed Depth)
$F_{u\_em} := 50ksi$	(Embed Fracture)	$t_{em} := 0.75in$	(Embed Thickness)

$A_{em} := d_{em} \cdot t_{em} = 1.5 \cdot in^2$

Concrete Anchors: **5/8" Diameter D2L**

$d_{d2l} := 0.625in$	(Anchor Diameter)	$N_{d2l\_T} := 4$	(Tension Anchors per Connection)
$f_{uta\_d2l} := 61ksi$	(Anchor Tensile Strength)	$N_{d2l\_V} := 8$	(Shear Anchors per Corner)

Concrete Anchor Tension Reinforcement: **3/8" Diameter Prestressing Strands**

$d_{ps} := 0.375in$	(Strand Diameter)	$A_{ps} := 0.085in^2$	(Strand Area)
$f_{ps} := 270ksi$	(Strand Strength)	$N_{ps} := 2.5$	(Strands per Connection)

Concrete Anchor Shear Reinforcement: **D7.5 WWR**

$d_{wwr} := 0.3055in$	(WWR Diameter)	$A_{wwr} := 0.0733in^2$	(WWR Area)
$f_{y\_wwr} := 60ksi$	(WWR Yield)	$N_{wwr} := 3$	(Number of WWR)

Phi & Omega Safety Factors

$\phi_1 := 0.75 \quad \phi_2 := 0.90 \quad \phi_3 := 1 \quad \phi_4 := 0.65$

Shear Frame and PCP Dimensions

$$V_{pcp} := \frac{P_{ram} \cdot L}{f} = 100.9 \cdot kip \qquad M_{pcp} := V_{pcp} \cdot h = 9990.0 \cdot kip \cdot in$$

$$V_{corner} := \frac{P_{ram} \cdot L}{2f} = 50.5 \cdot kip \qquad T_{con\_o} := \frac{M_{pcp}}{2\left(w_o + \frac{w_i^2}{w_o}\right)} = 43.3 \cdot kip \qquad T_{con\_i} := \frac{T_{con\_o} \cdot w_i}{w_o} = 30.0 \cdot kip$$

$$V_{em} := \frac{A_{em}}{A_{em} + A_{wwr}} \cdot V_{corner} = 48.1 \cdot kip \qquad V_{wwr} := \frac{A_{wwr}}{A_{em} + A_{wwr}} \cdot V_{corner} = 2.4 \cdot kip$$

Strength of Embeds and Anchors

Embed Tension Yield (AISC J4.1)

$V_1 := F_{y\_em} \cdot A_{em} \cdot \phi_2$

$V_1 = 48.6 \cdot kip$

Anchor Shear Reinforcement Instead of Concrete Breakout (ACI D.6.2.9)

$V_2 := N_{wwr} \cdot A_{wwr} \cdot f_{y\_wwr} \cdot \phi_1$

$V_2 = 9.9 \cdot kip$

D2L Anchor Tension Rupture (ACI D.5.1)

$A_{d21} := \pi \cdot (0.5 \cdot d_{d21})^2 = 0.31 \cdot in^2$

$T_1 := N_{d21\_T} \cdot f_{uta\_d21} \cdot A_{d21} \cdot \phi_1$

$T_1 = 56.1 \cdot kip$

Anchor Tension Reinforcement Instead of Concrete Breakout (ACI D.5.2.9)

$T_2 := N_{ps} \cdot A_{ps} \cdot f_{ps} \cdot \phi_1$

$T_2 = 43 \cdot kip$

D2L Anchor Shear Rupture (ACI D.6.1)

$V_3 := N_{d21\_V} \cdot f_{uta\_d21} \cdot A_{d21} \cdot \phi_4$

$V_3 = 97.3 \cdot kip$

Concrete Side Face Anchor Shear Breakout (ACI D.6.2)

$c_{a1} := 1.5in$ $\phi_{ed\_V} := 1$ $\phi_{c\_V} := 1.0$ $c_{a2} := 20in + 2 \cdot 1.5 \cdot c_{a1} = 24.5 \cdot in$ $l_e := 8 \cdot d_{d21} = 5.0 \cdot in$

$\phi_{ec\_V} := 1.0$ $\phi_p := 2.0$ $\phi_{h\_V} := 1.0$ $f_c := 8767 \cdot psi^2$

$A_{vc} := c_{a2} \cdot 1.5 \cdot c_{a1} = 55.1 \cdot in^2$

$A_{vco} := 4.5 \cdot (c_{a1})^2 = 10.1 \cdot in^2$

$V_b := \left[8 \cdot \left(\frac{l_e}{d_{d21}} \right)^{0.2} \cdot \sqrt{d_{d21}} \right] \cdot 1 \cdot \sqrt{f_c} \cdot (c_{a1})^{1.5} = 1.6 \cdot kip$

$V_{cbg} := \frac{A_{vc}}{A_{vco}} \cdot \phi_{ec\_V} \cdot \phi_{ed\_V} \cdot \phi_{c\_V} \cdot \phi_{h\_V} \cdot V_b \cdot \phi_p = 18.0 \cdot kip$ (Shear Capacity per Corner)

$2 \cdot V_{cbg} = 35.9 \cdot kip$ (Shear Capacity per Embed)

Unity Check

$\frac{T_{con\_o}}{T_1} = 0.771$	$\frac{T_{con\_o}}{T_2} = 1.01$	$\frac{V_{em}}{V_1} = 0.990$	$\frac{V_{wwr}}{V_2} = 0.24$	$\frac{V_{em} + V_{corner}}{V_3} = 1.01$	$\frac{T_{con\_o}}{T_1} + \frac{V_{wwr}}{V_3} = 0.80$

A.2.5.2 Detail D.2 Weld Capacity

Frame Load, Frame Geometry, and Connection Geometry				Loads at Corners of Connections				Weld Strength			
P =	26.3	kip		T_{con_o} =	15.4	kip		ΦR_n =	5.6	kip/in	
V =	35.9	kip		V_{con_o} =	9.0	kip					
M =	3550.5	kip*in		T_{con_i} =	10.7	kip					
L =	150	in		V_{con_i} =	9.0	kip					
f =	110	in									
w_o =	78	in		Fillet Weld and Base Metal Parameters				Base Metal Check			
w_i =	54	in									
h =	99	in	WT9x35.5								
b_f =	7.64	in		D =	4	Size		t_{f_min} =	0.19	in	
t_f =	0.81	in		F_{exx} =	70.0	ksi		t_{w_min} =	0.38	in	
d =	9	in		Φ =	0.75						
t_w =	0.495	in		F_y =	50.0	ksi		Unity = 0.23			
h_w =	3	in		F_u =	65.0	ksi		Unity = 0.77			
h_{bs} =	4	in									
WT to PCP Connection in the Plane of the Faying Surface				**WT to Girder Connection in the Plane of the Faying Surface**				**WT to Girder Connection in the Plane of the Faying Surface**			
L =	7.64	in		L =	23.525	in					
I_x =	0.00	in^4/in		$\bar{y}$ =	2.85	in					
I_y =	37.16	in^4/in		I_x =	174.98	in^4/in					
I_p =	37.16	in^4/in		I_y =	38.17	in^4/in					
e =	3.50	in		I_p =	213.15	in^4/in					
c_x =	3.82	in		e =	2.85	in					
c_y =	0.00	in		c_x =	3.82	in	CG to A	c_x =	0.25	in	CG to B
				c_y =	2.85	in	CG to A	c_y =	5.34	in	CG to B
R_{px} =	1.17	kip/in									
R_{py} =	0.00	kip/in		R_{px} =	0.38	kip/in		R_{px} =	0.38	kip/in	
R_{mx} =	0.00	kip/in		R_{py} =	0.65	kip/in		R_{py} =	0.65	kip/in	
R_{my} =	3.23	kip/in		R_{mx} =	0.34	kip/in		R_{mx} =	0.64	kip/in	
				R_{my} =	0.46	kip/in		R_{my} =	0.03	kip/in	
R_{xy} =	3.43	kip/in									
				R_{xy} =	1.33	kip/in		R_{xy} =	1.23	kip/in	
WT to Girder Connection Normal to Plane of the Faying Surface				**WT to Girder Connection Normal to Plane of the Faying Surface**				**WT to Girder Connection Normal to Plane of Faying Surface**			
R_{pz} =	2.0	kip/in		R_{mz} =	3.1	kip/in	CG to A	R_{mz} =	0.2	kip/in	CG to B
R_{mz} =	0.0	kip/in		R_{mz} =	1.8	kip/in	CG to A	R_{mz} =	3.3	kip/in	CG to B
R_z =	2.0	kip/in		R_z =	4.9	kip/in		R_z =	3.5	kip/in	
WT to PCP Connection Max Load on Weld				**WT to Girder Connection Max Load on Weld**				**WT to Girder Connection Max Load on Weld**			
R_{max} =	4.0	kip/in		R_{max} =	5.1	kip/in		R_{max} =	3.7	kip/in	
Unity = 0.71				Unity = 0.91				Unity = 0.66			

A.3 SHEAR FRAME TEST RESULTS

A.3.1 Loading Beam Twist

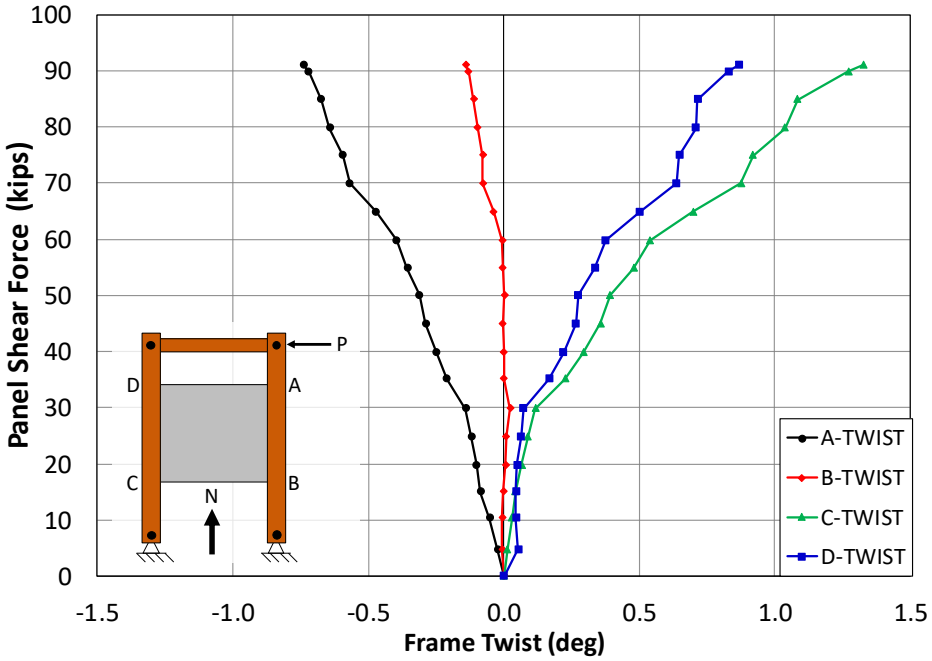

Figure A.7: Twist Behavior of the Shear Frame for PCP Detail A.1.MAX

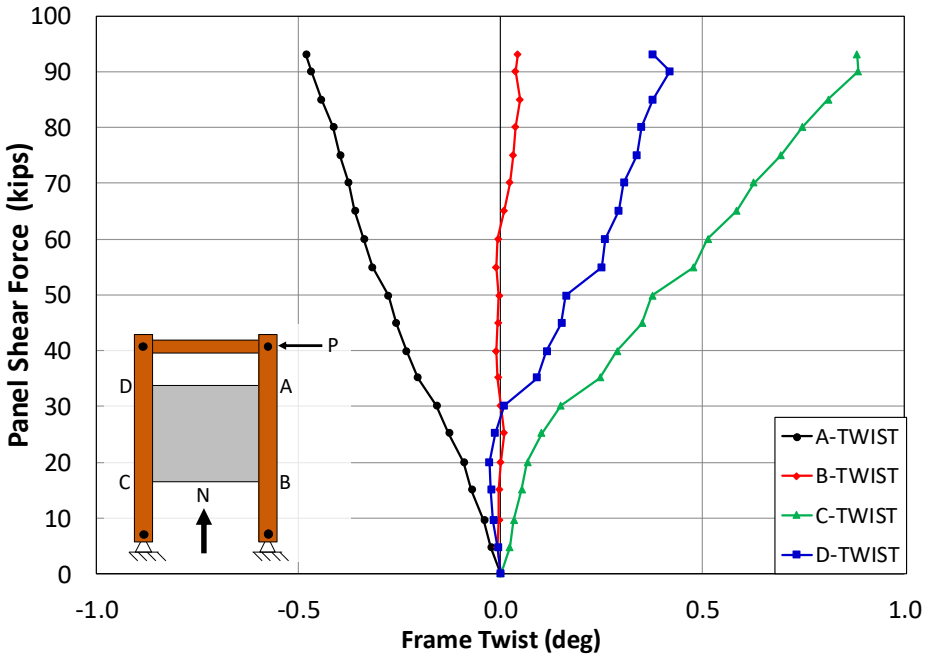

Figure A.8: Twist Behavior of the Shear Frame for PCP Detail B.1.MAX

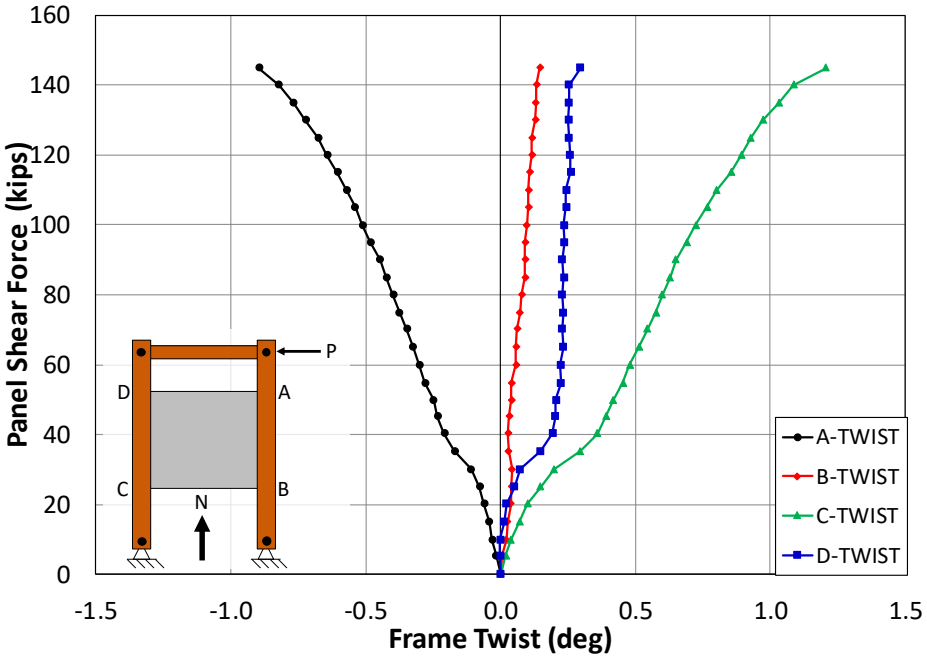

Figure A.9: Twist Behavior of the Shear Frame for PCP Detail C.2.MAX

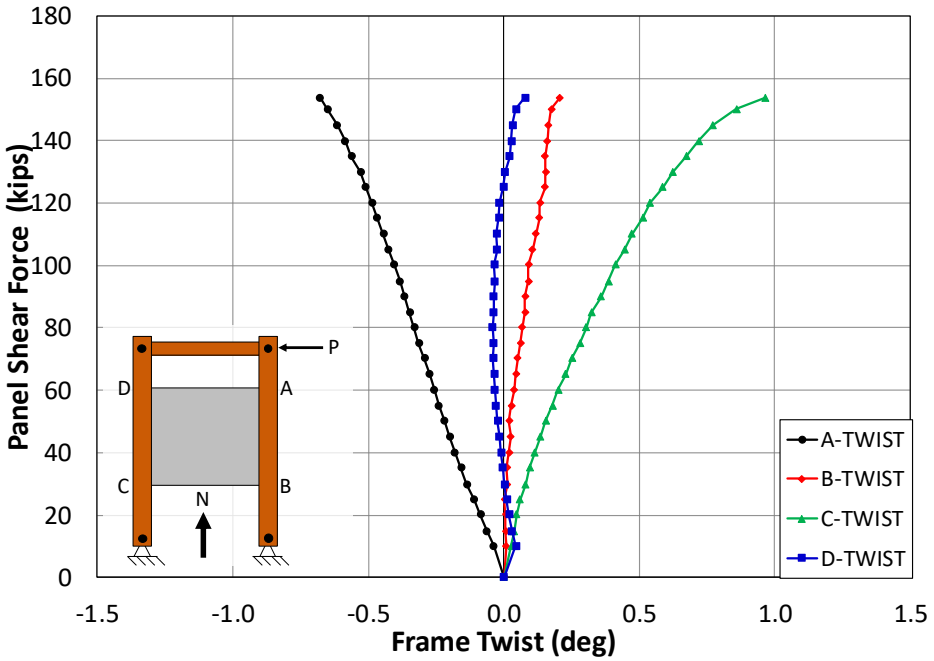

Figure A.10: Twist Behavior of the Shear Frame for PCP Detail D.2.MAX

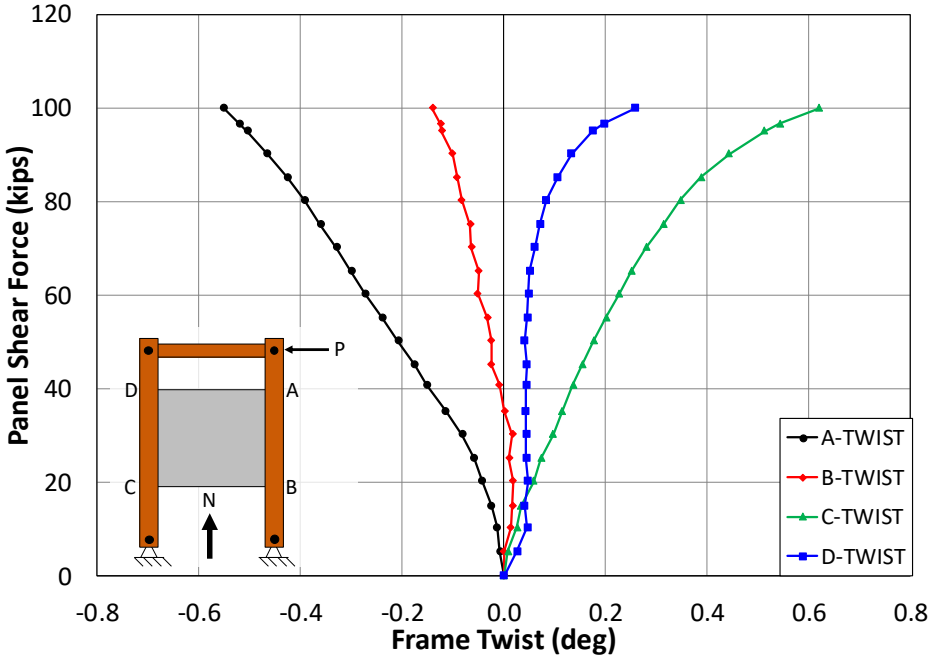

Figure A.11: Twist Behavior of the Shear Frame for PCP Detail A.1.MIN

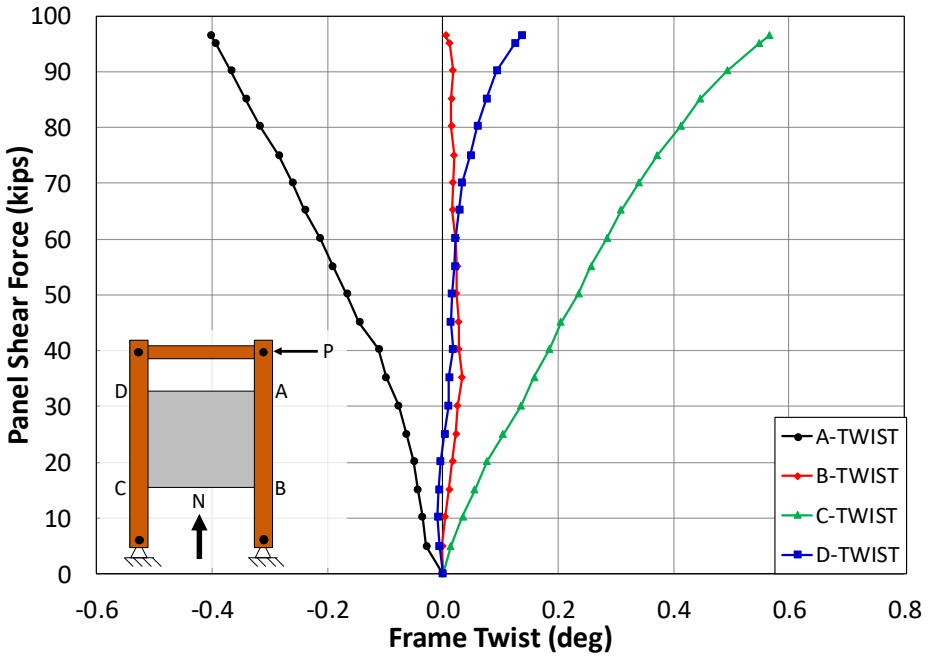

Figure A.12: Twist Behavior of the Shear Frame for PCP Detail B.1.MIN

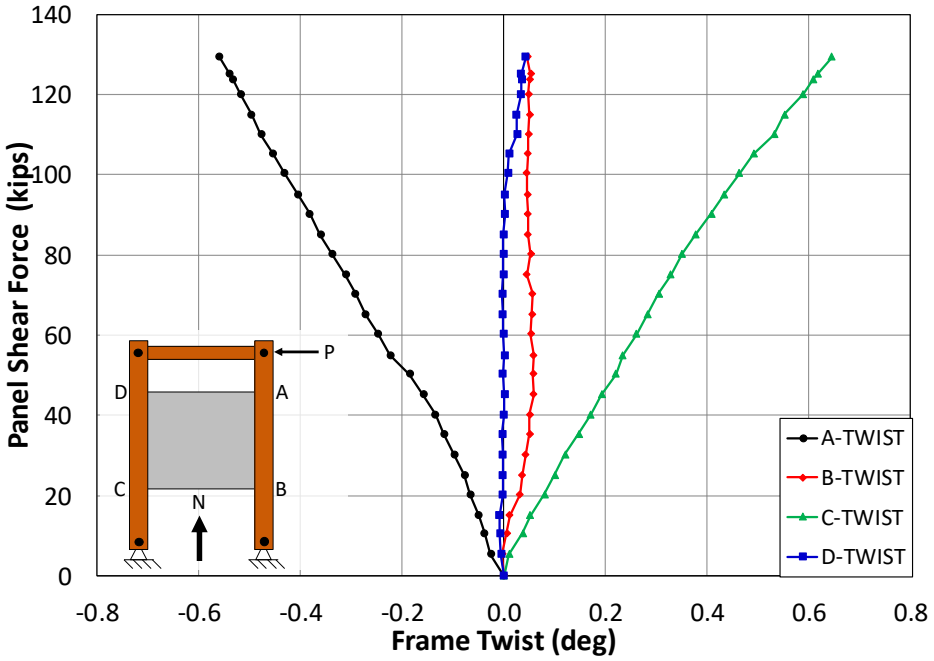

Figure A.13: Twist Behavior of the Shear Frame for PCP Detail C.2.MIN

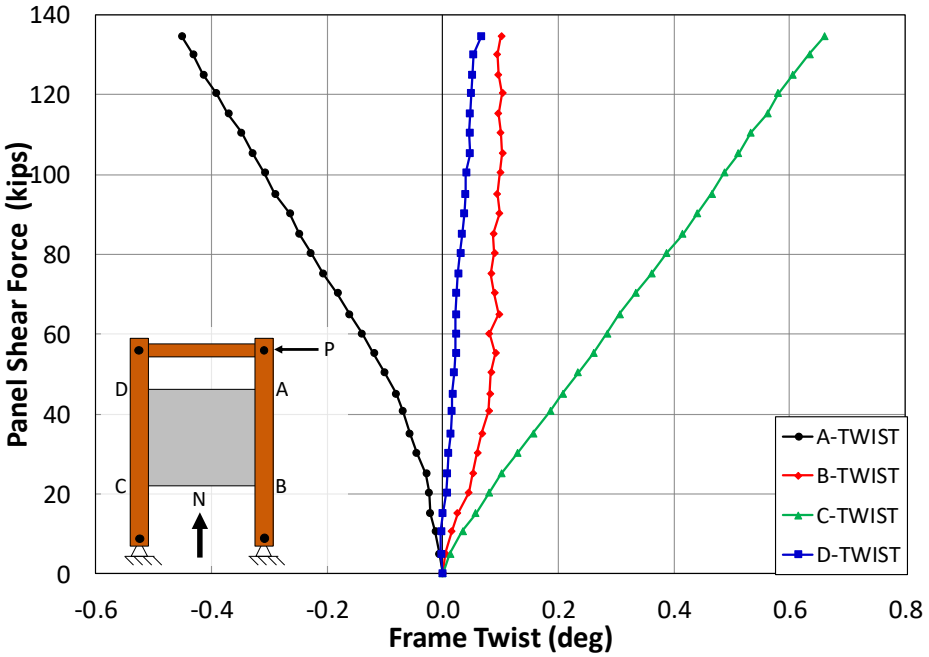

Figure A.14: Twist Behavior of the Shear Frame for PCP Detail D.2.MIN

A.3.2 Frame Lateral Displacements

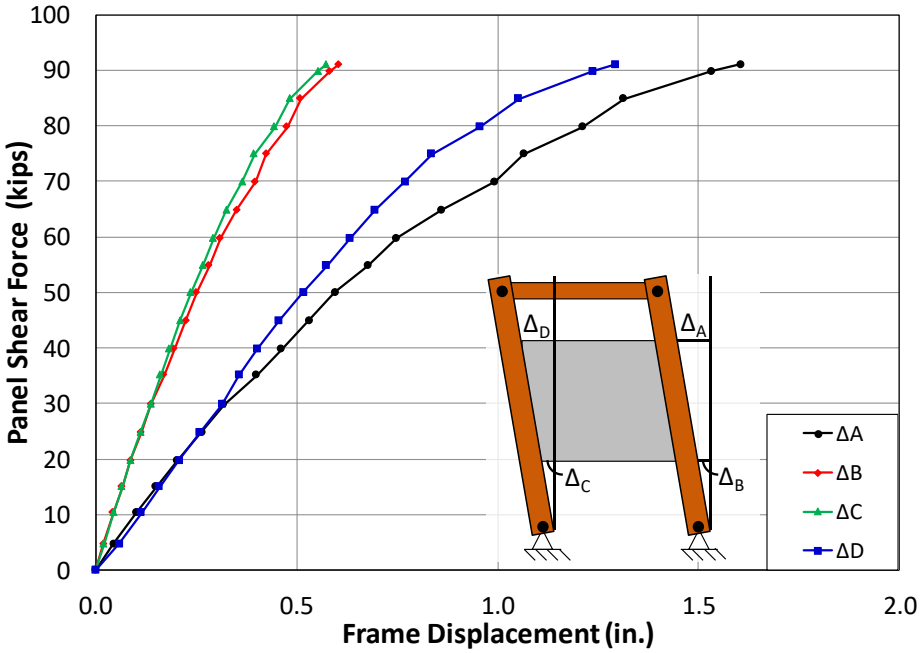

Figure A.15: Loading Beam Shear Center Lateral Displacement for PCP Detail A.1.MAX

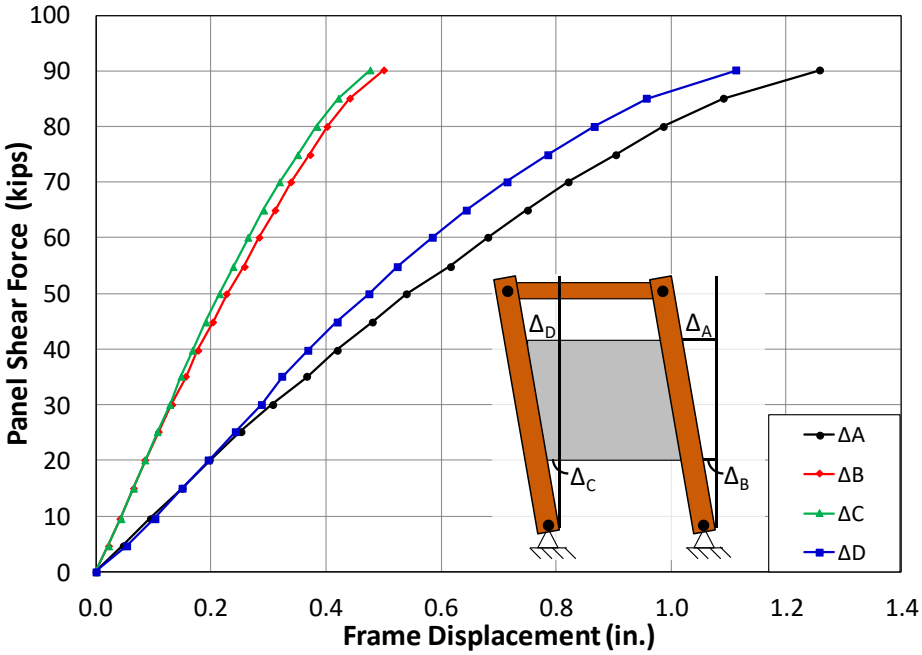

Figure A.16: Loading Beam Shear Center Lateral Displacement for PCP Detail B.1.MAX

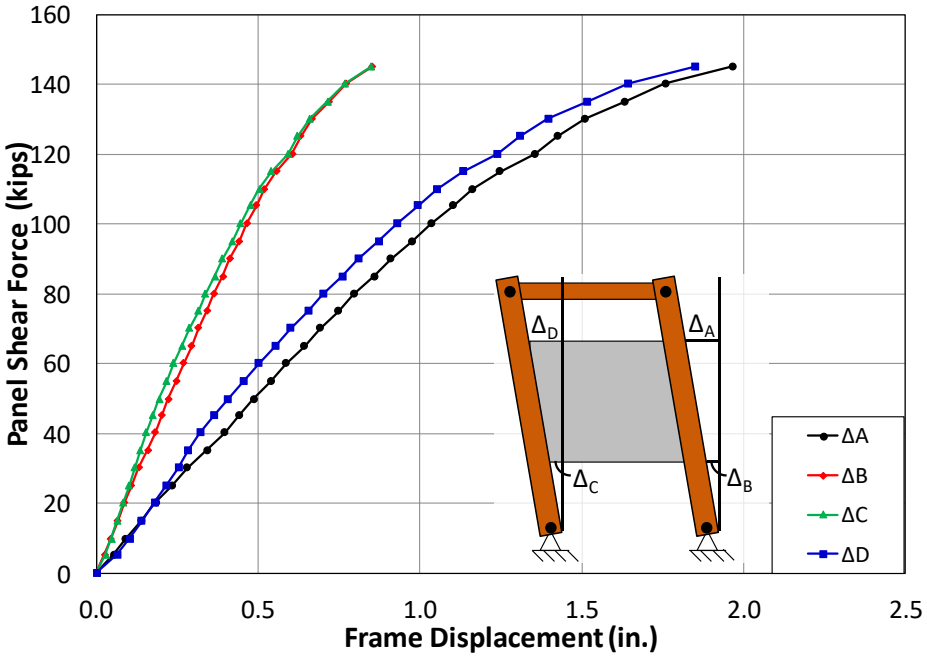

Figure A.17: Loading Beam Shear Center Lateral Displacement for PCP Detail C.2.MAX

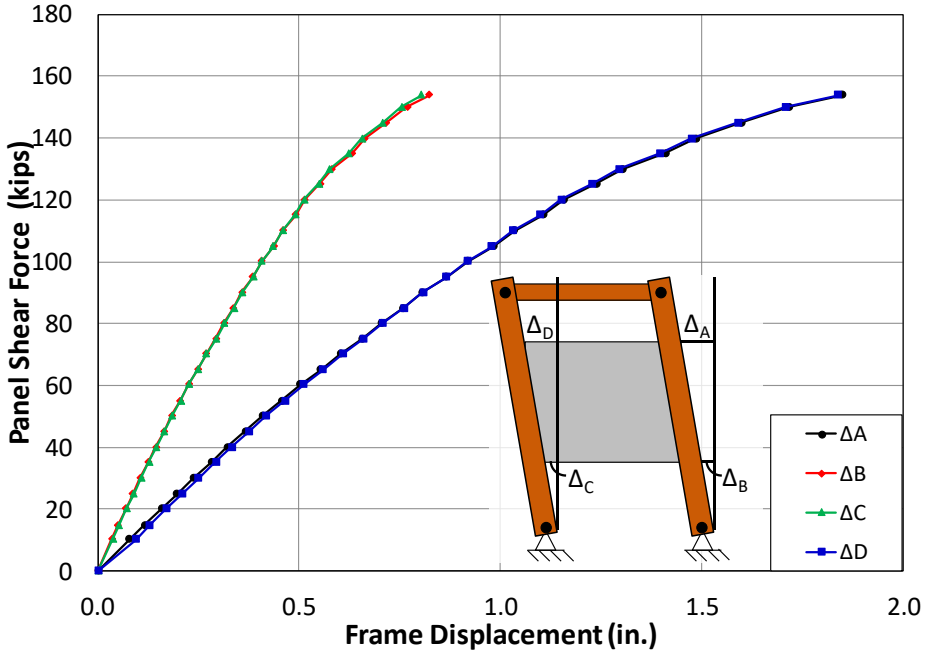

Figure A.18: Loading Beam Shear Center Lateral Displacement for PCP Detail D.2.MAX

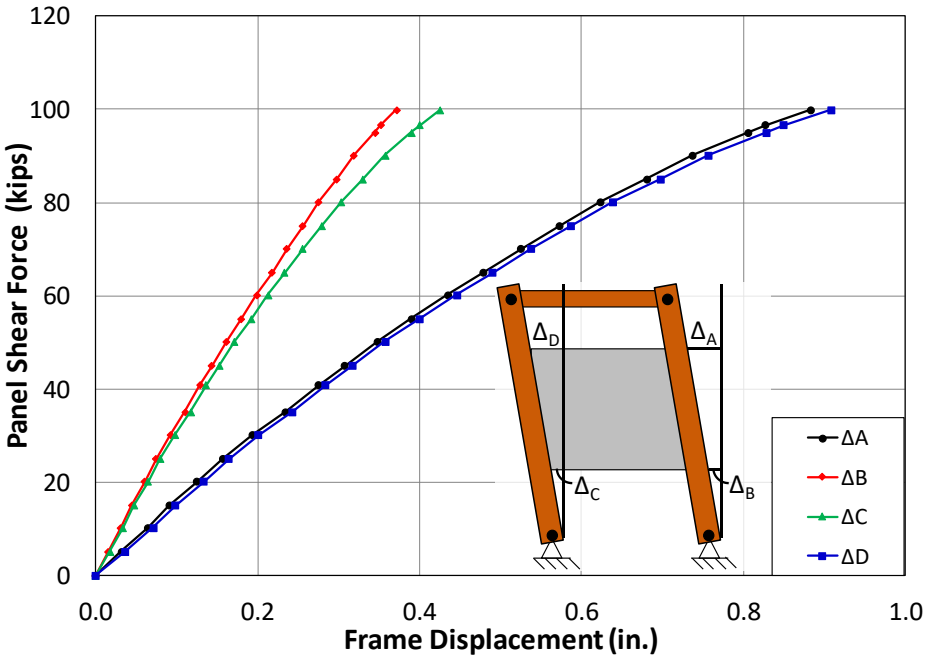

Figure A.19: Loading Beam Shear Center Lateral Displacement for PCP Detail A.1.MIN

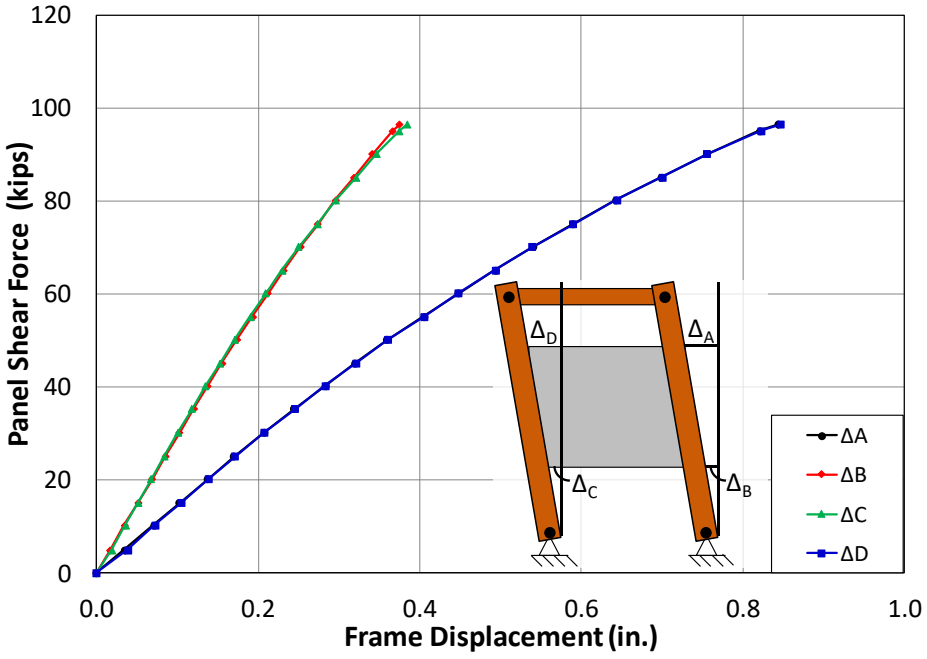

Figure A.20: Loading Beam Shear Center Lateral Displacement for PCP Detail B.1.MIN

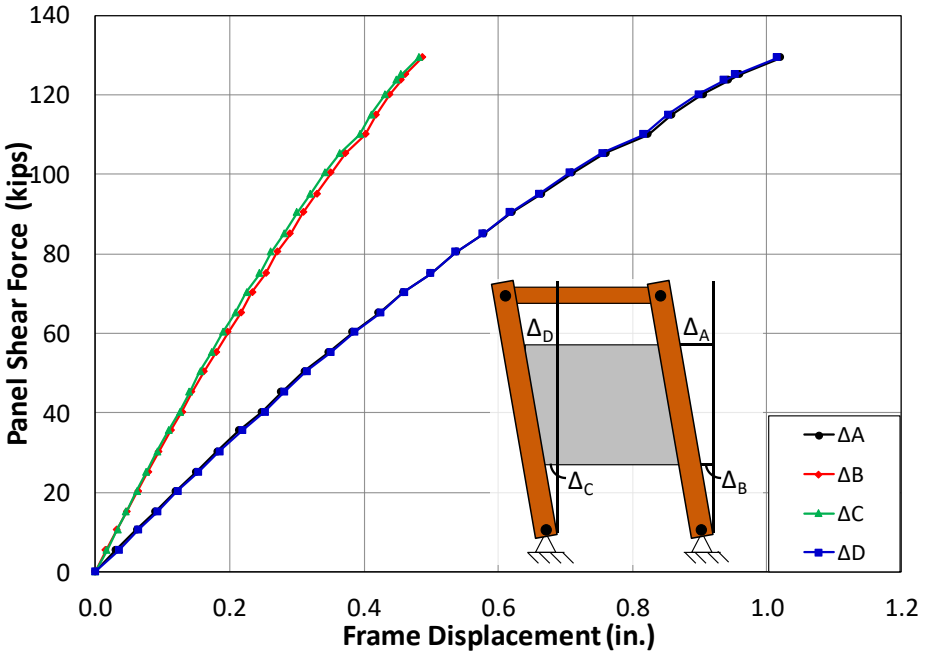

Figure A.21: Loading Beam Shear Center Lateral Displacement for PCP Detail C.2.MIN

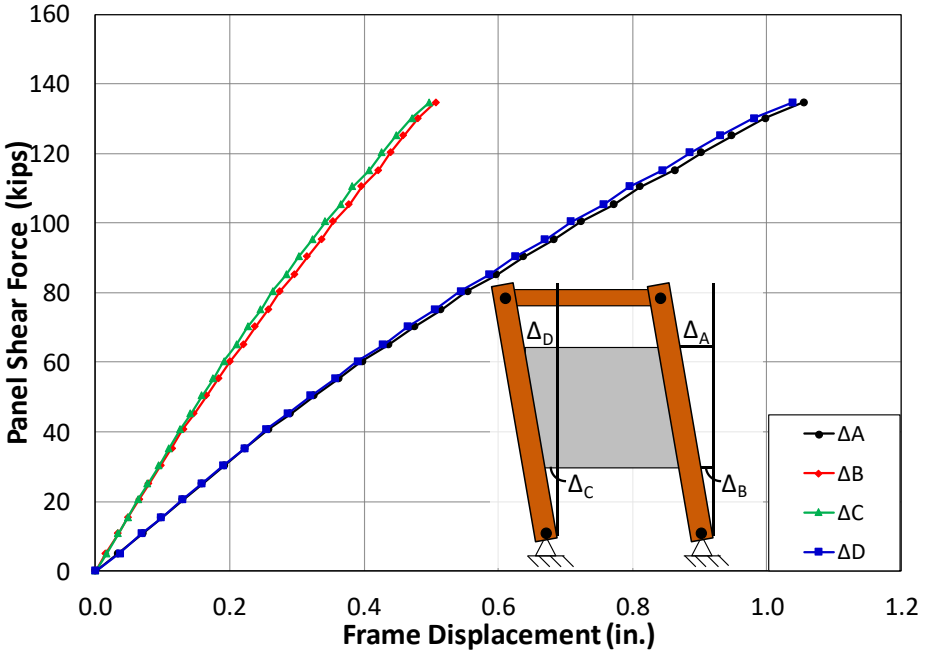

Figure A.22: Loading Beam Shear Center Lateral Displacement for PCP Detail D.2.MIN

A.3.3 PCP Ultimate Capacity Results

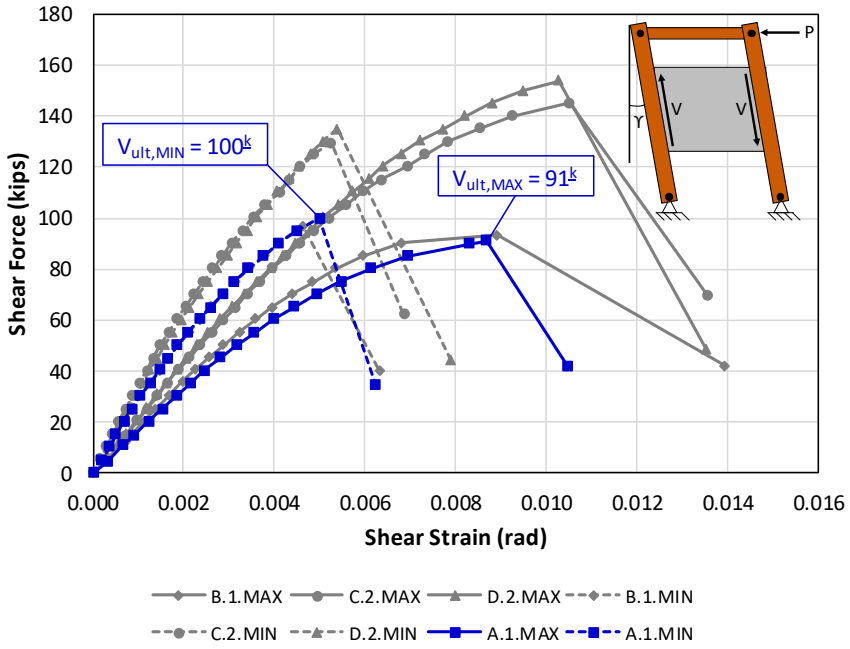

Figure A.23: Shear Behavior up to Ultimate Load for PCP Detail A.1

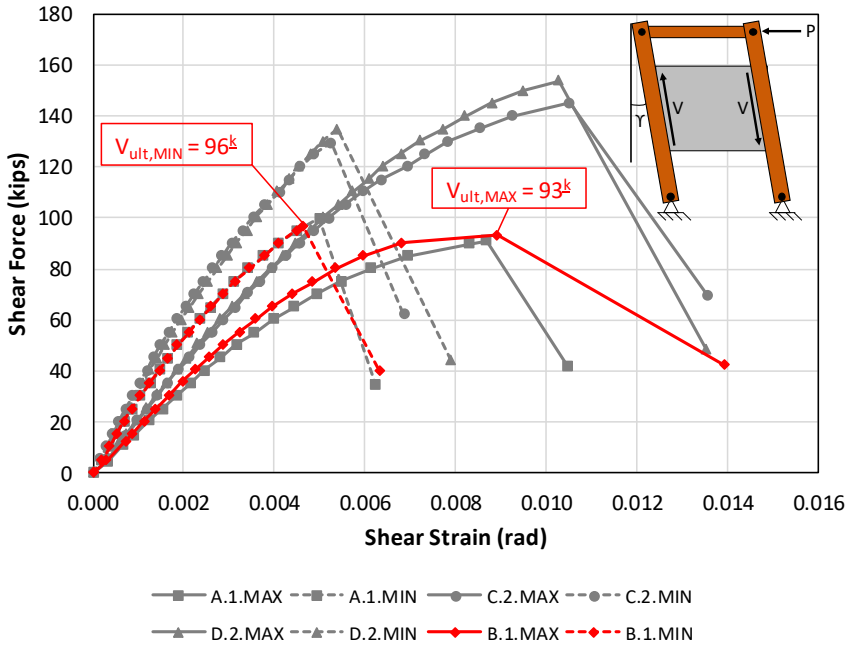

Figure A.24: Shear Behavior up to Ultimate Load for PCP Detail B.1

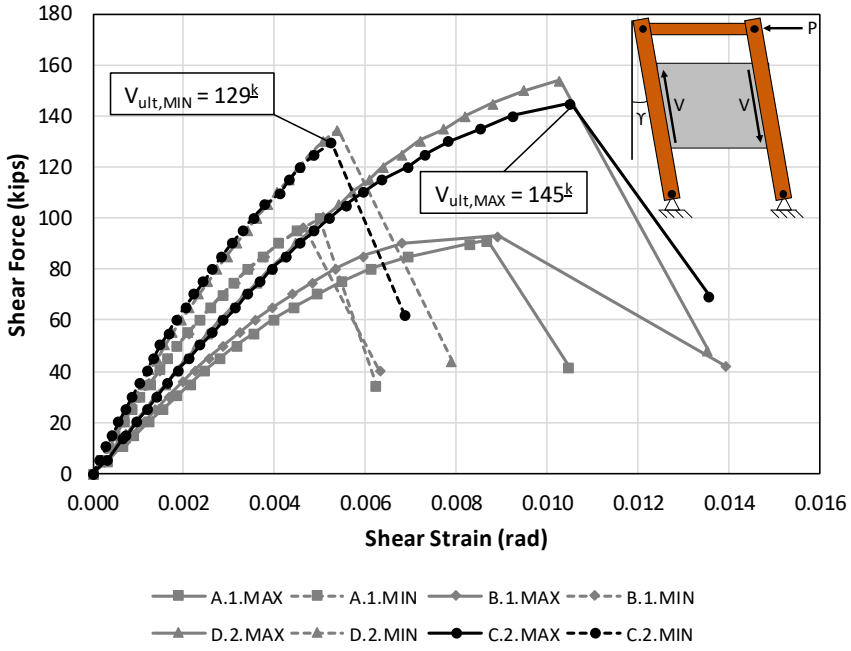

Figure A.25: Shear Behavior up to Ultimate Load for PCP Detail C.2

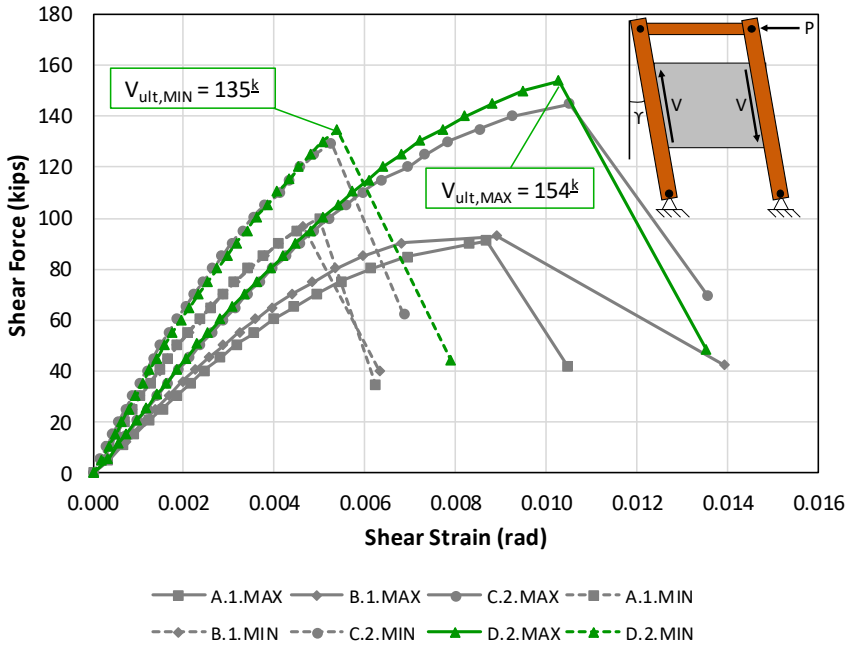

Figure A.26: Shear Behavior up to Ultimate Load for PCP Detail D.2

A.3.4 PCP Shear Stiffness Results

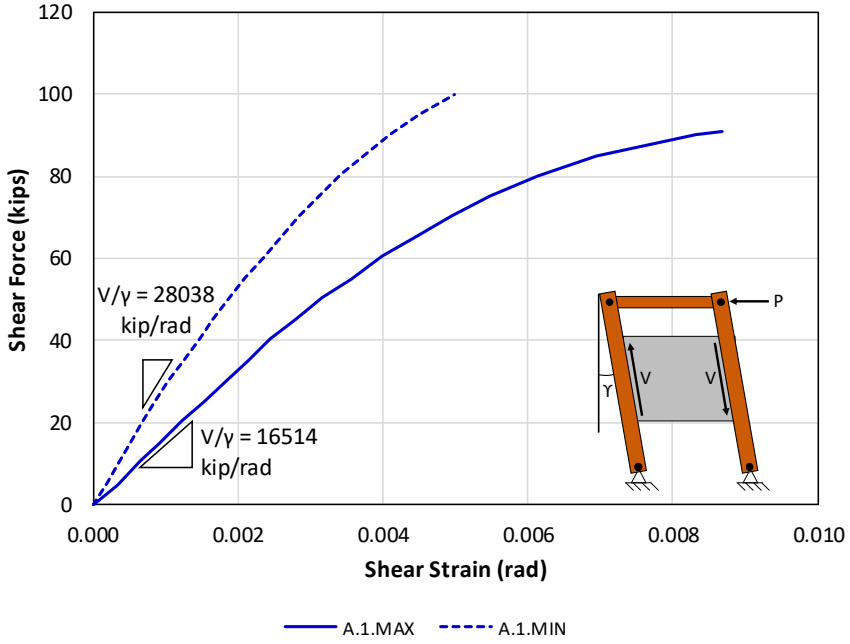

Figure A.27: Shear Stiffness Behavior for PCP Detail A.1

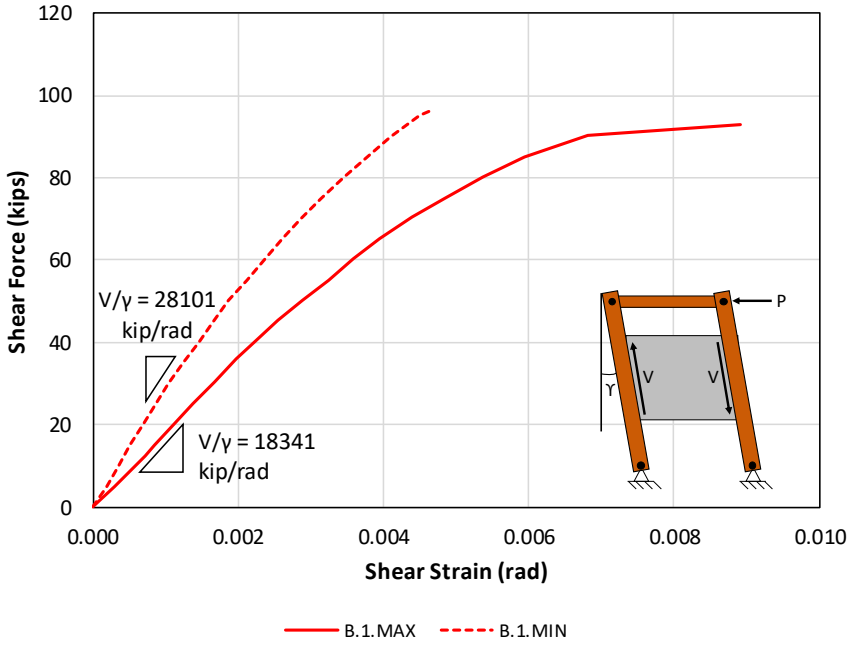

Figure A.28: Shear Stiffness Behavior for PCP Detail B.1

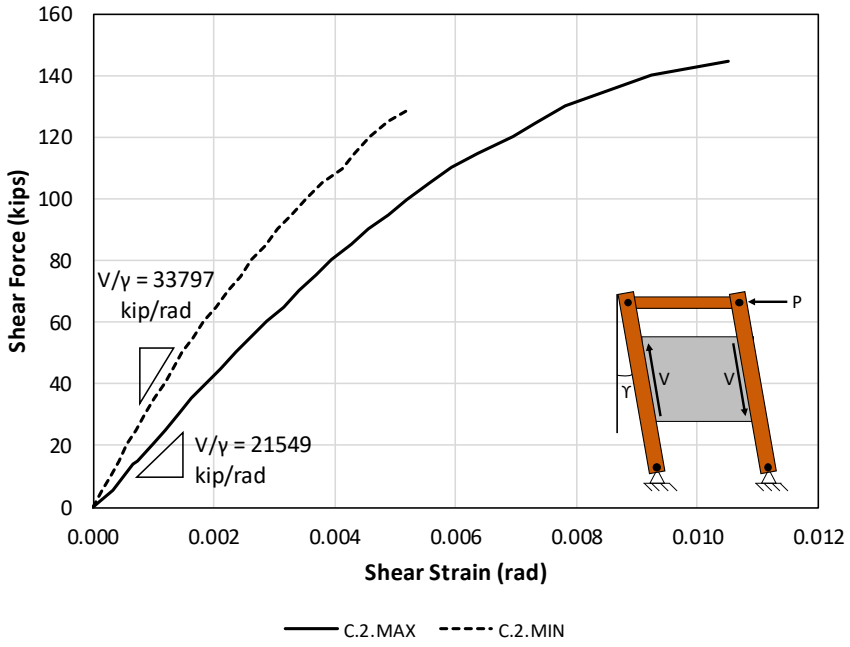

Figure A.29: Shear Stiffness Behavior for PCP Detail C.2

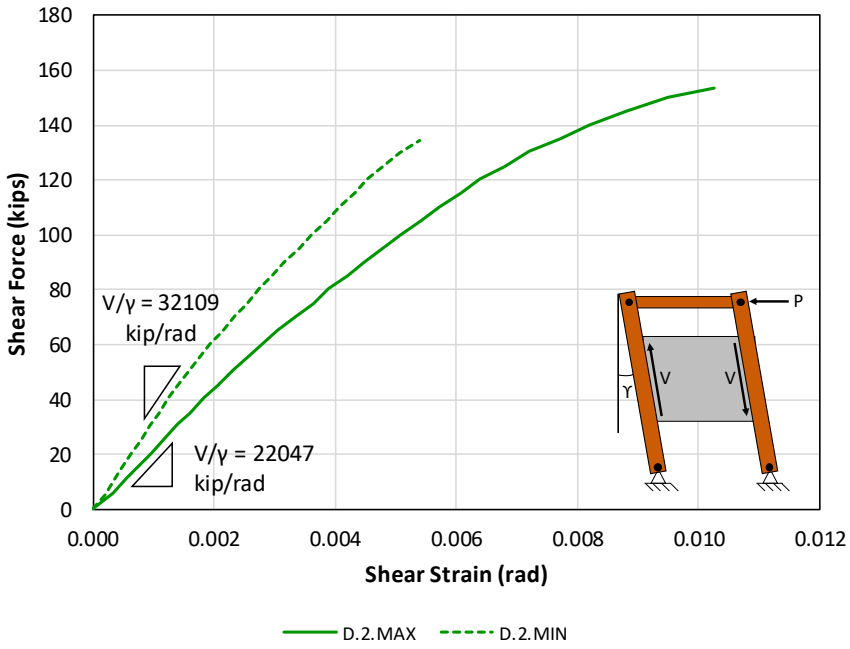

Figure A.30: Shear Stiffness Behavior for PCP Detail D.2

A.3.5 PCP Embed Behavior Results

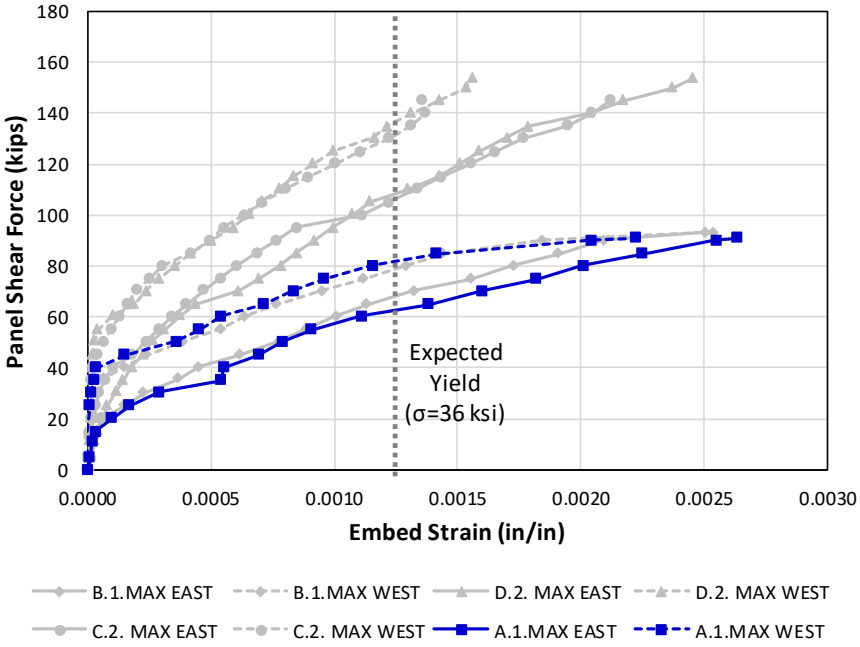

Figure A.31: Axial Strain Measured in Relation to Panel Shear for PCP Detail A.1.MAX

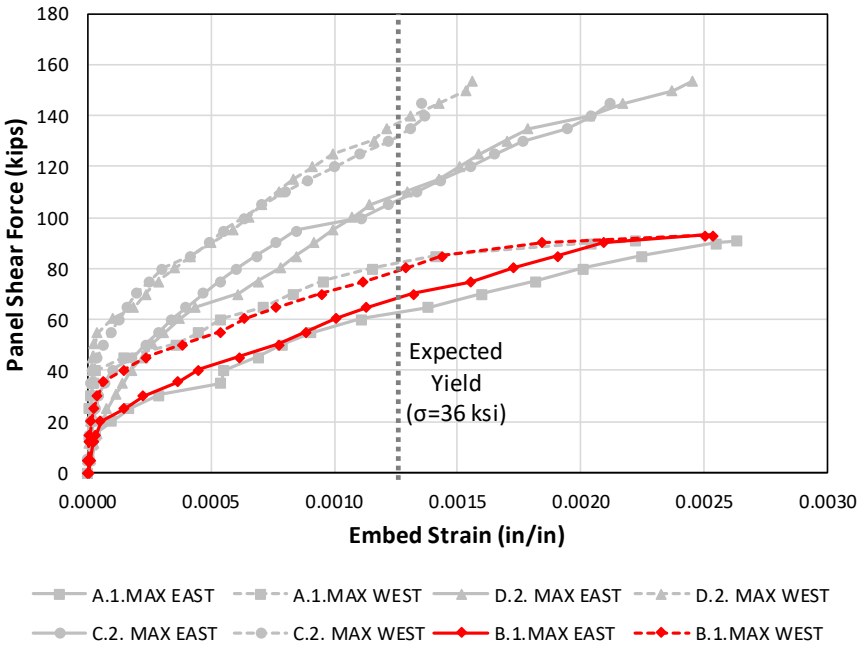

Figure A.32: Axial Strain Measured in Relation to Panel Shear for PCP Detail B.1.MAX

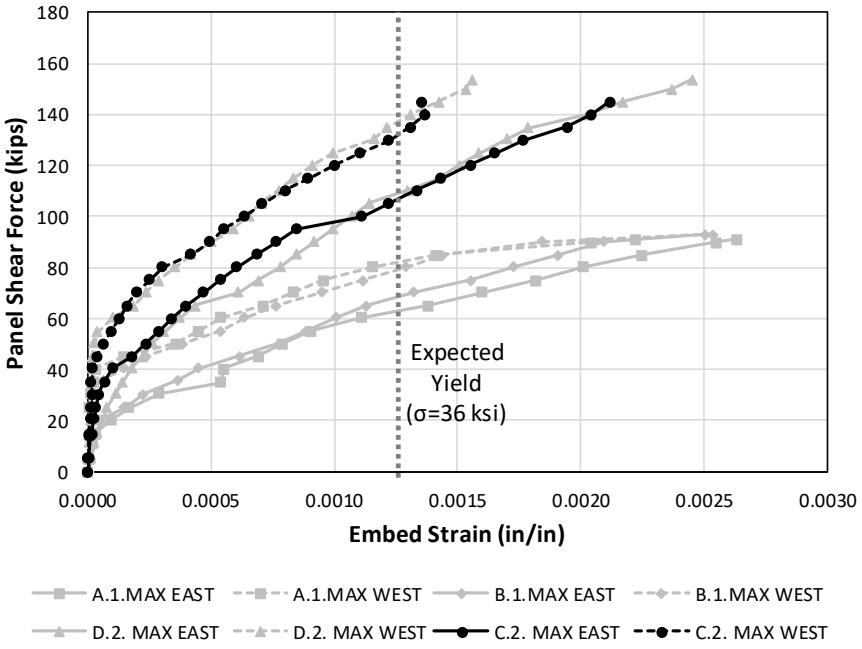

Figure A.33: Axial Strain Measured in Relation to Panel Shear for PCP Detail C.2.MAX

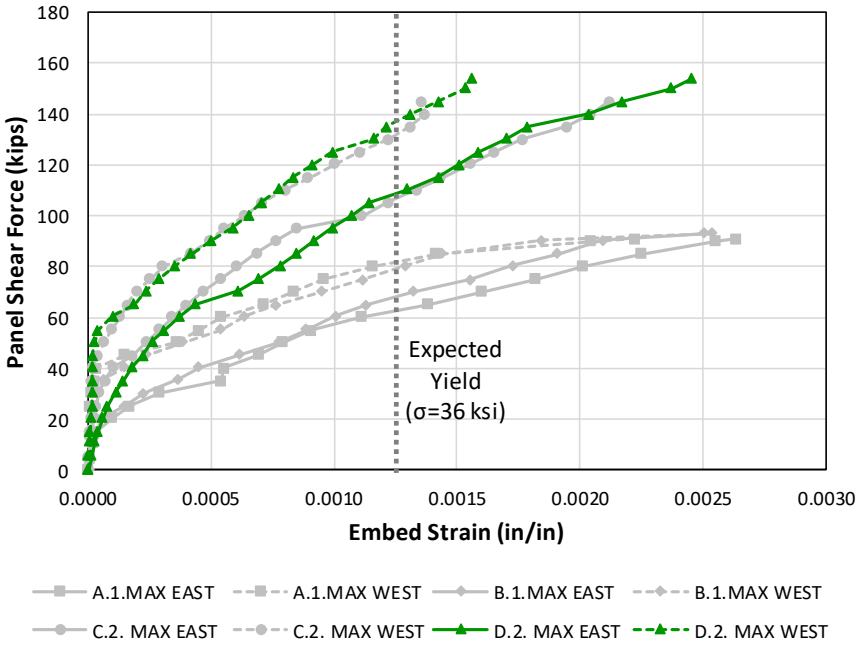

Figure A.34: Axial Strain Measured in Relation to Panel Shear for PCP Detail D.2.MAX

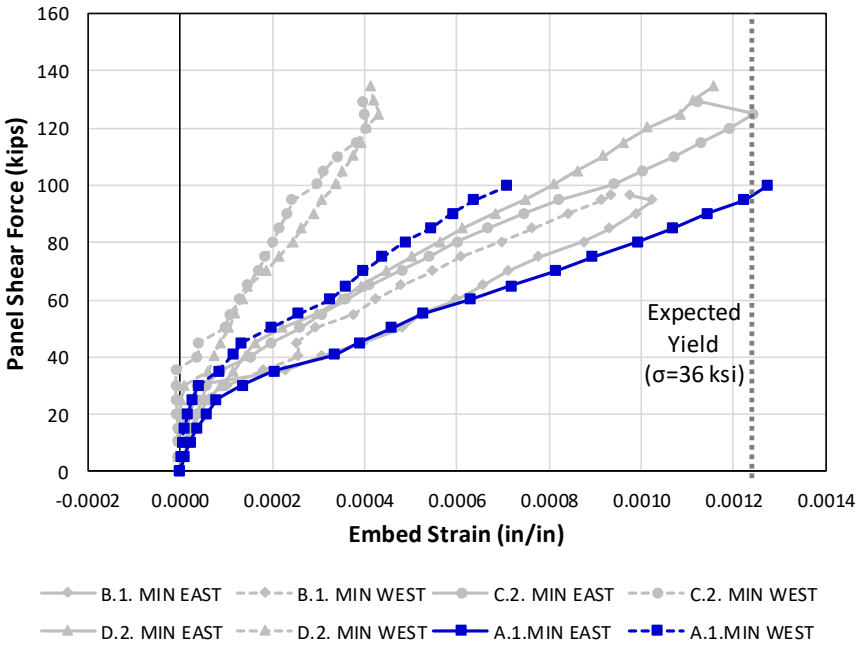

Figure A.35: Axial Strain Measured in Relation to Panel Shear for PCP Detail A.1.MIN

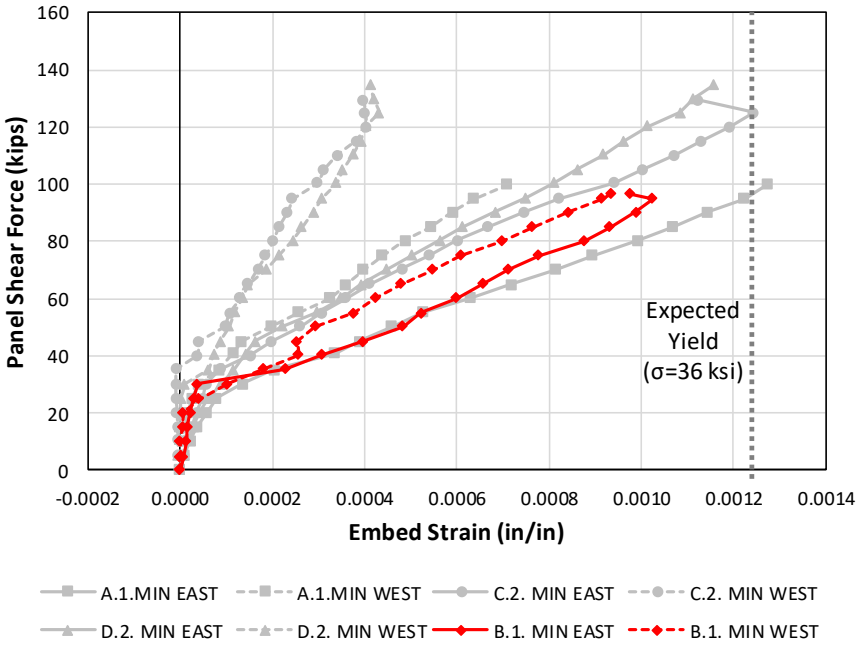

Figure A.36: Axial Strain Measured in Relation to Panel Shear for PCP Detail B.1.MIN

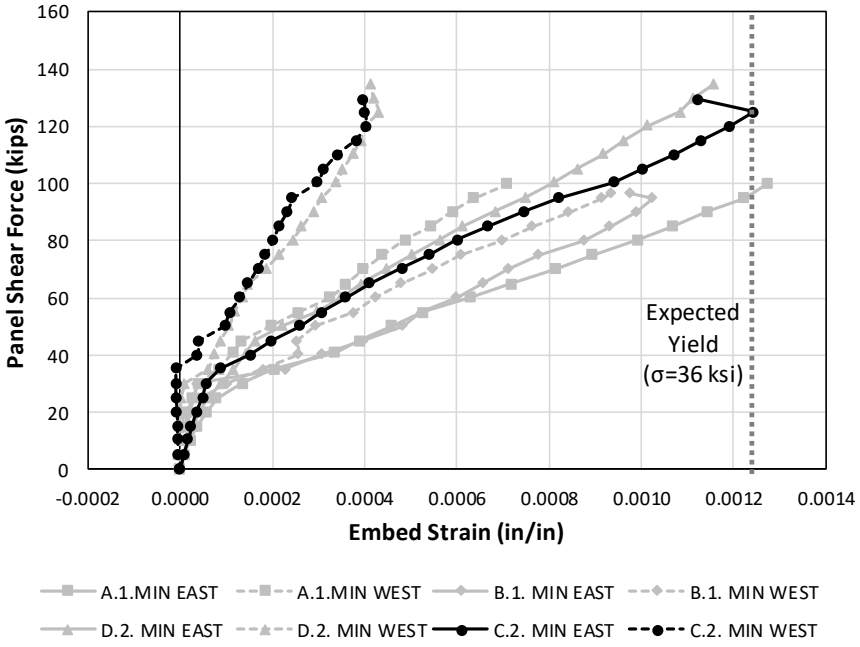

Figure A.37: Axial Strain Measured in Relation to Panel Shear for PCP Detail C.2.MIN

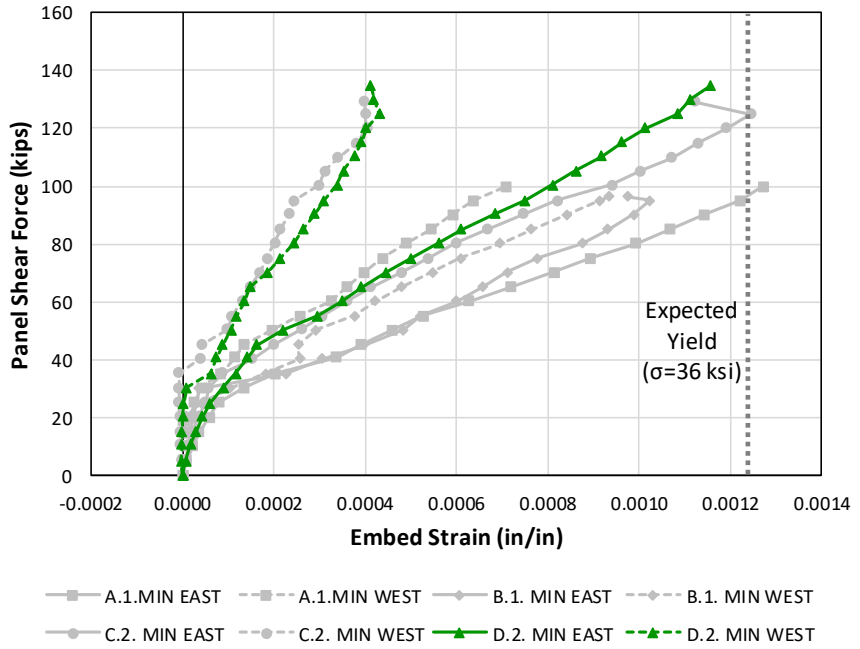

Figure A.38: Axial Strain Measured in Relation to Panel Shear for PCP Detail D.2.MIN

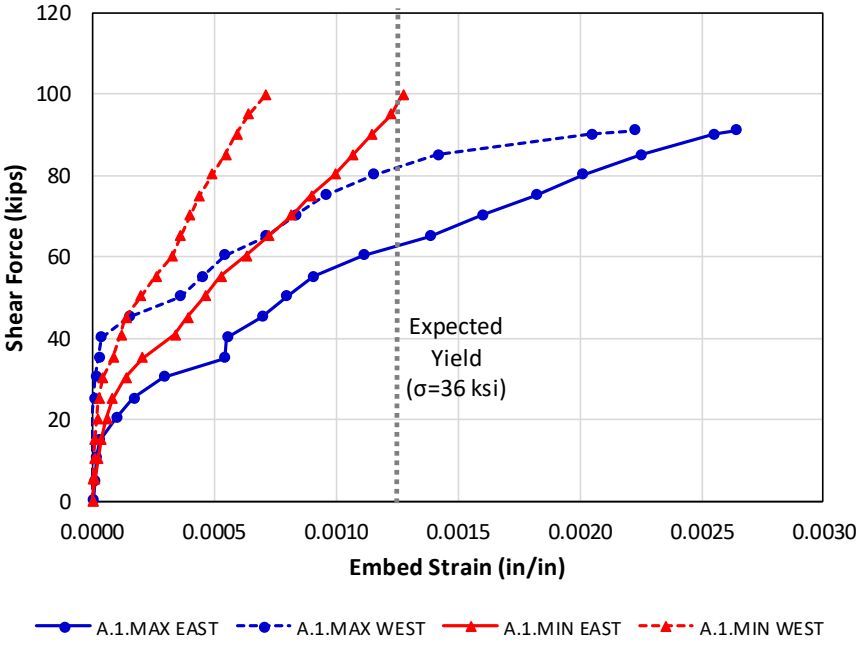

Figure A.39: Axial Strain Comparison for PCP Details A.1.MAX and A.1.MIN

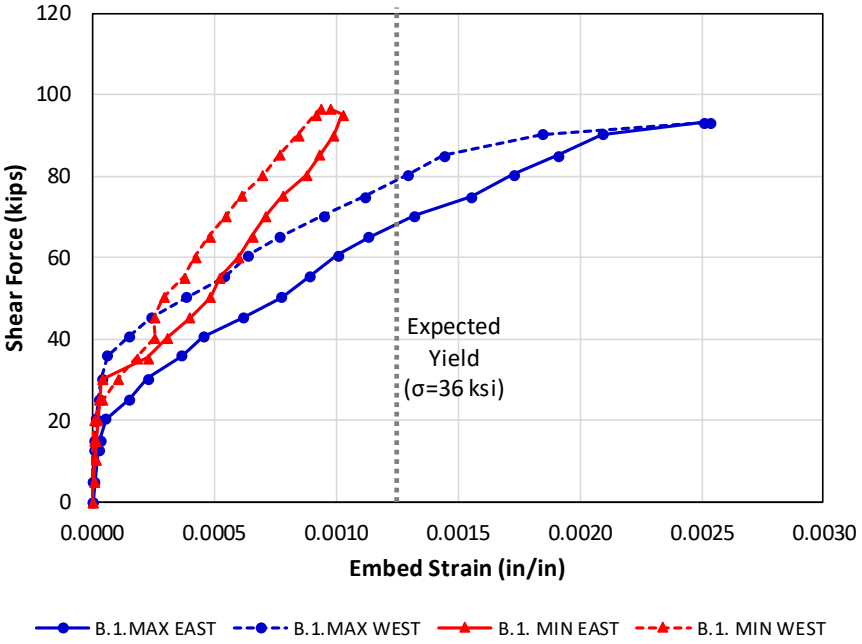

Figure A.40: Axial Strain Comparison for PCP Details B.1.MAX and B.1.MIN

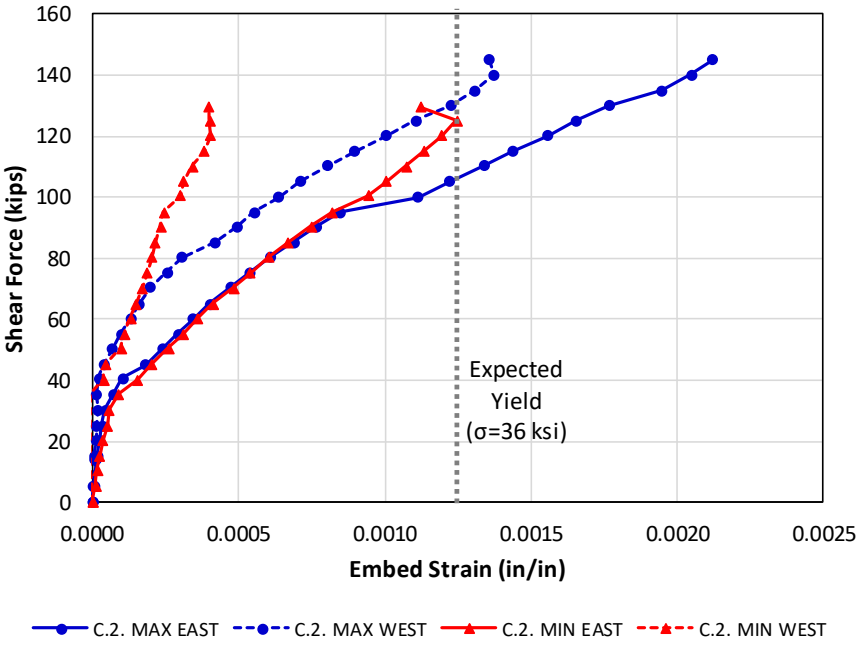

Figure A.41: Axial Strain Comparison for PCP Details C.2.MAX and C.2.MIN

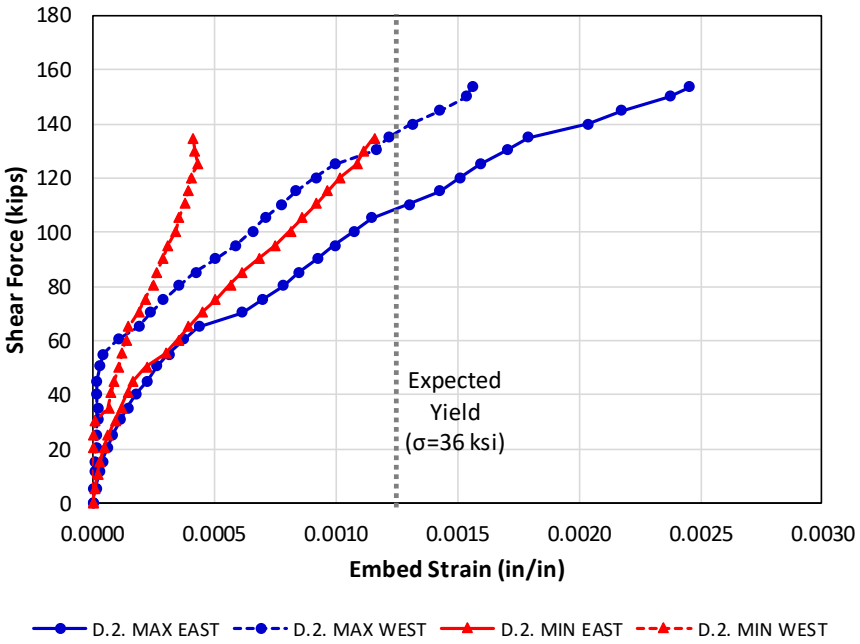

Figure A.42: Axial Strain Comparison for PCP Details D.2.MAX and D.2.MIN

A.4 PCP ULTIMATE LOAD CRACKING PATTERNS

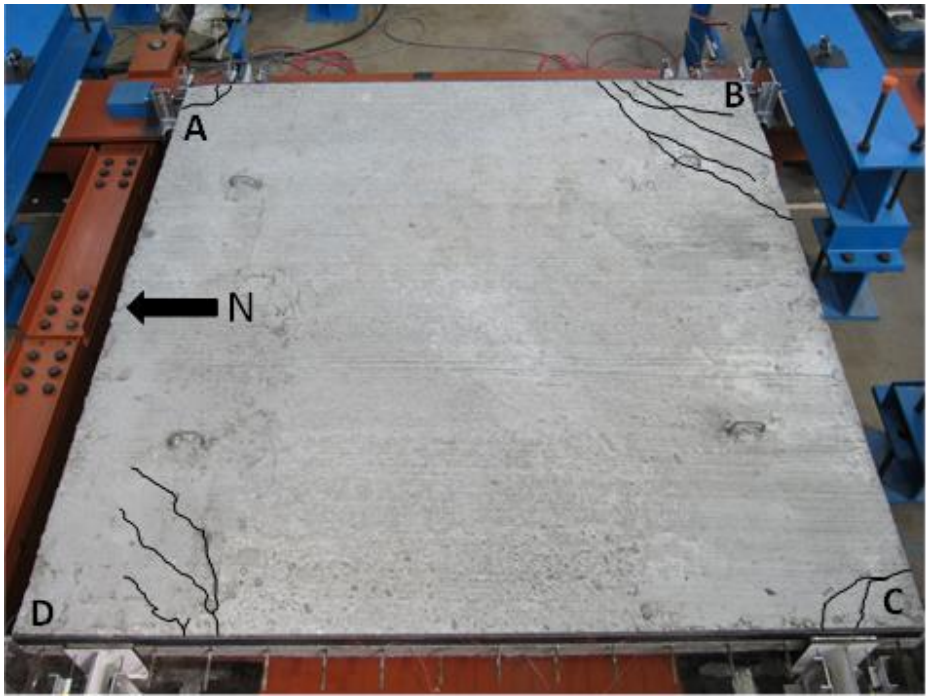

Figure A.43: Cracking Behavior at Ultimate Load for PCP Detail A.1.MAX

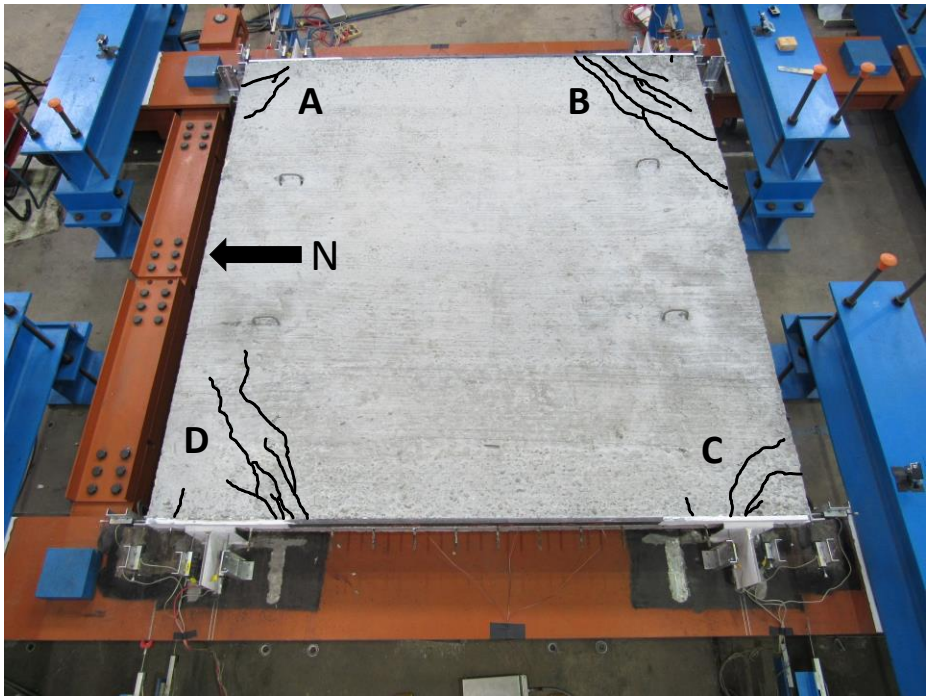

Figure A.44: Cracking Behavior at Ultimate Load for PCP Detail B.1.MAX

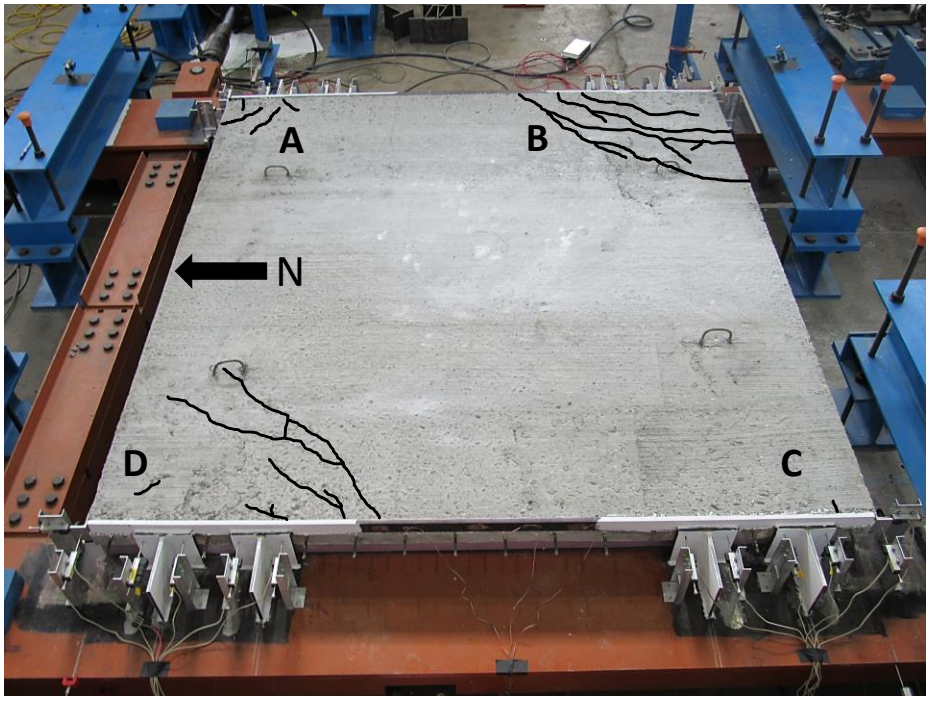

Figure A.45: Cracking Behavior at Ultimate Load for PCP Detail C.2.MAX

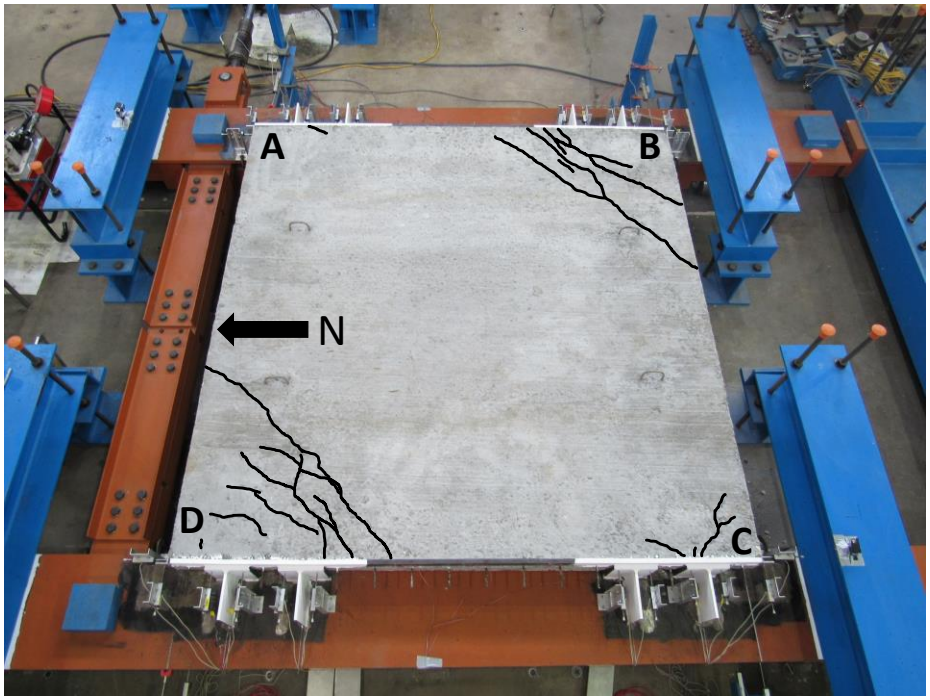

Figure A.46: Cracking Behavior at Ultimate Load for PCP Detail D.2.MAX

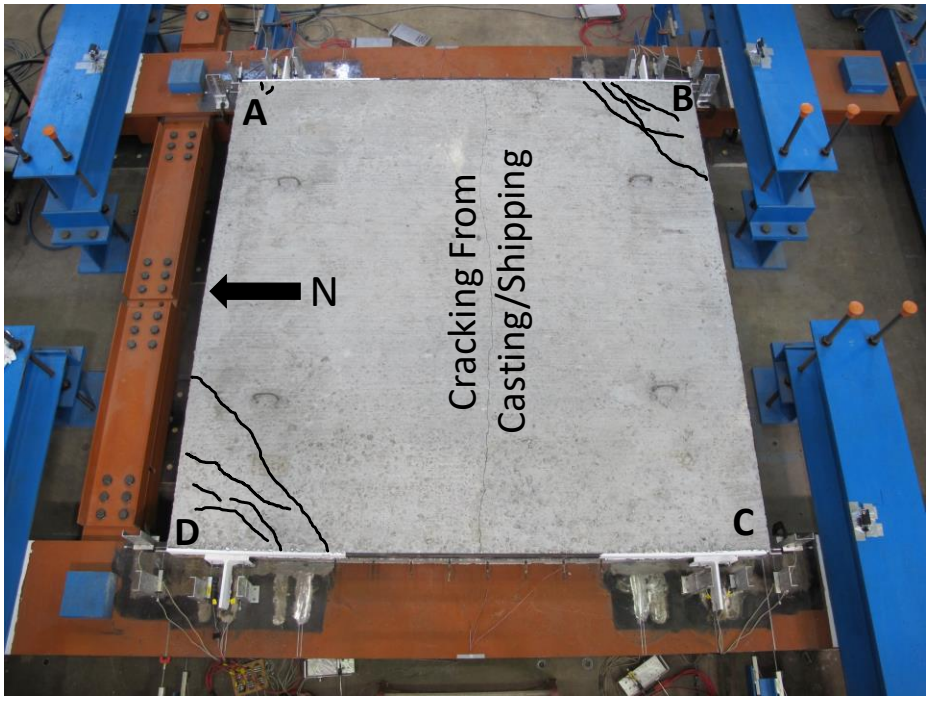

Figure A.47: Cracking Behavior at Ultimate Load for PCP Detail A.1.MIN

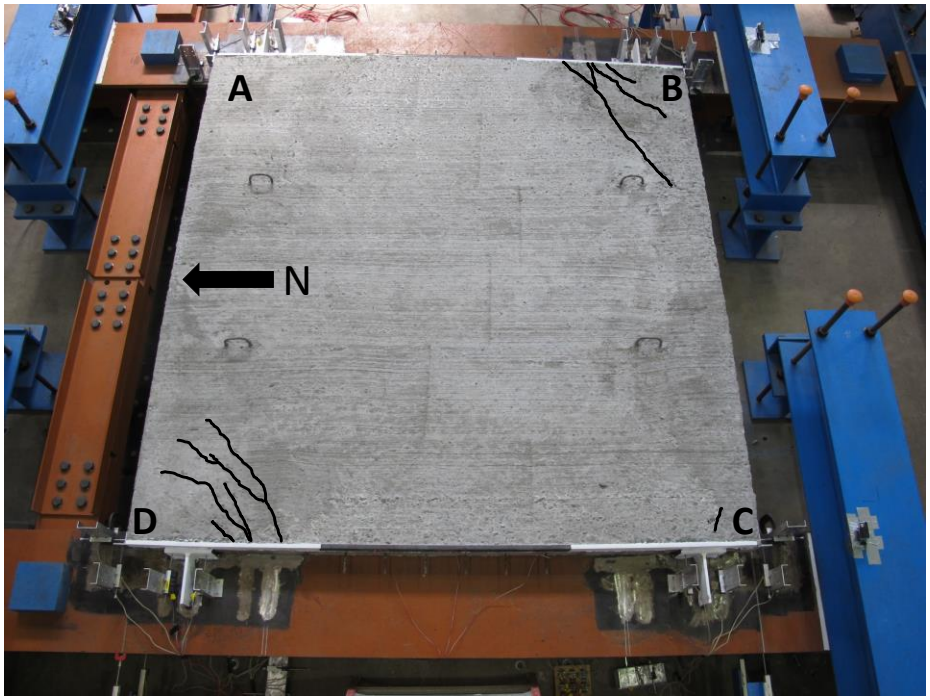

Figure A.48: Cracking Behavior at Ultimate Load for PCP Detail B.1.MIN

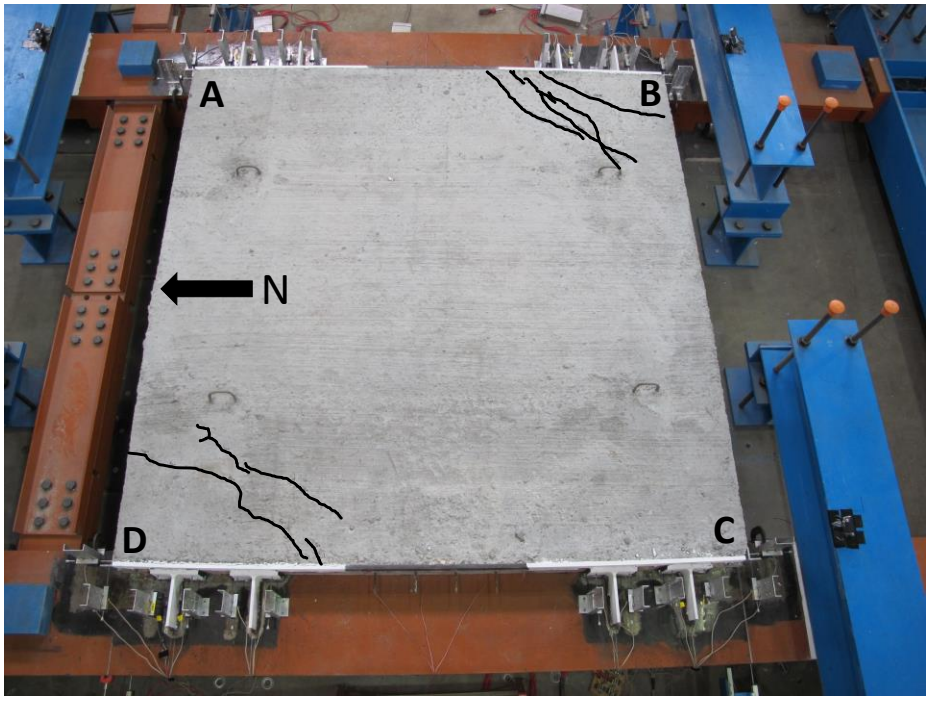

Figure A.49: Cracking Behavior at Ultimate Load for PCP Detail C.2.MIN

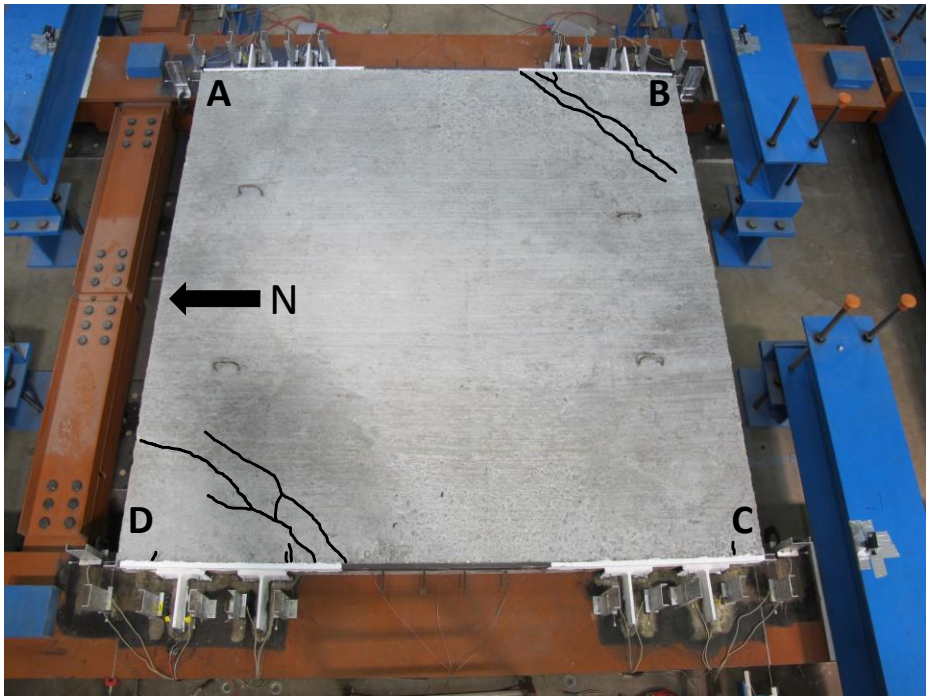

Figure A.50: Cracking Behavior at Ultimate Load for PCP Detail D.2.MIN

References

AASHTO, A. A. (2014). *Load and Resistance Factor Design (LRFD) Bridge Design Specifications, Seventh Edition.* Washington, D.C.

AISC. (2011). *Steel Construction Manual, 14th Edition.*

Currah, R. M. (1993, August). Shear Strength and Shear Stiffness of Permanent Steel Bridge Deck Forms. *M.S. Thesis*. The University of Texas at Austin.

Egilmez, O. O. (2005). Lateral Bracing of Steel Bridge Girders by Permanent Metal Deck Forms. *Ph.D. Dissertation*. The University of Houston.

Errera, S., & Apparao, T. (1976). Design of I-shaped beams with diaphragm bracing. *J. Struct. Div., 102(4)*, 769-781.

Galambos, T. V. (1998). *Guide to stability design criteria for metal structures.* New York: Wiley.

Haskins, M. (2015, January). *What Is a Girder Bridge?* Retrieved from Civil Engineering: https://erkrishneelram.wordpress.com/tag/girder-bridges/

Helwig, T. A. (1994). Lateral bracing of Bridge Girders by Metal Deck Forms. *Ph.D. Dissertation*. The University of Texas at Austin.

Helwig, T. A., & Frank, K. H. (1999). Stiffness Requirements for diaphragm bracing of beams. *J. of Struct. Engr., ASCE, Vol. 125, No. 11*, 1249-1256.

Helwig, T. A., & Yura, J. A. (1995). *Bracing for Stability.*

Helwig, T. A., & Yura, J. A. (2008a). Shear Diaphragm Bracing of Beams I: Stiffness and Strength. *Journal of Structural Engineering, 134(3)*, 348-356.

Helwig, T. A., & Yura, J. A. (2008b). Shear diaphragm bracing of beams. II: Design Requirements. *Journal of Structural Engineering, 134(3)*, 357-363.

Helwig, T. A., Frank, K. H., & Yura, J. A. (1997). Lateral-Torsional Buckling of Singly-Symmetric I-Beams. *ASCE Journal of Structural Engineering*, Vol. 123, No. 9, pp. 1172-1179.

Jetann, C. A. (2003). Stiffness and Strength of Metal Bridge Deck Forms with Stiffened Connection Details. *M.S. Thesis*. University of Houston.

Lawson, R., & Nethercot, P. (1985). Lateral Stability of I-beams Restrained by Profiled Sheeting. *The Struct. Engr., London, 63B(1)*, 3-13.

McCammon, V. E. (2015, December). In-Plane Shear Strength and Stiffness of Precast Concrete Panels. *M.S. Thesis*. The University of Texas at Austin.

Nethercot, D., & Trahair, N. (1975). Design of diaphragm-braced I-beams. *J. Struct. Div., 101(10)*, 2045-2061.

Roskos et al. (2017). Partial Depth Precast Concrete Deck Panels on Curved Bridges. *Proceedings of the Annual Stability Conference.* San Antonio: Structural Stability Research Council.

Timoshenko, S. P., & Gere, J. M. (1961). Theory of Elastic Stability, Second Edition. New York: McGraw-Hill Book Company, Inc.

TxDOT. (2006). *Prestressed Concrete Panel Deck Details.* Retrieved from Bridge Division Standard: http://austinprestress.com/pdf/pcpstde2.pdf

TxDOT. (2010). *Prestressed Concrete Panel Fabrication Details.* Retrieved from Bridge Division Standard: http://austinprestress.com/pdf/pcpstde1.pdf

Winter, G. (1960). Lateral Bracing of Columns and Beams. *ASCE Transactions, Vol. 125*, 809-825.

Yura, J. A. (2001). Fundamentals of Beam Bracing. *Engineering Journal, AISC, 1st Quarter*, 11-26.

Yura, J. A., & Helwig, T. A. (2014). Stability Bracing of Columns and Frames. *North American Steel Construction Conference.* Toronto: Structural Stability Research Council.

Vita

John Kintz was born in Geneva, Illinois and raised in Sugar Grove, Illinois. He attended the University of Iowa for his undergraduate education, receiving his Bachelor of Science in Engineering degree in civil engineering in May of 2015. During his time as an undergraduate, John worked as a teaching assistant and was heavily involved in Iowa's ASCE student chapter, particularly as a two-time captain of the steel bridge team. These experiences, in addition to several civil engineering internships, cultivated his interest for further education in structural engineering. In August 2015, he enrolled in the graduate school at The University of Texas at Austin Cockrell School of Engineering to pursue a master's degree.

Permanent email: jrkintz20@gmail.com

This thesis was typed by the author.